Alma Mater Studiorum – Università di Bologna

DOTTORATO DI RICERCA IN

Scienze Chimiche

Ciclo XXV

Settore Concorsuale di afferenza: 03/B1

Settore Scientifico disciplinare: CHIM/03

PHOTOACTIVE CARBON NANOSTRUCTURES:
FROM MULTICOMPONENT ARRAYS TO NANOMATERIALS

Presentata da: Joanna Maria Malicka

Coordinatore Dottorato

Prof.ssa Adriana Bigi

Relatore

Prof.ssa Paola Ceroni

Correlatore

Dr. Nicola Armarol

Esame finale anno 2013

Preface

Carbon possesses the unique ability to form sp^3-, sp^2- and sp-hybridized networks of atoms that allow to generate a collection of allotropes, which exist also as nanoscale materials. The emergence of carbon nanostructures occurred through serendipity and experimental advances resulting first in the discovery of fullerene, followed by that of of carbon nanotubes, nanohorns, and graphene. The multifaceted world of carbon nanostructures with their exceptional physical and chemical properties and nanoscale size created new opportunities in materials science opening the way to a vast range of potential applications.

The versatile properties of carbon nanomaterials are reflected in the multidisciplinary character of my doctoral work, where I take advantage of the opportunities offered by fullerenes and carbon nanotubes in constructing novel functional materials. This work is composed of three independent chapters, each of them presenting a different approach in the design of multicomponent arrays and materials based on carbon nanostructures. Each chapter begins with an introduction describing the desired properties of a carbon allotrope to be part of a given system as well as a general overview and state-of-the-art, followed mainly by a discussion on the photophysical investigations and the analytical characterization methods applied.

In Chapter 1, fullerenes are explored as electron and energy acceptors to be utilized in light energy conversion – a vital task to implement renewable energy technologies in the context of an ever increasing global demand for energy. This chapter presents two works on innovative fullerene-based covalent arrays for basic studies on photoinduced energy and electron transfer. In the first part, a fullerene hexa-adduct functionalized with twelve p-conjugated oligomers was investigated and virtually quantitative energy transfer was proved. The second part describes electrochemical and photophysical studies on fullerene systems equipped with a light harvesting antenna (oligophenyleneethynylene-type), and suitable

electron donor(s), namely ethynylferrocenyl or 4-ethynylphenyl phenothiazine. It is shown that photoinduced energy and electron transfer occur.

Chapter 2 describes the use of carbon nanotubes as optically silent scaffolds in a novel luminescent hybrid material. This is composed of multiwalled carbon nanotubes (MWCNTs) covalently functionalized with a second-generation polyamidoamine dendron, bearing four positively charged terminals per grafted moiety, which were subsequently ion-paired with a negatively charged and highly luminescent europium complex. The structure and integrity of the hybrid was demonstrated by various characterization techniques, such as XPS, electron microscopy and DOSY NMR. Photophysical analysis of this array shows that MWCNTs act as photochemically inert scaffolds with negligible UV-Vis absorption compared to the europium complex, with no quenching activity. As a result, the studied hybrid shows the characteristic bright luminescence of europium ions and is practically indistinguishable compared to the incorporated complex alone.

Chapter 3 shows one more application of carbon nanotubes, this time as single walled nanotubes. In such work, a functionalized squaraine dye capable of undergoing ultrasound-induced self-assembly was synthesized and fully characterized. Rapid cooling of a hot solution of the dye to 0 ℃ resulted in self-assembled precipitates consisting of two types of nanostructures, rings and ill-defined short fibers, likely to be originated from distinct primary nuclei. The application of ultrasound modifies the conditions for the supersaturation-mediated nucleation, generating only one kind of nuclei and prompting the formation of crystalline fibrous structures, inducing gelation of solvent molecules. These studies revealed a nucleation growth mechanism for the observed self-assembly, an aspect rarely studied in the area of sonication-induced gelation. In order to investigate the effects of nanoscale substrates on the sonication induced self-assembly, a minuscule amount of single walled carbon nanotubes has been added, which leads to acceleration of the self-assembly through a heterogeneous

nucleation process that ultimately affords a supramolecular nanotape-like morphology. This study demonstrates that self-assembly of functional dyes can be judiciously manipulated by an external stimulus and can be further controlled by the addition of carbon nanostructures as dopants.

In the overall work briefly summarized above, carbon nanostructures are incorporated in novel photoactive functional systems constructed through different types of interactions – covalent bonds, ion-pairing or self-assembly. The variety of properties exhibited by carbon nanostructures are successfully explored by assigning them a different role in a specific array. Due to their complex and innovative structures, all of the systems were extensively investigated by a number of analytical techniques. The experimental activities discussed in this doctoral thesis were mostly devoted to photochemistry and photophysics, but other methods like cyclic voltammetry, IR/NMR spectroscopies have been also applied. All the presented systems serve as a testbed for exploring the properties of carbon nanostructures in multicomponent arrays, which may be advantageous in the design and preparation of new photovoltaic or optoelectronic devices, as well as in the design and control of self-assembly processes.

Chapter 1

Energy and Electron Transfer in Fullerene-Based Covalent Multicomponent Systems

1.1. Introduction

Fullerenes, discovered in 1985,[1] attracted a lot of attention because of their beautiful structural features and intriguing physical properties. With no doubt, the milestone in the research on this carbon allotrope was in 1990 when the groups of Krätschmer and Fostiropoulos described the procedure for mass production of the most popular member in the fullerene family, C_{60}, based on the arc discharge of graphite electrodes.[2] Once C_{60} and C_{70} fullerenes became commercially accessible, the research community has intensively explored the properties of these materials and importantly, protocols for the functionalization of C_{60} were quickly established.[3] Studies on fullerenes coincided with a growing awareness related to the escalating demand for energy and the depletion of fossil fuels.[4] These global problems have fostered the research on artificial photosynthesis, organic photovoltaics and other approaches that aim at investigating the conversion solar energy into electricity or fuels. A key fundamental process on the way to these goals is the production of photoinduced charge separated states, for which fullerenes are perfectly suited as electron acceptors.[4b,5]

To better understand fundamental photophysical processes that govern light energy conversion, namely energy and electron transfer, a variety of arrays where fullerenes are combined with suitable electron donors have been investigated. Fullerenes were assembled with electron acceptors by covalent bonding,[5d,6c] supramolecular interactions,[6] as well as mechanical linking (rotaxanes).[7] Photoinduced energy or electron transfer have been reported for a variety of fullerene-based donor-acceptor conjugates where porphyrins,[8] phtalocyanines,[6c] (oligo)thiophenes,[9] oligovinylenes[8f] are among the most utilized electron donating moieties. As a further development, more sophisticated structures of higher order, like triads, tetrads or fullerodendrimers have been proposed, assigning specific roles to the grafted moieties in order to perform light harvesting and charge separation in nanoarchitectures.[3d,5d,8a,11]

Herein, two systems designed to accomplish photoinduced energy or electron transfer in fullerene-based covalent arrays are described, each representing a different approach to photoinduced events. First, studies on a fullerene hexakis adduct are described, where the effect of the symmetrical, shell-like arrangement of chromophores on photoinduced energy transfer is investigated. Another system combines fullerene with two individual moieties with a specific role. i.e. a light-harvesting antenna and an electron donor.

Photophysical and electrochemical properties of C_{60}

C_{60} absorbs light across the UV and visible spectral regions (Figure 1).[5d] Upon photoexcitation, the lowest lying singlet excited state of C_{60} is populated ($^1C_{60}$*, ~1.7 eV[12]), which undergoes intersystem crossing to populate the lowest triplet excited state ($^3C_{60}$*, 1.5 eV[13]) with high yield (>99%). In spite of this dominant deactivation pathway, a weak fluorescence band originating from the $^1C_{60}$* → C_{60} transition can be detected around 700 nm, with quantum yield ~ 0.0001 and lifetime around 1.3 ns.[12,14] The phosphorescence originating from the fullerene triplet excited state can observed only below 5K[15] or, at 77 K,[16] in rigid media containing heavy atoms, for example ethyl iodide (Figure 1).[5d]
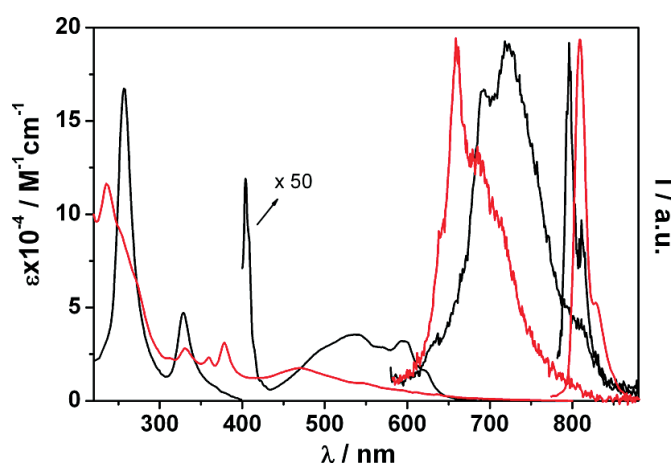
Figure 1. Absorption and fluorescence spectra of C_{60} (black) and C_{70} (red), in CH_2Cl_2. The narrow profiles above 800 nm are the phosphorescence spectra in ethyl iodide at 77 K.[5d]

At room temperature, the lifetime of $^3C_{60}^*$ was determined to be 40 μs[17] and 60 μs[7a] by transient absorption in benzene and dichloromethane, respectively. The experimental conditions are very strict in order to avoid triplet-triplet annihilation.[18] The triplet lifetime can be measured only at diluted concentrations applying weak excitation powers, with no traces of oxygen in a solution. Importantly, energy transfer between $^3C_{60}^*$ and oxygen is in fact a sensitization process, which enables indirect monitoring of the fullerene triplet thanks to the emission of oxygen in its singlet state ($^1O_2^*$, "singlet oxygen") generated according to the process:[5d]

$$F \xrightarrow{h\nu_{UV-vis}} {}^1F^* \xrightarrow{isc} {}^3F^* \xrightarrow{O_2} F + {}^1O_2^* \rightarrow F + O_2 + heat + h\nu_{1270\,nm}$$
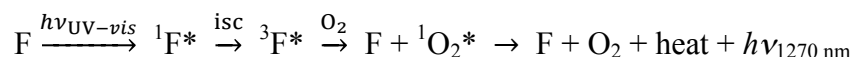
Although the majority of $^1O_2^*$ deactivates nonradiatively, the band in the near-infrared region is easily detectable and is a convenient indication of the presence of $^3C_{60}^*$ in solution.[19]

The plethora of applications of fullerenes in materials science results from its outstanding electron affinity.[5a] In fact, C_{60} can reversibly accept up to six electrons with the first reduction potential placed in the range between - 0.3 - 0.4 eV vs. saturated calomel electrode (SCE).[20] The reduction potentials can be determined by cyclic voltammetry and the resulting values depend on the experimental conditions, e.g. solvent or supporting electrolyte. Reduction (as well as oxidation) of fullerene becomes easier upon excitation to its singlet or triplet electronic excited state and this characteristic is advantageous for the design of systems aimed at photoinduced electron- and energy-transfer.[5a]

1.2. Photoinduced Energy Transfer in a T_h-Symmetrical Hexakis Adduct of C_{60} Substituted with π-Conjugated Oligomers

1.2.1. Introduction

Among the innumerable fullerene hybrids designed to study photoinduced processes, hexakis-adducts have been scarcely explored.[21] This is mainly due to the difficulties associated with their synthesis, when compared to mono- or bis-functionalized derivatives.[22] However, hexa-substituted fullerenes have unique and advantageous features for the design of photoactive materials. The three-dimensional addition pattern enables symmetrical functionalization of the fullerene sphere with a multitude of chromophores, with formation of compact materials. Moreover, hexa-substituted fullerene remains a good energy acceptor.[21c]

The investigated multicomponent system is composed of a fullerene core and 12 peripheral organic conjugated oligomers (each substitution brings two oligomers) and is depicted in Figure 2.
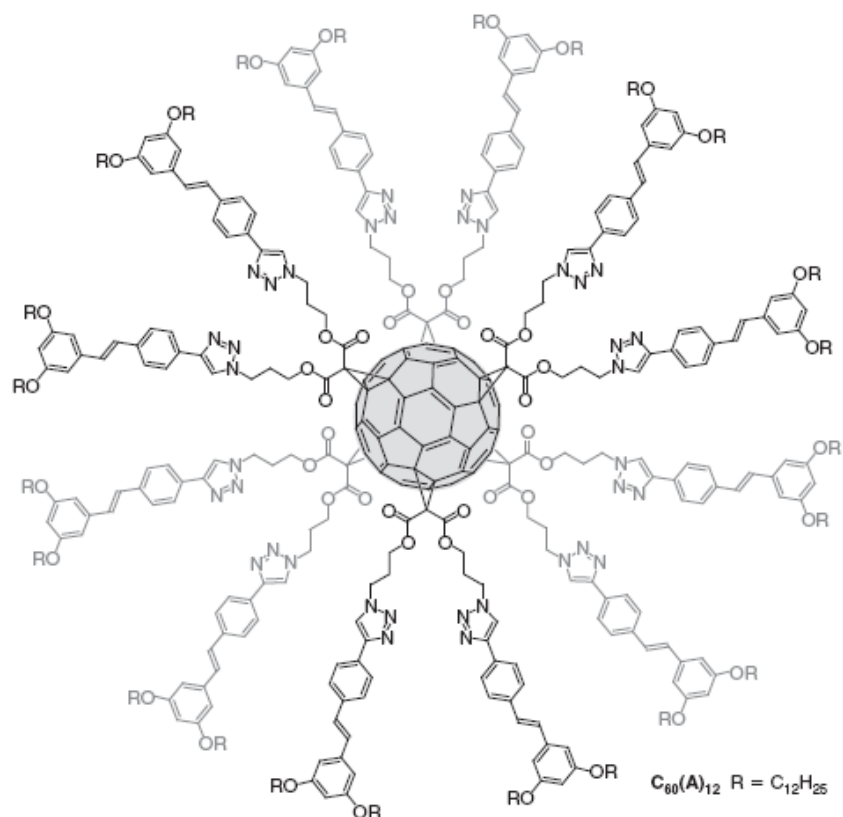
Figure 2. Molecular structure of the investigated fullerene hexakis-adduct.

Efficient synthesis of this compound was possible by applying post-functionalization of a simple fullerene hexakis-adduct, which was first synthesized in a one-pot reaction of C_{60} and a suitable malonate derivative bearing terminals azide groups with 62% yield. Next, 12 peripheral moieties were grafted onto the functionalized fullerene core by copper mediated Huisgen 1,3 dipolar cycloaddition of azides and alkynes, affording the final molecule. In order to understand the properties of this complex hexa-adduct, reference compounds **A** and **$C_{60}(Ph)_{12}$** were also synthesized and are depicted in Figure 3. Details of the synthesis of the investigated system **$C_{60}(A)_{12}$** together with **A** and **$C_{60}(Ph)_{12}$** can be found in ref. 23 and 24.
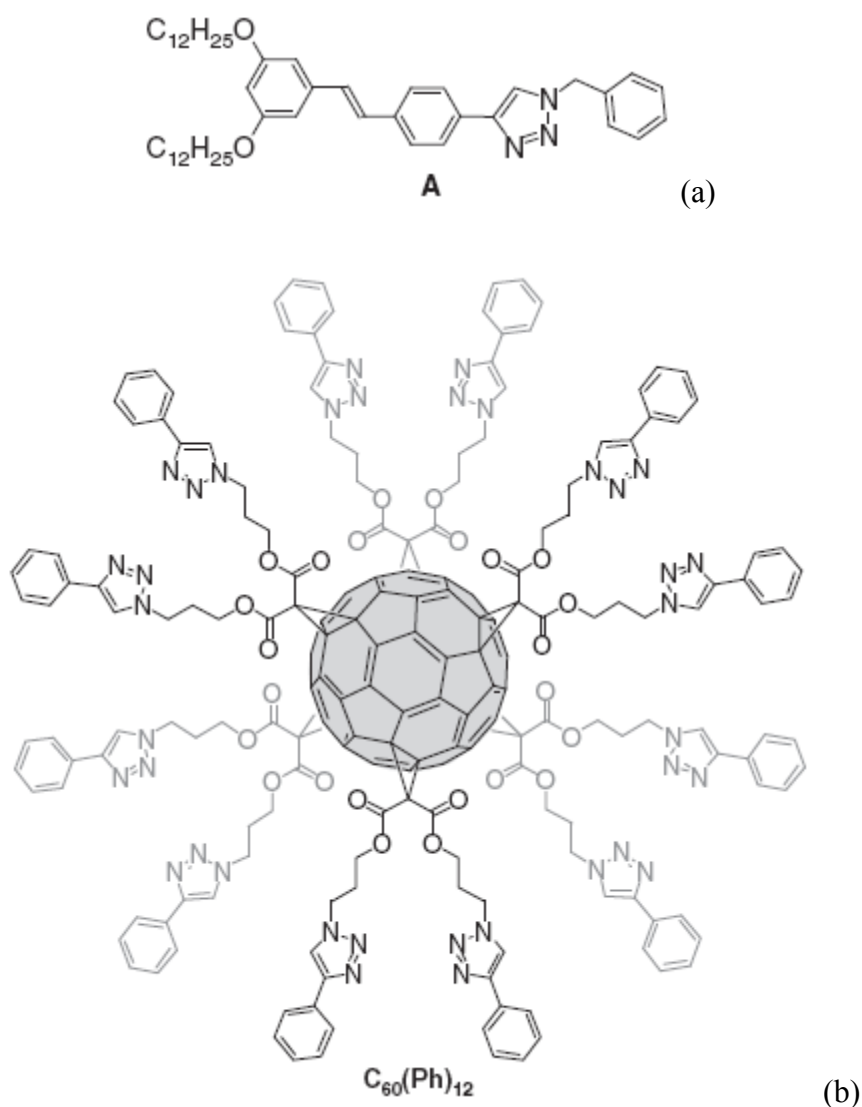
Figure 3. Reference compounds to compare electrochemical and photophysical properties of the target hexakis multichromophoric system; (a) conjugated oligomer, **A** – a model for the grafted pendants; (b) hexa-substituted fullerene, **C₆₀(Ph)₁₂** – a model for the fullerene core.

Electrochemical properties were studied by cyclovoltammetry (CV) and Osteryoung square wave voltammetry (OSWV). Compound **A** is a weak electron donor characterized by two oxidation potentials at +1.46 V and +1.66 V versus SCE. Both oxidation processes are irreversible. One reduction process was detected at high potential, i.e. -2.12 V versus SCE. In the case of the target compound **C₆₀(Ph)₁₂** an irreversible oxidation process was detected at +1.50 V, which corresponds to the oxidation of the shell moieties. In the cathodic region,

irreversible reduction at -1.56 V vs. SCE was observed and is attributed to the reduction of the hexa-substituted fullerene core,[25] which is higher compared to non-functionalized C_{60}. Electrochemical studies revealed a relatively high HOMO-LUMO gap that disfavours electron transfer processes.

Photophysical properties of the T_h symmetrical fullerene hexakis-adduct were studied in detail and are described in the following section.

1.2.2. Photophysical properties

The ground state absorption spectra of the hexakis-adduct $C_{60}(A)_{12}$, its reference compounds **A** and $C_{60}(Ph)_{12}$[23] in CH_2Cl_2 are shown in Figure 4. The model hexa-substituted fullerene $C_{60}(Ph)_{12}$ shows extensive absorption in the UV-Vis region and the compound **A** has an intense absorption centered at 335 nm. Compound $C_{60}(A)_{12}$ exhibits a molar absorptivity of nearly 400,000 M^{-1} cm^{-1} at 335 nm owing to the presence of 12 **A** units around the central fullerene core. However, extinction coefficient of $C_{60}(A)_{12}$ is not the sum of the extinction coefficients of its model compounds, which may be attributed to a somehow different conjugation pattern in model compounds and the final structure and/or may indicate intramolecular interactions between the 12 external oligomer units.
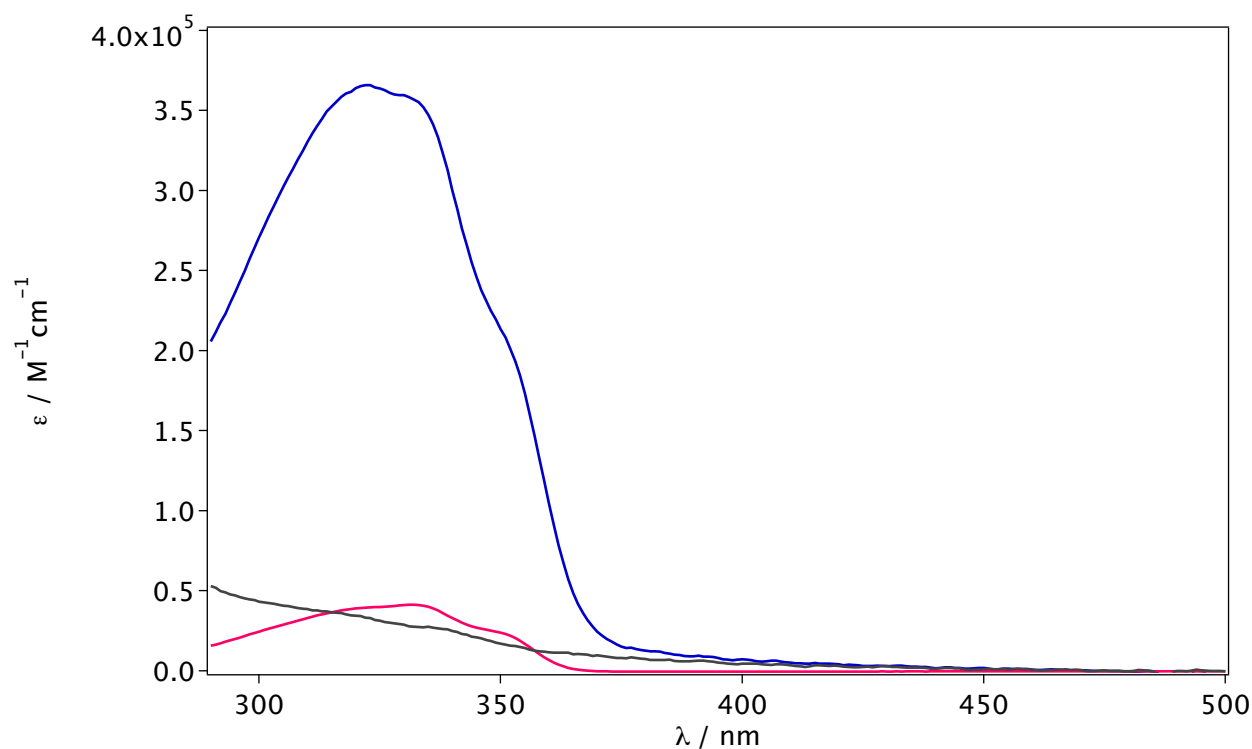
Figure 4. Electronic absorption spectrum of **A** (pink), **C$_{60}$(Ph)$_{12}$** (grey), **C$_{60}$(A)$_{12}$** (blue) in CH$_2$Cl$_2$ solution.

The emission spectra of **A**, **C$_{60}$(Ph)$_{12}$**, and **C$_{60}$(A)$_{12}$** are depicted in Figure 5 and the related photophysical parameters are summarized in Table 1. Model compound **A** is a strong fluorophore with an emission maximum around 385 nm (Φ_{em} = 0.4; τ = 1.0 ns). The fullerene reference compound **C$_{60}$(Ph)$_{12}$** shows a very weak fluorescence band centered around 670 nm (Φ_{em} = 0.0002; τ = 1.7 ns).
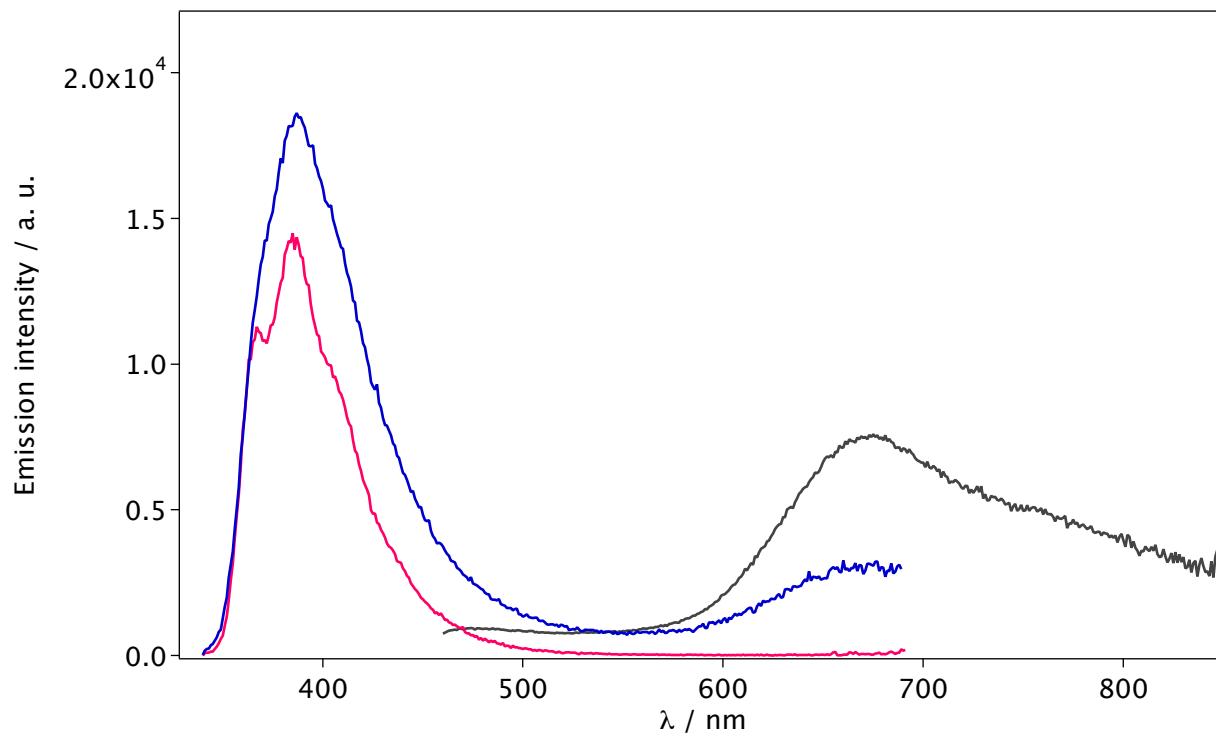
Figure 5. Emission profiles of **A** (pink), $C_{60}(Ph)_{12}$ (grey), $C_{60}(A)_{12}$ (blue)$_2$ in CH_2Cl_2 solution ($\lambda_{exc} = 325$ nm).

Table 1. Fluorescence properties of compounds **A**, $C_{60}(Ph)_{12}$, and $C_{60}(A)_{12}$ in CH_2Cl_2.

	λ_{max} [nm]	$\Phi_{fluorescence}$	τ [ns]
A	385	0.4	1
$C_{60}(Ph)_{12}$	670	0.0002	1.7
$C_{60}(A)_{12}$	388, 670	0.001 (388 nm)[A]	2[B]
		0.0002 (670 nm)[A]	

A: Residual emission from the appended conjugated oligomer fragments.
B: Determined for the emission at 670 nm, using a cut-off filter at 550 nm.

The fluorescence spectra of model compounds recorded at 77 K (CH_2Cl_2) are depicted in Figure 6. Notably, the spectrum of **A** shows a shift towards lower energy ($\lambda_{max} = 425$ nm) as compared to 298 K. This unusual temperature trend in the fluorescence spectra is probably related to the presence of a wide range of conformers in the rigid matrix within **A** structures,[26]

with emission observed predominantly from the lowest energy conformer. On the contrary, model compound $C_{60}(Ph)_{12}$ showed a shift of 30 nm towards the higher energy side ($\lambda_{max} =$ 640 nm).
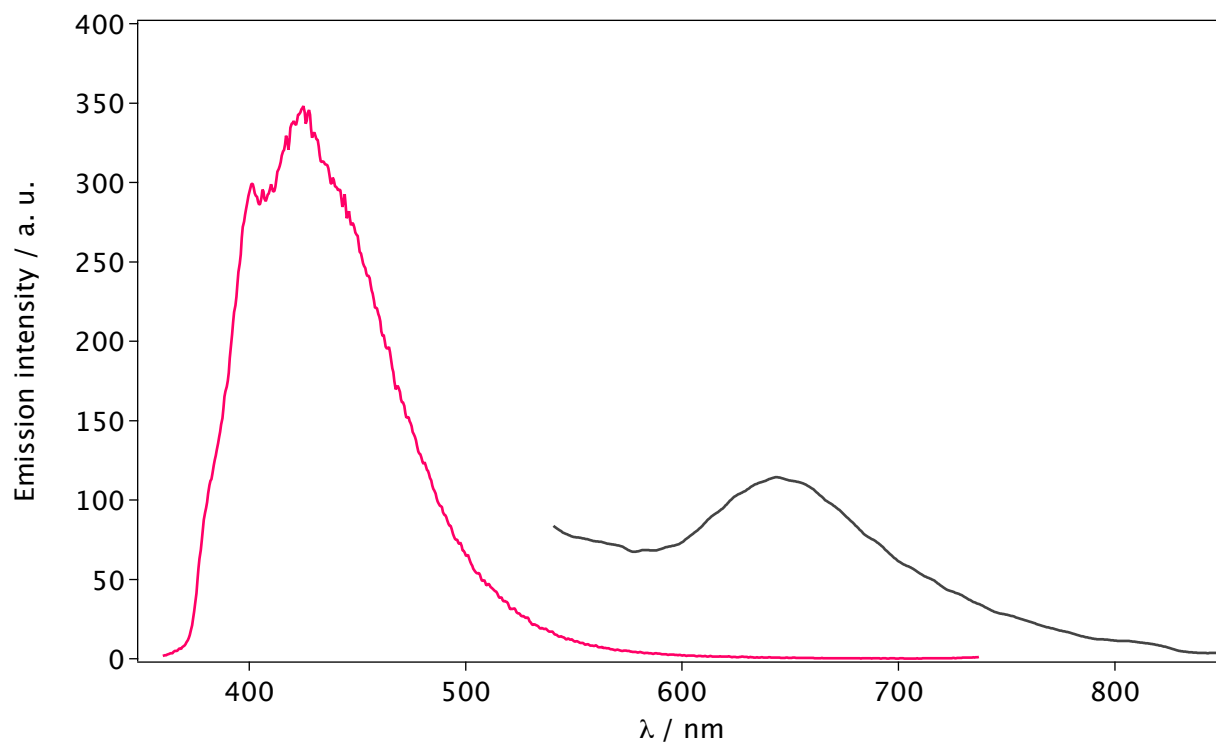
Figure 6. Emission spectra of **A** (pink) and $C_{60}(Ph)_{12}$ (grey) in CH_2Cl_2 at 77 K recorded by exciting at 325 nm.

Upon excitation of $C_{60}(A)_{12}$ at 335 nm, more than 90% of the light is absorbed by the peripheral **A** moieties. The **A**-centered fluorescence intensity of $C_{60}(A)_{12}$ is indeed dramatically quenched when compared with **A** (three orders of magnitude lower, see Table 1) while, at the same time, a broad band above 600 nm is clearly observable. This band was further characterized by recording the emission spectrum with a cut-off filter at 550 nm and compared with that of a model compound $C_{60}(Ph)_{12}$ having the same optical density at the exciting wavelength and recorded under identical conditions (Figure 7). Notably, both

16

samples $C_{60}(A)_{12}$ and $C_{60}(Ph)_{12}$ exhibit quite similar emission profiles and comparable intensity. One the other hand, if the same experiment is done for $C_{60}(A)_{12}$ and $C_{60}(Ph)_{12}$ having the same concentrations, the band above 600 nm is one order of magnitude higher for $C_{60}(A)_{12}$ relative to the reference fullerene. These observations are consistent with the occurrence of a virtually quantitative A - C_{60} singlet energy transfer process via the Förster mechanism since the fluorescence profile of A (350–500 nm) overlaps with the absorption tail of the fullerene hexa-adduct core. This energy transfer mechanism was further supported by recording the excitation spectrum for $C_{60}(A)_{12}$ at λ_{em} = 670 nm, which exactly matches the absorption spectrum of model compound A (Figure 8).
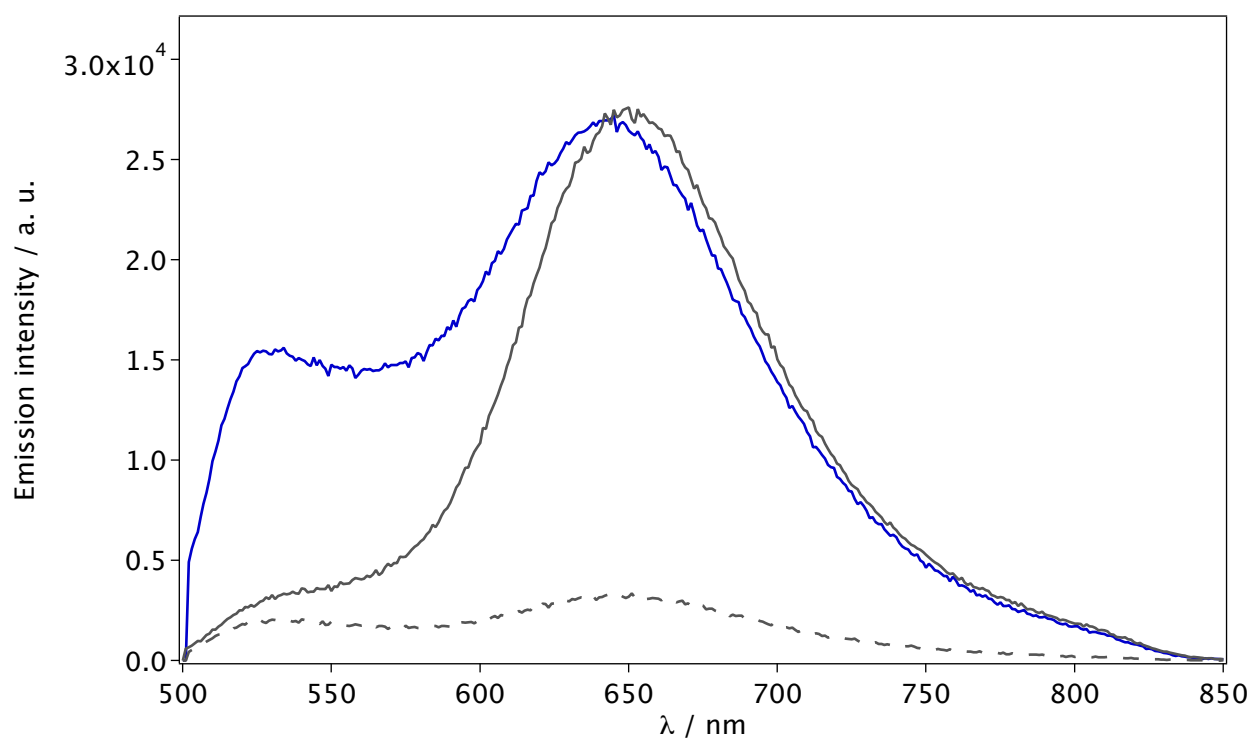
Figure 7. Comparison of emission spectra of $C_{60}(A)_{12}$ (blue) and $C_{60}(Ph)_{12}$ having (i) same optical density at 335 nm (o.d. = 0.15, grey full line) and (ii) same concentration (4.2 10^{-7}, grey dashed line) as $C_{60}(A)_{12}$. Emission spectra were collected upon excitation at 335 nm and with a cut-off filter at 550 nm in front of the emission monochromator.
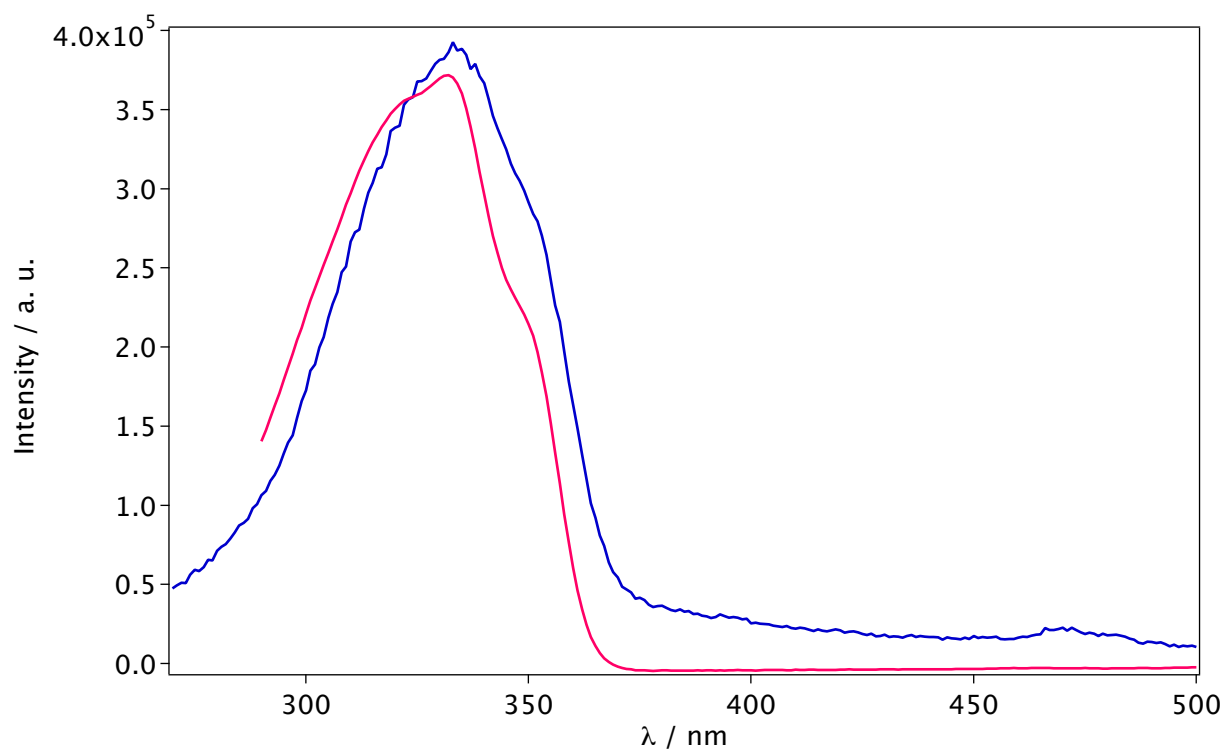
Figure 8. Absorption spectrum of **A** (pink) and excitation spectrum $C_{60}(A)_{12}$ (blue); λ_{em} = 670 nm with a cut-off filter at 515 nm, CH_2Cl_2.

1.2.3. Conclusion

A T_h-symmetrical fullerene hexakis-adduct with grafted 12 organic conjugated oligomers forming a shell-core ensemble was studied by steady state and time resolved absorption and emission spectroscopy in dichloromethane at room temperature and 77 K. The studies revealed virtually quantitative intramolecular energy transfer upon excitation of the peripheral chromophores. The investigated compound is an efficient light harvesting system capable of channelling the light energy from the shell to the core by singlet-singlet energy transfer. This first system paves the way towards more elaborated compact photoactive devices in which a potent electron donating group is additionally incorporated to the system, thus allowing an electron transfer upon the initial energy transduction event to the C_{60} core.

1.3. Photophysical and Electrochemical Properties of a Novel Antenna-Fullerene-Donor Architecture for Light Energy Conversion

1.3.1. Introduction

The conversion of solar power into useful chemical energy is mastered by Nature through photosynthesis and inspires researchers in the quest for efficient light energy harnessing.[5] In photosynthesis, the antenna module harvests sunlight and funnels the energy by singlet-singlet energy transfer to the reaction center where charge separation occurs thanks to a cascade of electron transfer events.[27] In literature, elaborated fullerene-based multicomponent systems, which mimic photosynthesis, are predominantly focused on the separation of the radical ion pair by multistep electron transfer obtained by attaching additional donor or acceptor moiety, and thus reducing the energy of the charge-separated state.[8b,8f,11d,28] On the other hand, systems that investigate cooperative energy and electron transfer are somehow less abundant.[29]

Herein, the electrochemical and photophysical properties of fullerene-based molecular architectures are reported where, in addition to an electron donor (ferrocene or phenothiazine) and an acceptor (fullerene), an oligophenyleneethynylene module (Figure 9) was employed as a light-harvesting antenna (**Ant**). Differently from many reported triads or tetrads, which usually aim to improve the stability of the radical ion pair by the attachment of a redox active unit, we use a moiety that does not undergo redox processes but transfers the excitation energy to the C_{60} unit generating the lowest singlet state ($^1C_{60}*$),[10a] from which the CS state can be formed. The light harvesting antenna unit is expected to enhance the conversion of light into the charge-separated state by populating the photoexcited state of the fullerene through an energy transfer mechanism, from which, in turn, a charge-separated state is generated in the presence of an efficient electron donor group via the fullerene singlet excited

state.
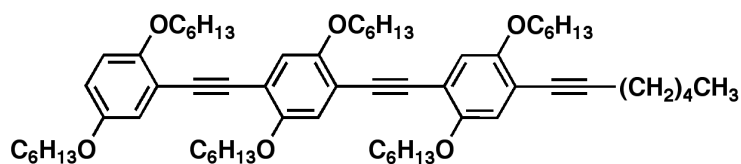
Figure 9. Oligophenyleneethynylene, the reference compound of the antenna module.

In one of the investigated arrays, a ferrocene derivative was incorporated as an electron donor (ethynylferrocenyl, **FC**, Figure 10a). Ferrocene, which is known as a good electron donor with low oxidation potential and high stability under the redox conditions,[30] was readily incorporated into the light harvesting systems to prolong the lifetime of the CS state. Ferrocene was combined with C_{60}-based arrays containing porphyrins[28a,8b,31], oligophenylenevinylenes[32], subphtalocyanines,[28c] boron dipyrrins[33] and others.[11d,34] In these systems, light is harvested by the chromophore, which forms a charge separated state, subsequently undergoing charge shift to form the ferrocene cation. Effective systems were obtained if ferrocene was used as a terminal unit in a multicomponent array that forms a sequence of a redox gradient.[28c,31a] However, in some cases no improvement[31b] or even quenching of the CS state by fullerene triplet was observed.[32]

In the second system, a phenothiazine derivative plays the role of an electron donating moiety (4-ethynylphenyl phenothiazine, **PTZ**, Figure 10b). Although not as often exploited as ferrocene, electron-donating properties of phenothiazine were also explored in fullerene-based light harvesting devices. Efficient light induced charge transfer was reported in systems combining fullerene and phenothiazine[35] as well as together with an additional light harvesting porphyrin unit.[8f]

The third system is a tetrad (Figure 10c), which combines both electron donors, antenna and fullerene and enables studies of the competition between phenothiazine and ferrocene in the electron transfer event.
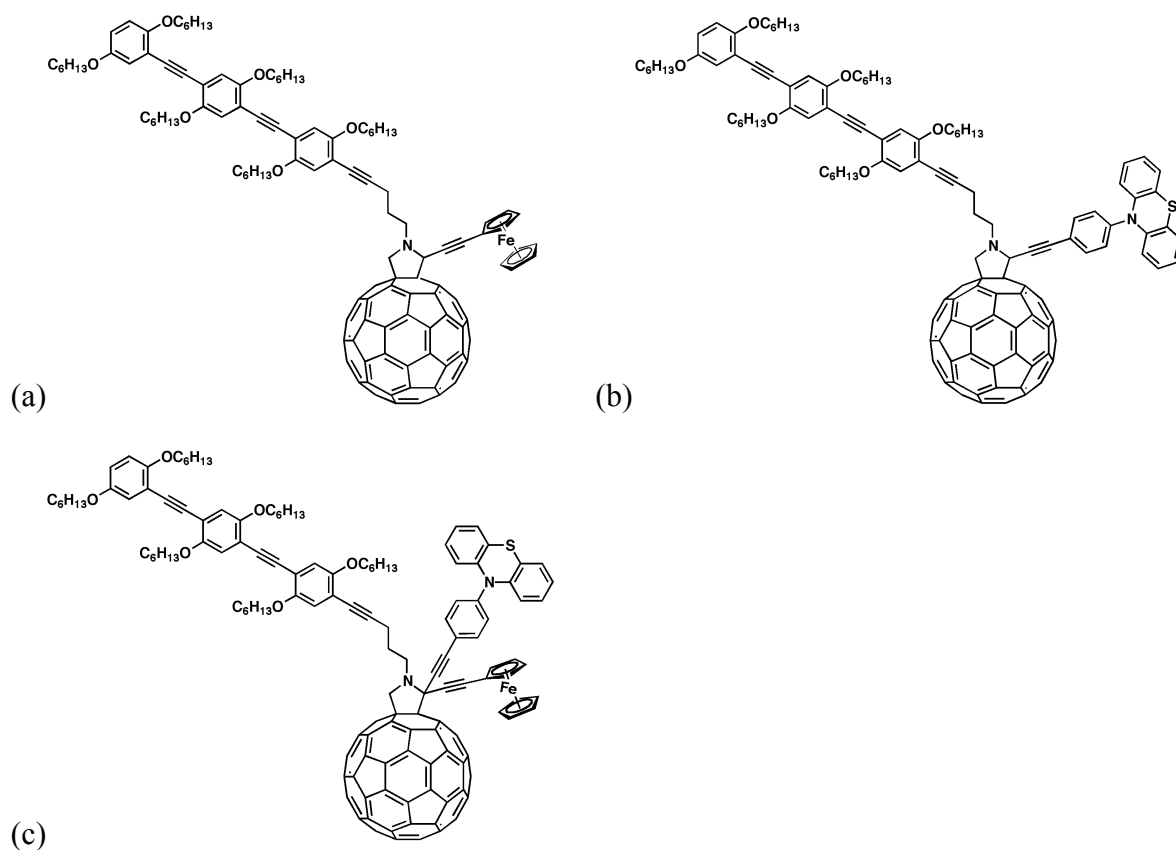
Figure 10. Multimodular arrays containing a light-harvesting antenna moiety and, as electron donor(s), (a) ferrocene, **Ant-F-FC**, (b) phenothiazine, **Ant-F-PTZ**, (c) phenothiazine and ferrocene, **Ant-F-PTZ-FC**.

In summary, a new design of fullerene-based molecular architectures was proposed, where, in addition to electron donor and acceptor, a light harvesting antenna was employed. The antenna unit is expected to enhance the conversion of light into the charge-separated state by populating the photoexcited state of the fullerene through an energy transfer mechanism, from which, in turn, charge-separated state is generated in the presence of an efficient electron donor moiety – be it ferrocene or phenothiazine. Properties of the target molecules **Ant-F-PTZ**, **Ant-F-FC**, **Ant-F-PTZ-FC** together with a collection of reference systems were

studied by cyclic voltammetry, steady-state absorption and luminescence, and will be discussed in the following sections.

1.3.2. Electrochemical properties

Within the electrochemical stability window (dichloromethane solution, 0.1 mmol L^{-1} tetrabutylammonium perchlorate, TBAP), the voltammogram of **F** shows three reversible reduction waves whose standard potentials do not change significantly for the dyad and of the triads (Table 2, Figure 11, 12, 13). **Ant** and **PTZ**, **FC** do not have reduction processes in the cathodic window. **FC** and **PTZ** show a quasi-reversible oxidation wave at 0.16 and 0.31 V vs. Fc/Fc$^+$, respectively, confirming good electron-donating character. The redox potentials measured for these reference compounds remain approximately the same in the triads (Figure 12 ,13). **Ant** shows an irreversible oxidation wave due to the overlapping of two processes, where the half wave potential related to the first shoulder is 0.70 V vs. Fc/Fc$^+$. Importantly, **Ant** has a relatively high oxidation potential when compared to **PTZ** and **FC** that prevents a redox role of the light harvesting moiety in the multicomponent arrays.
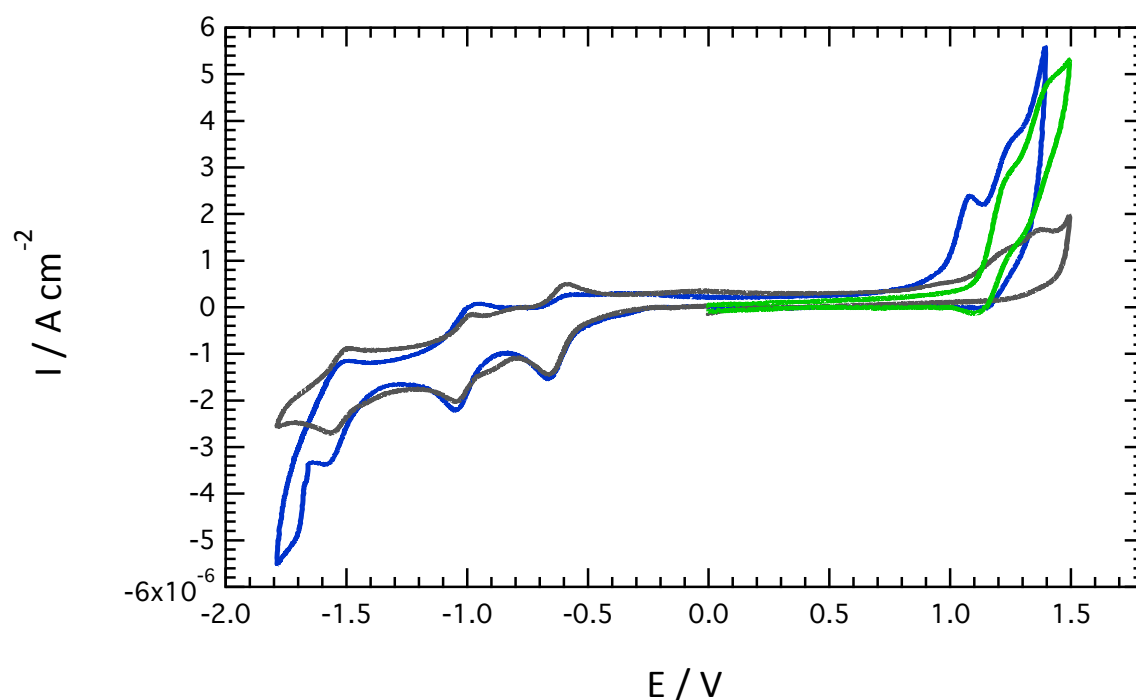
Figure 11. Cyclic voltammograms of **Ant** (green), **F** (grey), **Ant-F** (blue) in CH_2Cl_2 vs. SCE containing 0.1 mmol L^{-1} TBAP at 0.1 V ms^{-1} sweep rate.
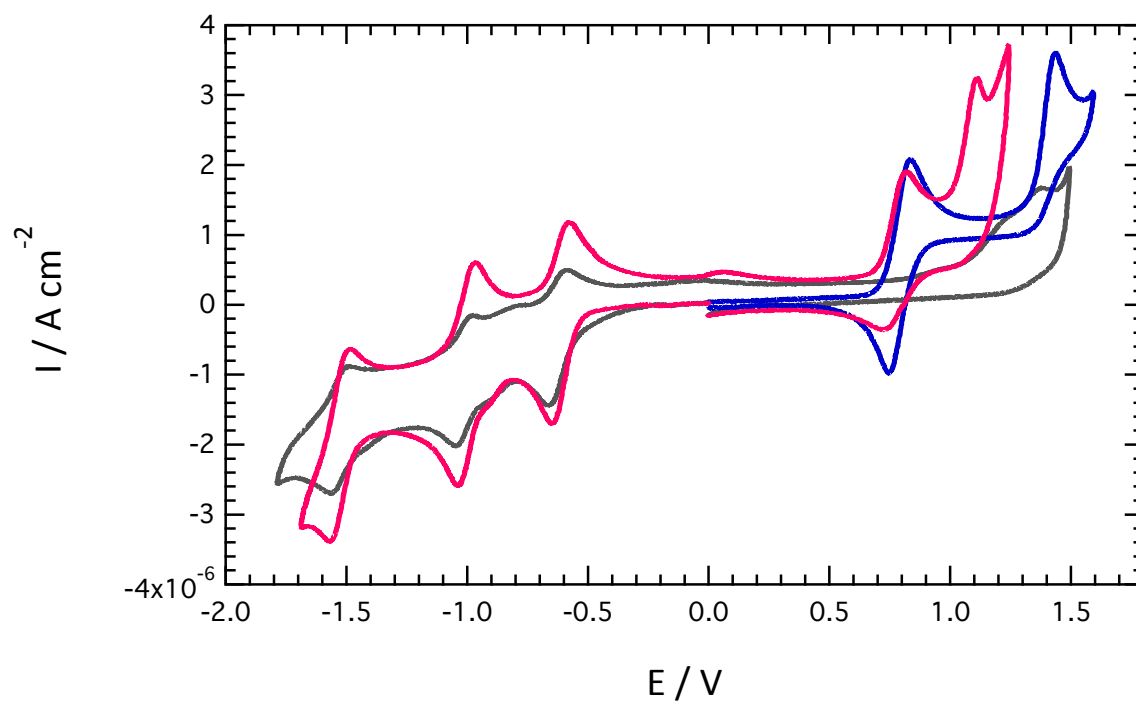
Figure 12. Cyclic voltammograms of **Ant-F-PTZ** (pink), **F** (grey), **Ant-F** (blue) in CH_2Cl_2 vs. SCE containing 0.1 mmol L^{-1} TBAP at 0.1 V ms^{-1} sweep rate.
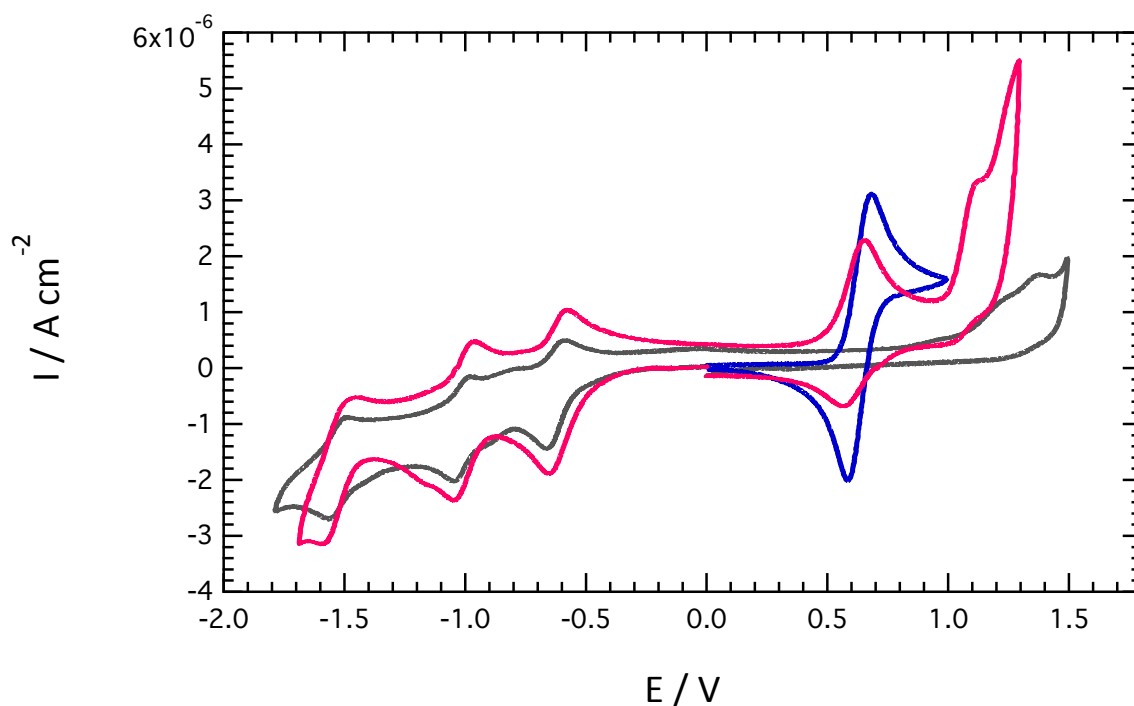
Figure 13. Cyclic voltammograms of **Ant-F-FC** (pink), **F** (grey), **Ant-F** (blue) in CH_2Cl_2 vs. SCE containing 0.1 mmol L^{-1} TBAP at 0.1 V ms^{-1} sweep rate.

Table 2. Standard redox potentials (V vs. Fc/Fc$^+$.) of FC, PTZ, Ant, F, Ant-F, Ant-F-FC, and Ant-F-PTZ in BN 0.1 mol·L^{-1} TBAP (in parenthesis half wave potentials).

	$E°_{ox2}$/V	$E°_{ox1}$/V	$E°_{red1}$/V	$E°_{red2}$/V	$E°_{red3}$/V
FC		0.16			
PTZ		0.31			
Ant	0.70				
F			-0.62	-1.02	-1.53
Ant-F	(0.59)		-0.61	-1.00	-1.52
Ant-F-FC	(0.59)	0.14	-0.61	-1.00	-1.52
Ant-F-PTZ	(0.59)	0.31	-0.62	-1.00	-1.53

1.3.3. Steady State Absorption and Luminescence Studies

Steady State Absorption

In Figure 14 are gathered the absorption spectra of the investigated compounds in toluene solution. The absorption spectrum of the reference electron donor modules **PTZ** and **FC** in toluene are characterized by moderate to low extinction coefficients, which is in line with literature data.[36] **PTZ** absorbs in the spectral window 290 – 400 nm with a maximum at 325 nm ($\varepsilon = 6 \times 10^3$ M^{-1}cm^{-1}). **FC** exhibits a weak band at $\lambda_{max} = 450$ nm ($\varepsilon = 10^2$ M^{-1}cm^{-1}), which is typical for ferrocene and arises from spin allowed *d-d* electronic transition.[36a] The reference antenna unit, **Ant**, absorbs in the range 290 – 440 nm with the maximum placed at 385 nm ($\varepsilon = 4.6 \times 10^4$ M^{-1}cm^{-1}, toluene) in line with similar oligophenyleneethynylenes.[10] The differences in the maxima and intensity of the absorption spectra of **Ant** and the electron donors allow very selective excitation of the antenna moiety in the multicomponent systems. The reference *N*-methylfulleropyrrolidine unit (**F**) exhibits broad absorption across the UV and visible regions, which is also in accordance with literature.[5d] Absorption spectra of the dyad **Ant-F**, triads **Ant-F-PTZ** and **Ant-F-FC**, as well as tetrad **Ant-F-PTZ-FC** are essentially the sum the absorption of their building blocks, indicating negligible intramolecular interactions in the ground state.
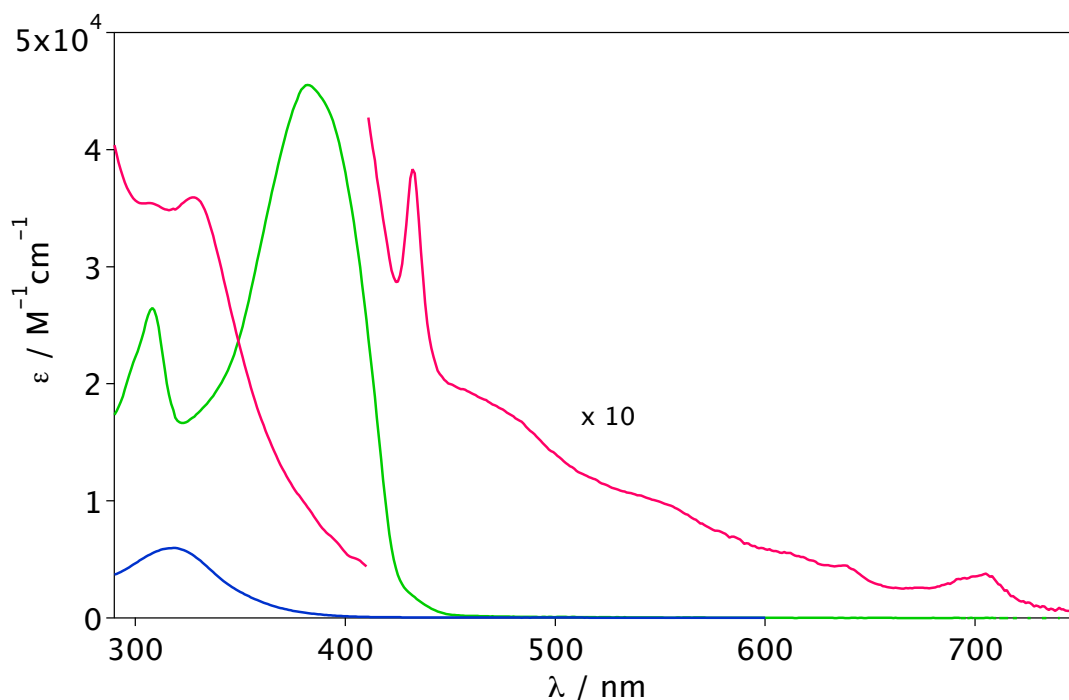
Figure 14. Absorption spectra of **Ant** (green), **PTZ** (blue) and **F** (pink) in toluene solution

Luminescence properties of the building blocks: Ant, PTZ, F and FC

The reference phenothiazine donor, **PTZ**, is weakly luminescent (λ_{max} = 450 nm, Φ_{em} = 0.01 in PhMe; Figure 15). As expected, **FC** does not exhibit detectable luminescence because of nonradiative deactivation from its low-lying triplet level.[37] **Ant** exhibits a strong fluorescence at λ_{max} = 420 nm (Φ_{em} = 0.64 in PhMe and 0.42 in PhCN, τ = 1.1 ns in both solvents), which is attributable to the deactivation from the lowest-lying singlet excited state (Figure 15). Similar quantum efficiencies and spectral features were earlier reported for other oligophenyleneethynylene or oligophenylenevinylene compounds.[10] **F** exhibits a weak fluorescence band typical of fulleropyrrolidines with λ_{max} = 710 nm, τ = 1.4 ns, $\Phi_{em} \approx$ 0.0001 in toluene and benzonitrile; Figure 16 in next section). These values are in accordance with literature data.[5d]
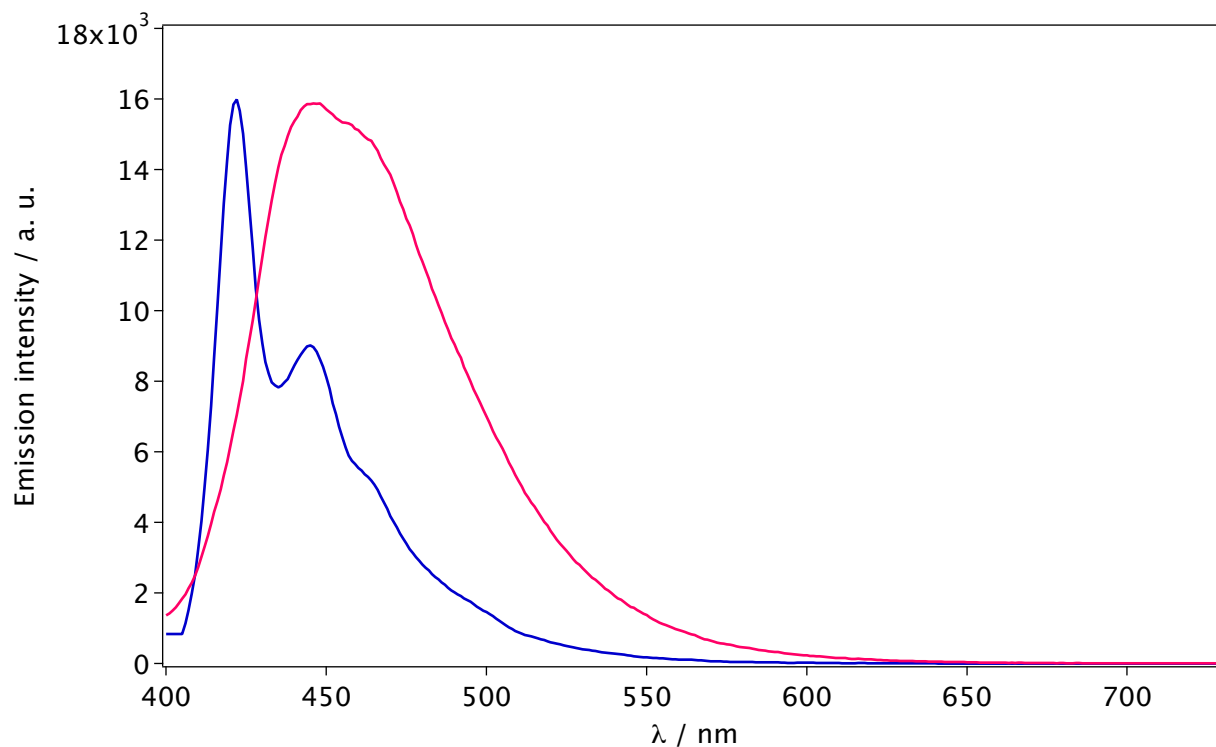
Figure 15. Normalized emission spectra of **Ant** (blue) and **PTZ** (pink) in toluene excited at 385 nm and 330 nm, respectively.

Ant-F dyad

The strong luminescence of the antenna is dramatically quenched by the fullerene moiety. In toluene, its fluorescence quantum yield at $\lambda_{exc} = 385$ nm drops from 0.64 to 0.0014, whereas, in benzonitrile, from 0.42 to 0.0049 (Table 3) indicating strong excited state intramolecular interactions between **F** and **Ant** and high quenching rate (10^{10}-10^{11} s^{-1}). The quenched lifetime of the antenna moiety is below the resolution of our instrumentation (30 ps). However, by applying deconvolution of the decay signals of the antenna moiety, lifetimes of about 25 ps are determined in both toluene and benzonitrile, which are attributable to the quenched fluorescence of the antenna moiety of **Ant-F**.

Upon excitation of the antenna, efficient sensitization of the *N*-methylfulleropyrrolidine moiety was observed for the dyad in both PhMe and PhCN (Figure 16). In toluene, when excited at $\lambda_{exc} = 385$ nm, the luminescence quantum yield of the fullerene core (emission in the range 660-850 nm) in **Ant-F** is exactly the same as in case of

27

the reference **F** compound, 4 x 10^{-4}. Accordingly, lifetime values (λ_{exc} = 371 nm) were measured to be 1.4 ns. These values are in accord with literature reports for *N*-methylfulleropyrrolidine[38] and result from the radiative decay of the singlet excited state.[5d] The same values of Φ_{em} and τ were obtained by the direct excitation of the fullerene sphere (λ_{exc} = 500 nm) confirming efficient energy transfer (Table 3).

In benzonitrile, upon excitation of the antenna, the luminescence of the fulleropyrrolidine moiety in **Ant-F** is somehow lower (Φ_{em} = 2.5 x 10^{-4}) compared to the reference **F** in the same solvent or to **Ant-F** in toluene (4 x 10^{-4}), which could indicate the presence of another quenching pathway (Figure 16). Nevertheless, upon selective excitation of the fulleropyrrolidine module in **Ant-F** (λ_{exc} = 500 nm), only slightly reduced quantum yield was obtained (3.5 x 10^{-4}) (Figure 16). Moreover, the singlet lifetime value of the fulleropyrrolidine moiety was determined to be 1.4 ns, regardless the excitation wavelength. These results suggest that the lower Φ_{em} of the **F** moiety in **Ant-F** in PhCN upon excitation of the antenna is not due to the formation of a charge separate state but, rather, to less efficient energy transfer in polar solvent (see Table 3 and discussion below), which was also observed in previously published work.[39]
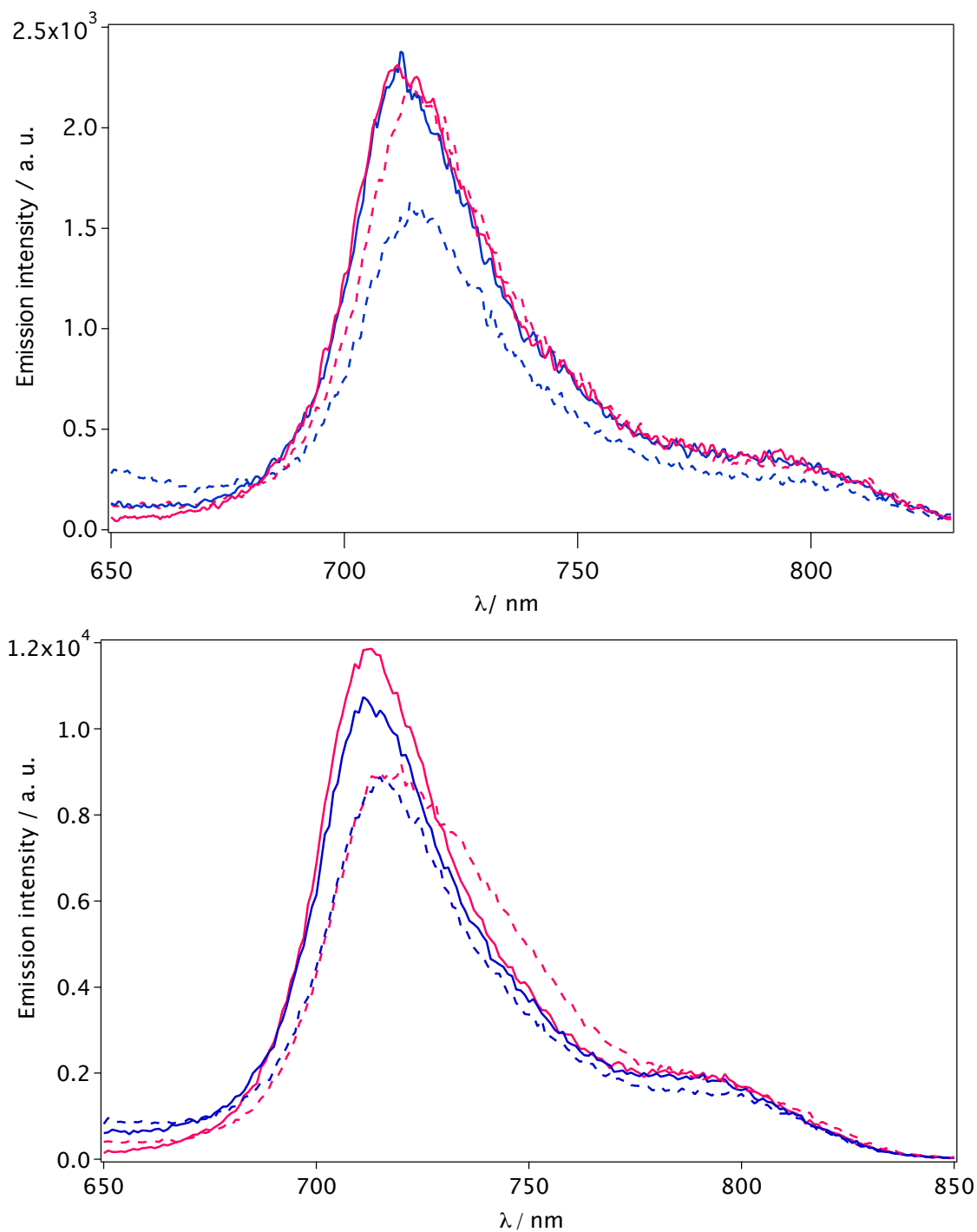
Figure 16. Fullerene-centered fluorescence of **Ant-F** (blue) compared to **F** (pink) in toluene (full line) and benzonitrile (dashed line) upon excitation of: (top) the antenna unit, $\lambda_{exc} = 385$ nm, (bottom) fullerene unit, $\lambda_{exc} = 500$ nm.

Since sensitization of the fulleropyrrolidine $^1C_{60}^*$ state is expected to be followed by

intersystem crossing to $^3C_{60}*$, emission of the sensitized singlet oxygen was investigated in the NIR region (Figure 17). It was found that the production of the $^3C_{60}*$ was practically identical for **Ant-F** in both solvents and equal to the reference fulleropyrrolidine moiety. This confirms an efficient sensitization of the fullerene excited states.
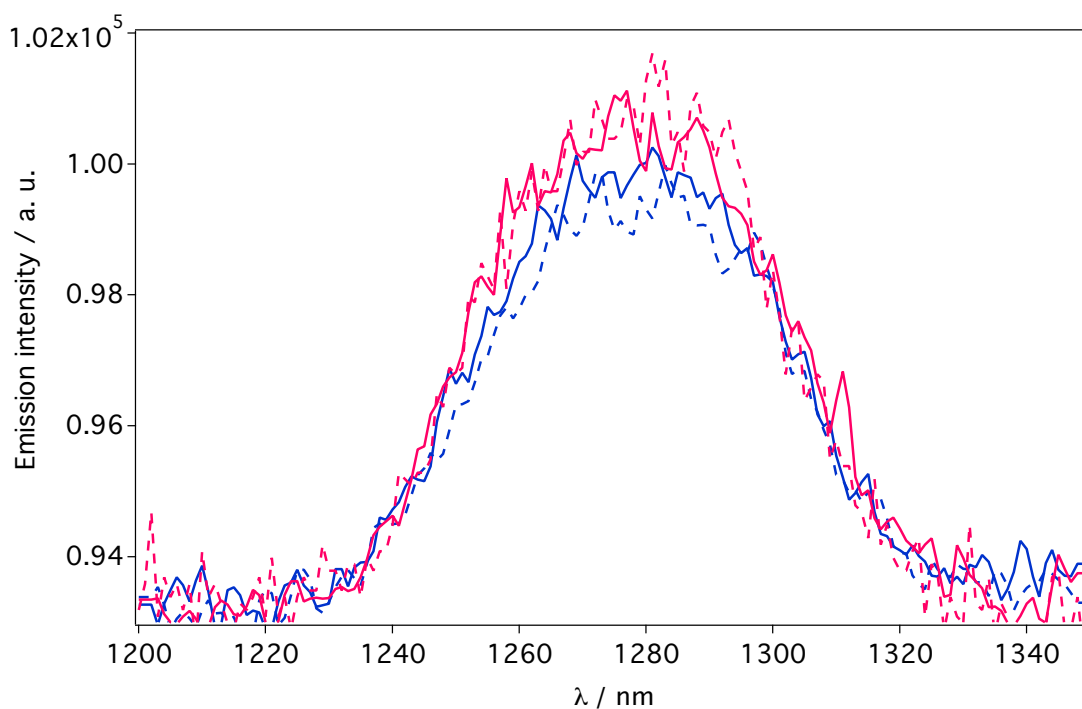
Figure 17. Sensitized $^1O_2*$ luminescence of **F** (pink) and **Ant-F** (blue) in toluene (full line) and benzonitrile (dashed line) solution, $\lambda_{ex} = 500$ nm.

In summary, the **F-Ant** dyad is an effective light harvesting module, suitable for the construction of triads that exhibit stepwise energy and electron transfer processes.

Table 3. Fluorescence lifetimes (τ) and quantum yield values (Φ).

Compound	Emission of **Ant** unit			Emission of **F** unit					
	$\Phi_{ex385nm}$		τ_{ex373}	$\Phi_{ex500nm}$		τ_{ex373} / ns		τ_{ex465} / ns	
	PhMe	PhCN	PhMe	PhMe	PhCN	PhMe	PhCN	PhMe	PhCN
Ant	0.64	0.43	1.1 ns	-	-	-	-	-	-
F	-	-		$4\,10^{-4}$	$4\,10^{-4}$	1.4	1.3	1.4	1.4
Ant-F	$1.4\,10^{-3}$	$4.9\,10^{-3}$	< 30 ps	$4\,10^{-4}$	$3\,10^{-4}$	1.4	1.4	1.4	1.4
Ant-F-PTZ	$2.0\,10^{-3}$	$4.2\,10^{-3}$	< 30 ps	$3\,10^{-4}$	-	1.5	0.7	1.6	0.8
Ant-F-FC	$1.7\,10^{-3}$	$4.9\,10^{-3}$	< 30 ps	-	-	-	-	-	-
Ant-F-PTZ-FC	$1.8\,10^{-3}$	$4.8\,10^{-3}$	< 30 ps	-	-	1.5	-	-	-

Ant-F-PTZ

Photophysical properties of the **Ant-F-PTZ** triad in toluene are similar to those of the **Ant-F** dyad. Quenching of luminescence and lifetime of the antenna moiety is observed and slightly less efficient sensitization of the fullerene emission as well as generation of the C_{60} triplet excited state (Figure 18, Table 3).

Dramatically different photophysical behaviour is observed in more polar benzonitrile, a solvent known for stabilizing charge-separated states.[5d] Upon excitation of the antenna, emission from the singlet excited state of the fulleropyrrolidine moiety is around 75% lower than in case of **F** and **Ant-F**. Likewise, direct excitation of the fulleropyrrolidine moiety results with ca. 60% decreased emission (Figure 18). This trend is confirmed by measurements of the lifetime of the fulleropyrrolidine singlet excited state, which is reduced to 0.7 ns for both direct (λ_{exc} = 465 nm) and sensitized excitation (λ_{exc} = 371 nm).
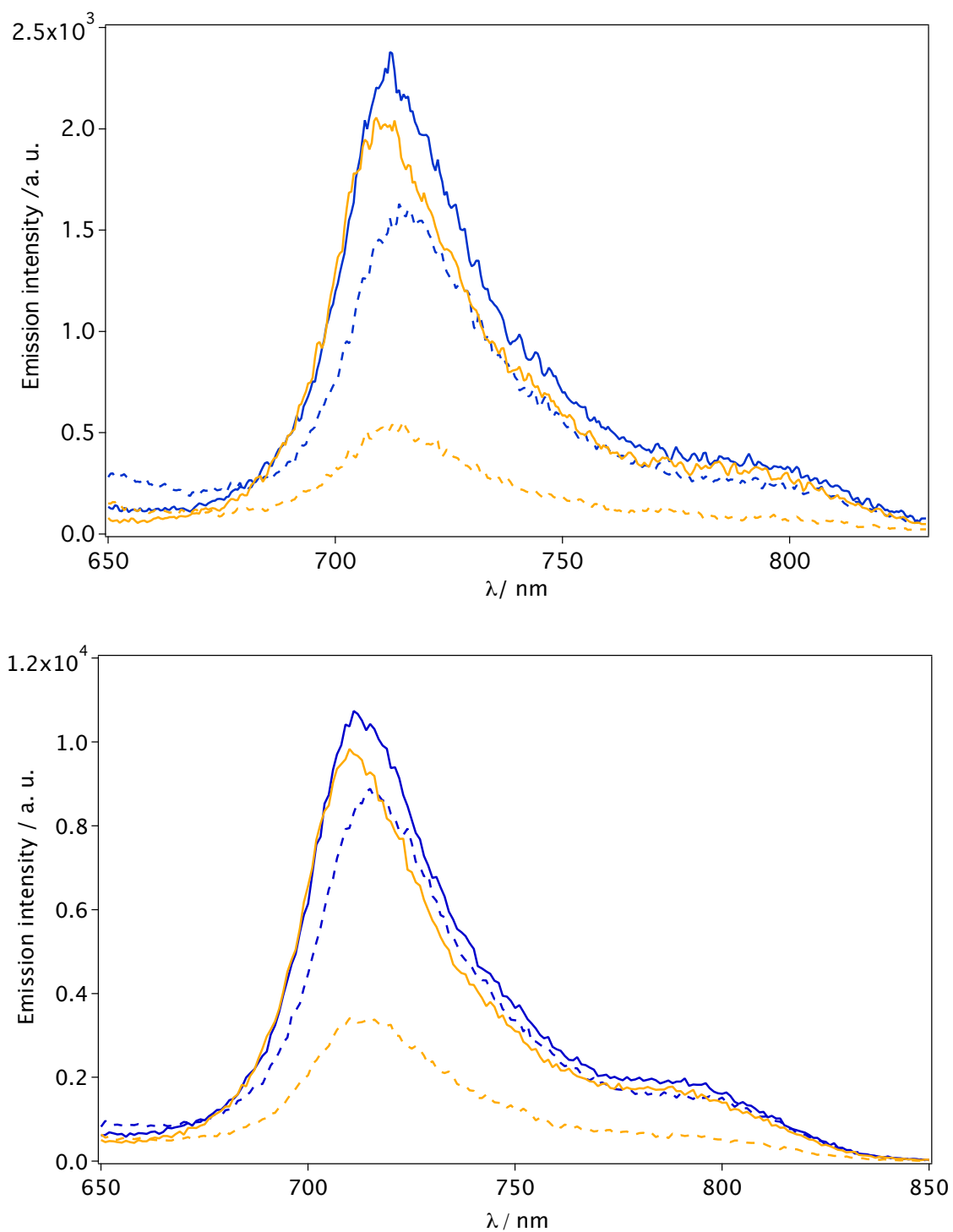
Figure 18. Fullerene-centered fluorescence of **Ant-F-PTZ** (yellow) and **Ant-F** (blue) in toluene (full line) and benzonitrile (dashed line) upon excitation of the antenna, $\lambda_{exc} = 385$ nm (top), and of the fullerene unit, $\lambda_{exc} = 500$ nm (bottom).

Only traces of fullerene triplet excited state are found, as obtained through sensitized NIR luminescence of $^1O_2^*$ (Figure 19). This indicates the presence of an additional quenching process in benzonitrile – *i.e.* formation of charge-separated state – as was previously observed for C_{60}-based systems incorporating phenothiazines as a donating moiety.[8f,35]
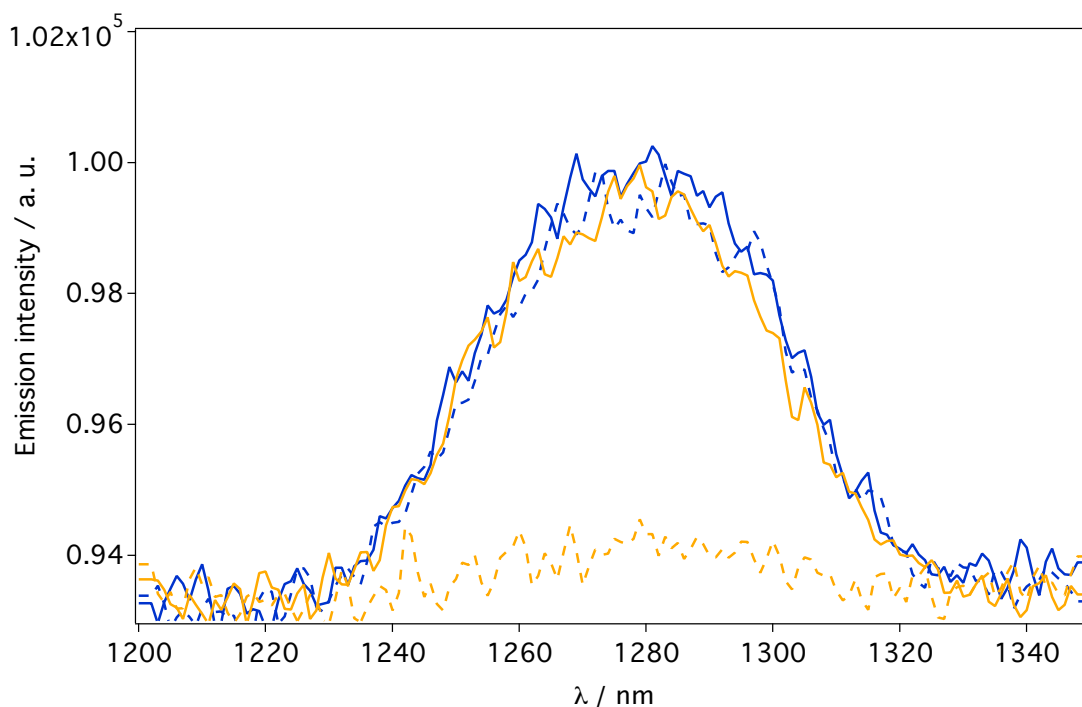
Figure 19. Sensitized $^1O_2^*$ luminescence of **Ant-F-PTZ** (yellow) and **Ant-F** (blue) in toluene (full line) and benzonitrile (dashed line) solution, $\lambda_{exc} = 500$ nm.

Ant-F-FC

When **FC** is used as donor, photophysical properties differ from those obtained with **Ant-F-Ant** and do not depend on the solvent polarity (Figure 20). Complete quenching of the fullerene singlet emission is observed regardless of the excitation wavelength, and no traces of $^3C_{60}^*$ were found in the sensitized singlet oxygen luminescence (Figure 21). This may be attributed to the photoinduced charge transfer[8f,11,28d] or energy transfer to the **FC** triplet state.[32]
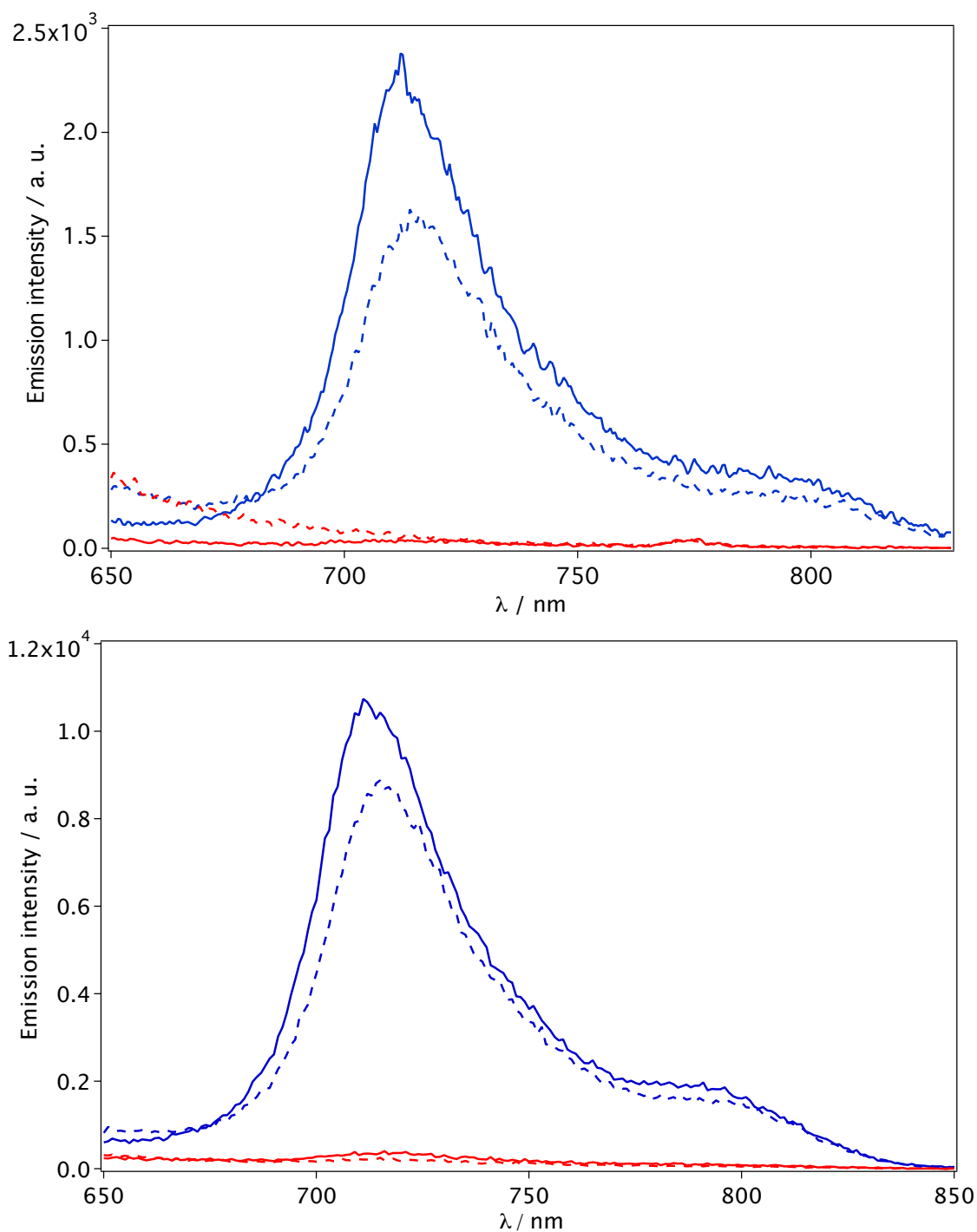
Figure 20. Fullerene-centered fluorescence of **Ant-F-FC** (red) and **Ant-F** (blue) in toluene (full line) and benzonitrile (dashed line) upon excitation of the antenna, λ_{exc} = 385 nm (top), and of the fullerene unit, λ_{exc} = 500 nm (bottom).

Figure 21. Sensitized $^1O_2^*$ luminescence of **Ant-F-FC** (red) and **Ant-F** (blue) in toluene (full line) and benzonitrile (dashed line) solution, λ_{ex} = 500 nm.

Ant-F-PTZ-FC

When both donors are attached to the antenna a competitive electron transfer may take place forming the **PTZ+-F-** or **FC+-F-** charge separated states. The possibility of quenching through the low-lying excited electronic level of the ferrocene unit cannot be precluded when the FC moiety is present.
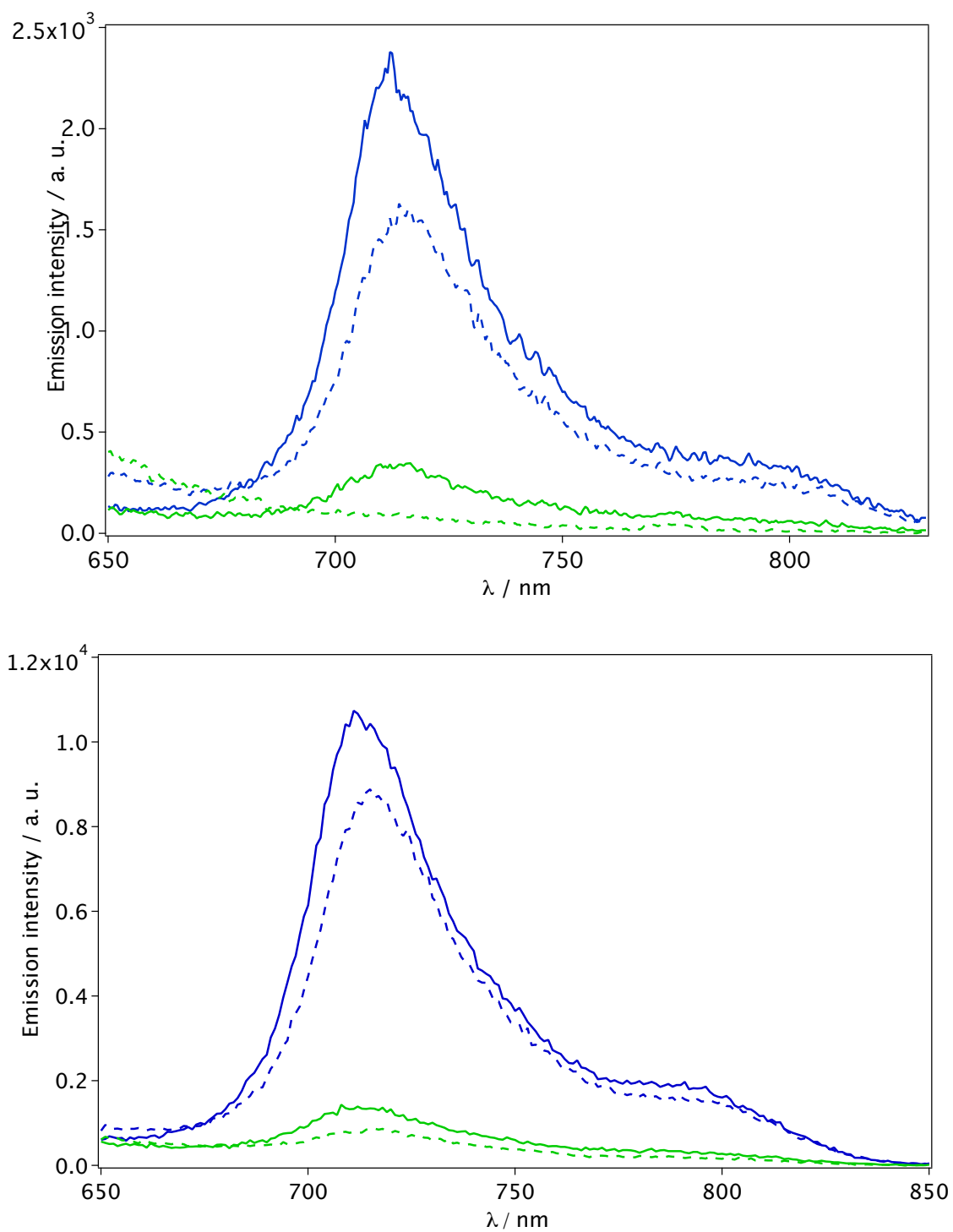
Figure 22. Fullerene-centered fluorescence of **Ant-F-PTZ-FC** (green) and **Ant-F** (blue) in toluene (full line) and benzonitrile (dashed line) upon excitation of the antenna, λ_{exc} = 385 nm (top), and of the fullerene units, λ_{exc} = 500 nm (bottom).
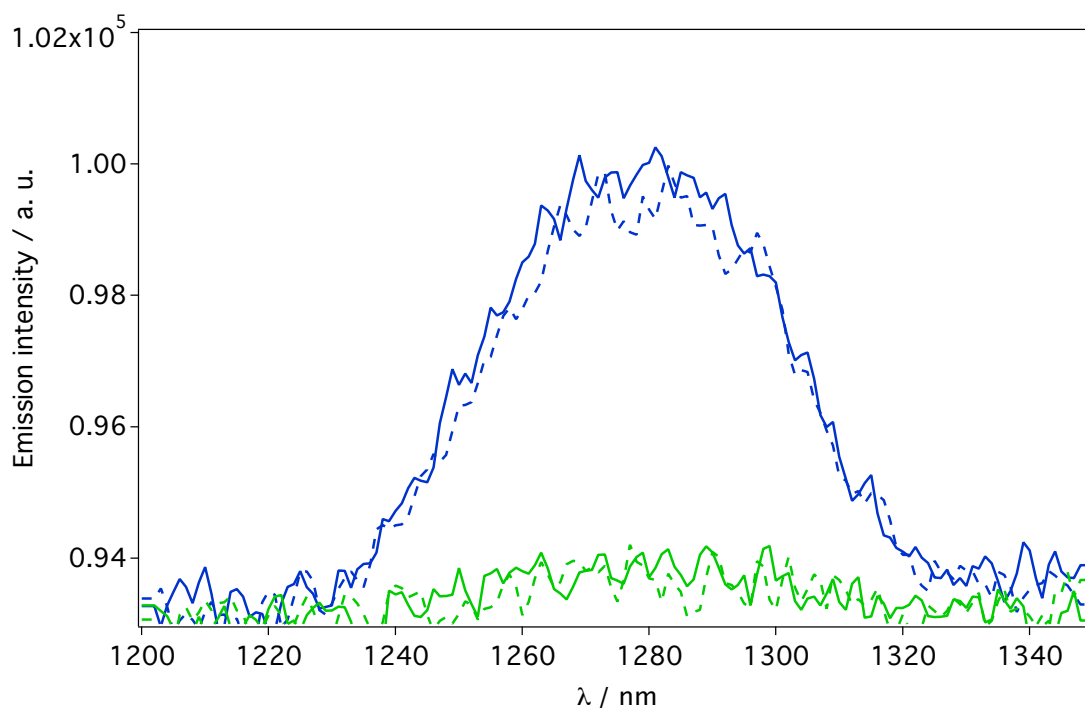
Figure 23. Sensitized $^1O_2^*$ luminescence of **Ant-F-PTZ-FC** (green) and **Ant-F** (blue) in toluene (full line) and benzonitrile (dashed line) solution, $\lambda_{exc} = 500$ nm.

1.3.4. Conclusion

In conclusion, the photophysical and electrochemical properties of novel fullerene-based multicomponent arrays incorporating an efficient light-harvesting oligophenyleneethynylene moiety along with ferrocene and/or phenothiazine derivatives as electron donors were investigated. Because of the relatively high oxidation potential, the light-capturing module does not compete in the electron transfer processes with the incorporatd electron donors characterized by the significantly better electron-donating properties. Efficient sensitization of the fullerene unit by the antenna moiety confirms the presence of photoinduced singlet-singlet energy transfer and populating the singlet excited state of the fullerene core, from which, in turn, the photoinduced charge separated state can be formed (Scheme 2). For the triad **Ant-F-PTZ** photoinduced electron transfer was observed in

polar solvent (benzonitrile), whereas for **Ant-F-FC** and **Ant-F-PTZ-FC** photophysical studies could not exclude quenching of the charge-separated state by low lying triplet state of ferrocene component. Studies with transient absorption spectroscopy are underway to obtain a deeper insight on this issue.
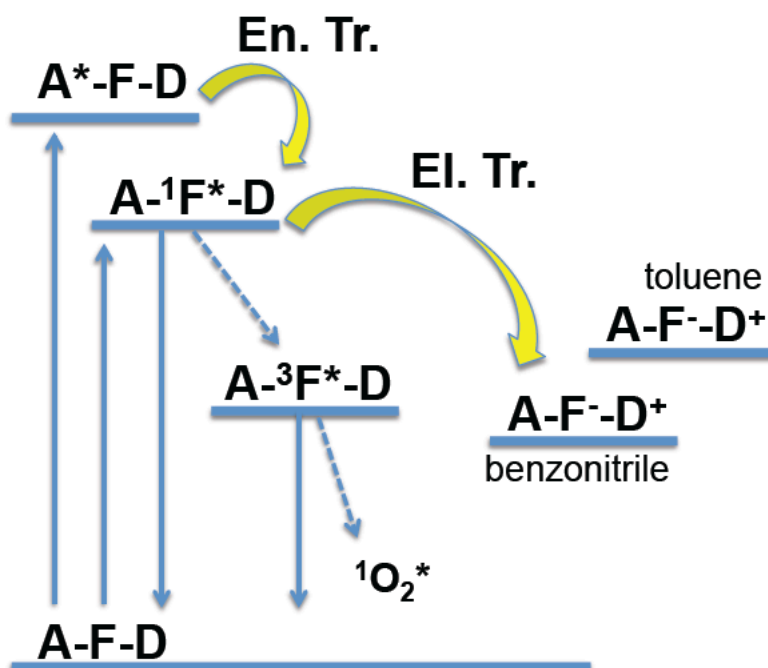
Scheme 2. Diagram schematically showing the energy levels and the envisaged photoinduced processes in the molecular array containing antenna, fullerene and electron donor (A-F-D).

References

(1)   Kroto, H. W.; Heath, J. R.; O'Brien, S. C.; Curl, R. F.; Smalley, R. E. *Nature* **1985**, *318*, 162-163.

(2)   Kratschmer, W.; Lamb, L. D.; Fostiropoulos, K.; Huffman, D. R. *Nature* **1990**, *347*, 354-358.

(3)   (a) Hirsh A. The chemistry of the fullerenes, Stuttgart: Thieme, **1994** (b) Nierengarten, J. F.; Eckert, J. F.; Felder, D.; Nicoud, J. F.; Armaroli, N.; Marconi, G.; Vicinelli, V.; Boudon, C.; Gisselbrecht, J. P.; Gross, M. *Carbon* **2000**, *38*, 1587–1598. (c) Thilgen, C.; Diederich, F. *Chem. Rev.* **2006**, *106*, 5049–5135. (d) Montellano López, A.; Mateo-Alonso, A.; Prato, M. *J. Mater. Chem.* **2011**, *21*, 1305-1318.

(4)   (a) Armaroli, N.; Balzani, V. Energy for a Sustainable World. From the Oil to a Sun Powered Future, Wiley-VCH, Weinheim, Germany, **2011**. (b) Guldi, D. M.; Sgobba, V. *Chem. Commun.* **2011**, *47*, 606-610.

(5)   (a) Guldi, D. M.; Prato, M. *Acc. Chem. Res.* **2000**, *33*, 695–703. (b) Günes, S.; Neugebauer, H.; Sariciftci, N. S. *Chem. Rev.* **2007**, *107*, 1324–1338. (c) Guldi, D. M.; Illescas, B. M.; Atienza, C. M.; Wielopolski, M.; Martín, N. *Chem. Soc. Rev.* **2009**, *38*, 1587. (d) Accorsi, G.; Armaroli, N. *J. Phys. Chem. C* **2010**, *114*, 1385–1403.

(6)   (a) Diederich, F.; Gómez-López, M. *Chem. Soc. Rev.* **1999**, *28*, 263–277. (b) Armaroli, N. Photochem. Photobiol. Sci. **2003**, *2*, 73-87. (c) Bottari, G.; la Torre, de, G.; Guldi, D. M.; Torres, T. *Chem. Rev.* **2010**, *110*, 6768–6816.

(7)   (a) Armaroli, N.; Diederich, F.; Dietrich Buchecker, C. O.; Flamigni, L.; Marconi, G.; Nierengarten, J. F.; Sauvage, J. P. *Chem. Eur. J.* **1998**, *4*, 406–416. (b) Watanabe, N.; Kihara, N.; Furusho, Y.; Takata, T.; Araki, Y.; Ito, O. *Angew. Chem.* **2003**, *115*, 705–707. (c) Sandanayaka, A. S. D.; Sasabe, H.; Araki, Y.; Furusho, Y.; Ito, O.; Takata, T. *J. Phys. Chem. A* **2004**, *108*, 5145–5155. (d)   Li, K.; Bracher, P. J.; Guldi, D. M.; Herranz, M. A.; Echegoyen, L.; Schuster, D. I. *J. Am. Chem. Soc.* **2004**, *126*, 9156–9157.

(8)   (a) Guldi, D. M. *Chem. Soc. Rev.* **2001**, *31*, 22–36. (b) Mateo-Alonso, A.; Ehli, C.; Guldi, D. M.; Prato, M. *J. Am. Chem. Soc.* **2008**, *130*, 14938–14939. (c) Aloukos, P.; Iliopoulos, K.;

Couris, S.; Guldi, D. M.; Sooambar, C.; Mateo-Alonso, A.; Nagaswaran, P. G.; Bonifazi, D.; Prato, M. *J. Mater. Chem.* **2011**, *21*, 2524. (d) Iehl, J.; Vartanian, M.; Holler, M.; Nierengarten, J.-F.; Delavaux-Nicot, B.; Strub, J.-M.; Van Dorsselaer, A.; Wu, Y.; Mohanraj, J.; Yoosaf, K.; Armaroli, N. *J. Mater. Chem.* **2011**, *21*, 1562. (e) Iehl, J.; Vartanian, M.; Holler, M.; Nierengarten, J.-F.; Delavaux-Nicot, B.; Strub, J.-M.; Van Dorsselaer, A.; Wu, Y.; Mohanraj, J.; Yoosaf, K.; Armaroli, N. *J. Mater. Chem.* **2011**, *21*, 1562. (f) Poddutoori, P. K.; Sandanayaka, A. S. D.; Zarrabi, N.; Hasobe, T.; Ito, O.; van der Est, A. *J. Phys. Chem. A* **2011**, *115*, 709–717.

(9)   (a) Ohkita, H.; Cook, S.; Astuti, Y.; Duffy, W.; Heeney, M.; Tierney, S.; McCulloch, I.; Bradley, D. D. C.; Durrant, J. R. *Chem. Commun.* **2006**, 3939. (b) Narutaki, M.; Takimiya, K.; Otsubo, T.; Harima, Y.; Zhang, H.; Araki, Y.; Ito, O. *J. Org. Chem.* **2006**, *71*, 1761–1768. (c) Nakamura, T.; Kanato, H.; Araki, Y.; Ito, O.; Takimiya, K.; Otsubo, T.; Aso, Y. *J. Phys. Chem. A* **2006**, *110*, 3471–3479. (d) MacLeod, J. M.; Ivasenko, O.; Fu, C.; Taerum, T.; Rosei, F.; Perepichka, D. F. *J. Am. Chem. Soc.* **2009**, *131*, 16844–16850.

(10)   Clifford, J. N.; Gu, T.; Nierengarten, J.-F. O.; Armaroli, N. *Photochem. Photobiol. Sci.* **2006**, *5*, 1165-1172.

(11)   (a) Matsuo, Y.; Maruyama, M.; Gayathri, S. S.; Uchida, T.; Guldi, D. M.; Kishida, H.; Nakamura, A.; Nakamura, E. *J. Am. Chem. Soc.* **2009**, *131*, 12643–12649. (b) Wijesinghe, C. A.; El-Khouly, M. E.; Blakemore, J. D.; Zandler, M. E.; Fukuzumi, S.; D'Souza, F. *Chem. Commun.* **2010**, *46*, 3301. (c) Matsuo, Y.; Ichiki, T.; Radhakrishnan, S. G.; Guldi, D. M.; Nakamura, E. *J. Am. Chem. Soc.* **2010**, *132*, 6342–6348. (d) Supur, M.; El-Khouly, M. E.; Seok, J. H.; Kay, K.-Y.; Fukuzumi, S. *J. Phys. Chem. A* **2011**, *115*, 14430–14437.

(12)   Sibley, S. P.; Argentine, S. M.; Francis A. H. *Chem. Phys. Lett.* **1992**, *188*, 187-193

(13)   Hung, R. R.; Grabowski, J. J. *J. Phys. Chem.* **1991**, *95*, 6073-6075.

(14)   (a) Kim, D. H.; Lee, M. Y.; Suh, Y. D.; Kim, S. K. *J. Am. Chem. Soc.* **1992**, *114*, 4429–4430. (b) Sun, Y. P.; Wang, P.; Hamilton, N. B. *J. Am. Chem. Soc.* **1993**, *115*, 6378– 6381. (c) Catalan, J.; Elguero, J. *J. Am. Chem. Soc.* **1993**, *115*, 9249–9252.

(15)   (a) Van den Heuvel, D. J.; Chan, I. Y.; Groenen, E. J. J.; Schmidt, J.; Meijer, G. *Chem. Phys. Lett.* **1994**, *231*, 111–118. (b) Hung, W. C.; Ho, C. D.; Liu, C. P.; Lee, Y. P. *J. Phys. Chem.* **1996**, *100*, 3927–3932.

(16)   Palewska, K.; Sworakowski, J.; Chojnacki, H.; Meister, E. C.; Wild, U. P. *J. Phys. Chem.* **1993**, *97*, 12167–12172.

(17)   Arbogast, J. W.; Darmanyan, A. P.; Foote, C. S.; Rubin, Y.; Diederich, F. N.; Alvarez, M. M.; Anz, S. J.; Whetten, R. L. *J. Phys. Chem.* **1991**, *95*, 11–12.

(18)   Dimitrijevic, N. M.; Kamat, P. V. *J. Phys. Chem.* **1992**, *96*, 4811–4814.

(19)   Armaroli, N.; Accorsi, G.; Felder, D.; Nierengarten, J. F. *Chem. Eur. J.* **2002**, *8*, 2314–2323.

(20)   Echegoyen, L.; Echegoyen, L. E. *Acc. Chem. Res.* **1998**, *31*, 593-601.

(21)   (a) Camps, X.; Dietel, E.; Hirsch, A.; Pyo, S.; Echegoyen, L.; Hackbarth, S.; Roder, B. *Chemistry* **1999**, *5*, 2362 (b) Guldi, D. M.; Luo, C.; Prato, M.; Troisi, A.; Zerbetto, F.; Scheloske, M.; Dietel, E.; Bauer, W.; Hirsch, A. *J. Am. Chem. Soc.* **2001**, *123*, 9166-9167. (d) Rancan, F.; Helmreich,M.; Molich, A.; Ermilov, E. A.; Jux, N.; Roder, B.; Hirsch, A.; Bohm, F. *Bioconjug. Chem.* **2007**, *18*, 1078-1086. (e) Regehly, M.; Ermilov, E. A.; Helmreich, M.; Hirsch, A.; Jux, N.; Roder, B. *J. Phys. Chem. B* **2007**, *111*, 998-1006. (f) Spanig, F.; Kovacs, C.; Hauke, F. Ohkubo, K.; Fukuzumi, S.; Guldi, D. M.; Hirsch, A. *J. Am. Chem. Soc.* **2009**, *131*, 8180-8195.

(22)   (a) Hirsch, A.; Lamparth, I.; Grosser, T.; Karfunkel, H. R. *J. Am. Chem. Soc.* **1994**, *116*, 9385-9386. (b) Hirsch, A.; Vostrowsky, O. *Eur. J. Org. Chem.* **2001**, 829-848. (c) Li, H.; Kitaygorodskiy, A.; Carino, R. A.; Sun, Y.-P.; *Org. Lett.* **2005**, *7*, 859-861. (d) Li, H.; Haque, S. A.; Kitaygorodskiy, A.; Meziani, M. J.; Torres-Castillo, M.; Sun, Y.-P. *Org. Lett.* **2006**, *8*, 5641-5643.

(23)   Iehl, J.; Pereira de Freitas, R.; Delavaux-Nicot, B.; Nierengarten, J.-F. *Chem. Commun.* **2008**, 2450-2452.

(24)   Iehl, J.; Holler, M.; Nierengarten, J.-F.; Yoosaf, K.; Malicka, J. M.; Armaroli, N.; Delavaux-Nicot, B. *Aust. J. Chem.* **2011**, *64*, 153-159.

(25)   Cardullo, F.; Seiler, P.; Isaacs, L.; Nierengarten, J.-F.; Haldimann, R. F.; Diederich, F.; Mordasini-Denti, T.; Thiel, W.; Boudon, C.; Gisselbrecht, J.-P.; Gross, M. *Helv. Chim. Acta* **1997**, *80*, 343-371.

(26)   Eckert, J.-F.; Nicoud, J.-F.; Nierengarten, J.-F.; Liu, S.-G.; Echegoyen, L.; Barigelletti, F.; Armaroli, N.; Ouali, L.; Krasnikov, V.; Hadziioannou, G. *J. Am. Chem. Soc.* **2000**, *122*, 7467-7479.

(27)   a) Deisenhofer, J.; Epp, O.; Miki, K.; Huber, R.; Michel, H. *J. Mol. Biol.* **1984**, *180*, 385. b) The Photosynthetic Reaction Center (Eds.: J. Deisenhofer, J. R. Norris), Academic Press, San Diego, **1993**; c) Kirmaier, C.; Holton, D. in The Photosynthetic Reaction Center, Vol II (Eds. : J. Deisenhofer, J. R. Norris), Academic Press, San Diego, **1993**, pp. 49 – 70 ; d) R. E. Blankenship, Molecular Mechanisms of Photosynthesis, Blackwell Sciences, Oxford, **2002**; e) Handbook of Photosynthesis, 2nd ed. (Ed.: M. Pessarakli), CRC, Boca Raton, **2005**; f) Photosynthetic Light Harvesting (Eds.: R. Cogdell, C. Mullineaux), Sprigner, Dordrecht, **2008**.

(28)   (a) Imahori, H.; Tamaki, K.; Araki, Y.; Sekiguchi, Y.; Ito, O.; Sakata, Y.; Fukuzumi, S. *J. Am. Chem. Soc.* **2002**, *124*, 5165–5174. (b) Oswald, F.; Islam, D. M. S.; Araki, Y.; Troiani, V.; la Cruz, de, P.; Moreno, A.; Ito, O.; Langa, F. *Chem. Eur. J.* **2007**, *13*, 3924–3933. (c) González-Rodríguez, D.; Carbonell, E.; Rojas, G. de M.; Castellanos, C. A.; Guldi, D. M.; Torres, T. *J. Am. Chem. Soc.* **2010**, *132*, 16488–16500. (d) Lee, S.-H.; Larsen, A. G.; Ohkubo, K.; Cai, Z.-L.; Reimers, J. R.; Fukuzumi, S.; Crossley M. J. *Chem. Sci.* **2012**, *3*, 257-269.

(29)   Imahori, H.; Sekiguchi, Y.; Kashiwagi, Y.; Sato, T.; Araki, Y.; Ito, O.; Yamada, H.; Fukuzumi, S. *Chem. Eur. J.* **2004**, *10*, 3184–3196.

(30)   Bao, D.; Millare, B.; Xia, W.; Steyer, B. G.; Gerasimenko, A. A.; Ferreira, A.; Contreras, A.; Vulley, V. I. *J. Phys. Chem. A* **2009**, *113*, 1259– 1267.

(31)   (a) Imahori, H.; Tamaki, K.; Guldi, D. M.; Luo, C.; Fujitsuka, M.; Ito, O.; Sakata, Y.; Fukuzumi, S. *J. Am. Chem. Soc.* **2001**, *123*, 2607–2617. (b) Poddutoori, P. K.; Sandanayaka, A. S. D.; Hasobe, T.; Ito, O.; van der Est, A. *J. Phys. Chem. B* **2010**, *114*, 14348–14357.

(32)   Figueira-Duarte, T. M.; Rio, Y.; Listorti, A.; Delavaux-Nicot, B.; Holler, M.; Marchioni, F.; Ceroni, P.; Armaroli, N.; Nierengarten, J.-F. *New J. Chem.* **2008**, *32*, 54-64.

(33)   Wijesinghe, C. A.; El-Khouly, M. E.; Blakemore, J. D.; Zandler, M. E.; Fukuzumi, S.; D'Souza, F. *Chem. Commun.* **2010**, *46*, 3301-3303.

(34)   (a) Seok, J. H.; Park, S. H.; El-Khouly, M. E.; Araki, Y.; Ito, O.; Kay, K.-Y. *Journal of Organometallic Chemistry* **2009**, *694*, 1818–1825. (b) Megiatto, J. D., Jr.; Li, K.; Schuster, D. I.; Palkar, A.; Herranz, M. A.; Echegoyen, L.; Abwandner, S.; de Miguel, G.; Guldi, D. M. *J. Phys. Chem. B* **2010**, *114*, 14408–14419.

(35)   (a) Thomas, K. G.; Biju, V.; Kamat, P. V.; George, M. V.; Guldi, D. M. *ChemPhysChem* **2003**, *4*, 1299–1307. (b) Sasaki, Y.; Araki, Y.; Ito, O.; Alam, M. M. *Photochem. Photobiol. Sci.* **2007**, *6*, 560-565. (c) Kawauchi, H.; Suzuki, S.; Kozaki, M.; Okada, K.; Islam, D. M. S.; Araki, Y.; Ito, O.; Yamanaka, K.-I. *J. Phys. Chem. A* **2008**, *112*, 5878–5884.

(36)   (a) Gray, H. B.; Sohn, Y. S.; Hendrickson, D. N. *J. Am. Chem. Soc.* **1971**, *93*, 3603–3612.

(37)   Araki, Y.; Yasumura, Y.; Ito, O. *J. Phys. Chem. B* **2005**, *109*, 9843–9848.

(38)   Peeters, E.; van Hal, P. A.; Knol, J.; Brabec, C. J.; Sariciftci, N. S.; Hummelen, J. C.; Janssen, R. A. J. *J. Phys. Chem. B* **2000**, *104*, 10174–10190.

(39)   Kanato, H.; Takimiya, K.; Otsubo, T.; Aso, Y.; Nakamura, T.; Araki, Y.; Ito, O. *J. Org. Chem.* **2004**, *69*, 7183–7189.

Luminescent Blooming of Dendronic Carbon Nanotubes through Ion-Pairing Interactions with an Eu^{III} Complex

2.1. Introduction

2.1.1. Carbon Nanotubes – a Framework Material for Multicomponent Functional Arrays.

Carbon nanotubes (CNTs) were first described by Iijima in 1991[1] and, since then, these one-dimensional macromolecules have fascinated chemists, physicists and material scientists, opening an entirely new field of research that has expanded spectacularly throughout two decades. The desirable and unique characteristics of CNTs, especially their electrical, mechanical, optical and thermal properties[2] make them potentially useful in many applications, such as composite fibers, optoelectronics devices, hydrogen storage, sensing, and biomedical applications (e.g. drug delivery) and many others.[2,3]

CNTs can be produced by various techniques, and the commonly used approaches are arc discharge,[4] laser ablation[5] and chemical vapor deposition, which includes high-pressure CO conversion (HiPco) and a method based on the Co-Mo catalyst (CoMoCat).[6] CNTs are made of a sp^2 bonded graphene carbon sheet rolled up to form a tube. The direction and angle at which the graphene sheet closes to form a tube is defined by chiral indices (n,m), which ultimately are responsible for differences in chemical and physical properties among the various types of CNTs.[2] Carbon nanotubes are classified as single-walled (SWCNTs), consisting only of one rolled-up graphene sheet, or multi-walled (MWCNTs), formed by several layers. While all MWCNTs have metallic nature, SWCNTs possess metallic or semiconducting character, depending on the chiral indices. As-prepared carbon nanotubes are always aggregated in tight bundles because their smooth, tubular shape and extended π-conjugated structure favor intermolecular van der Waals interactions and π-π stacking. They are also insoluble in most solvents, which makes handling and further processing of CNTs a very challenging task. Several techniques were applied for efficient manipulation of carbon nanotubes. CNTs can be functionalized noncovalently for example by polymers, surfactants

or DNA and this approach has been broadly reviewed.[7] CNTs can be also processed by means of covalent functionalization and also this subject has been reviewed.[8]

In the case of the materials studied herein, MWCNTs were first covalently functionalized with dendronic branches in order to become processable and serve as a stiff scaffold for the functional multicomponent array. For this purpose, we chose multi-walled carbon nanotubes because – unlike their single-walled counterparts – their electronic properties are less affected by the defects in sp^2 hybridization introduced by the formation of covalent bonds.

2.1.2. Lanthanide Complexes – Unique Luminophores in Hybrid Arrays

Luminescent rare earth complexes have attracted a lot of attention in the variety of fields, such as electronics[9] and medical imaging.[10] The importance of lanthanide ions (Ln) in photophysics stems from their extraordinary properties, particularly line-like emission bands and luminescence lifetimes in the millisecond time scale.[11] Luminescence of Ln ions originates from the parity forbidden transitions between the *f* orbitals. This type of transition is responsible for the long luminescence lifetime as well as for the very weak extinction coefficient.[11] To enhance excitation in spite of the weak absorption in the UV-Vis range, lanthanide ions are often coordinated with ligands that play the role of light harvesting antennas.[11] The sensitization process is driven by energy transfer and is schematically depicted in Figure 1.
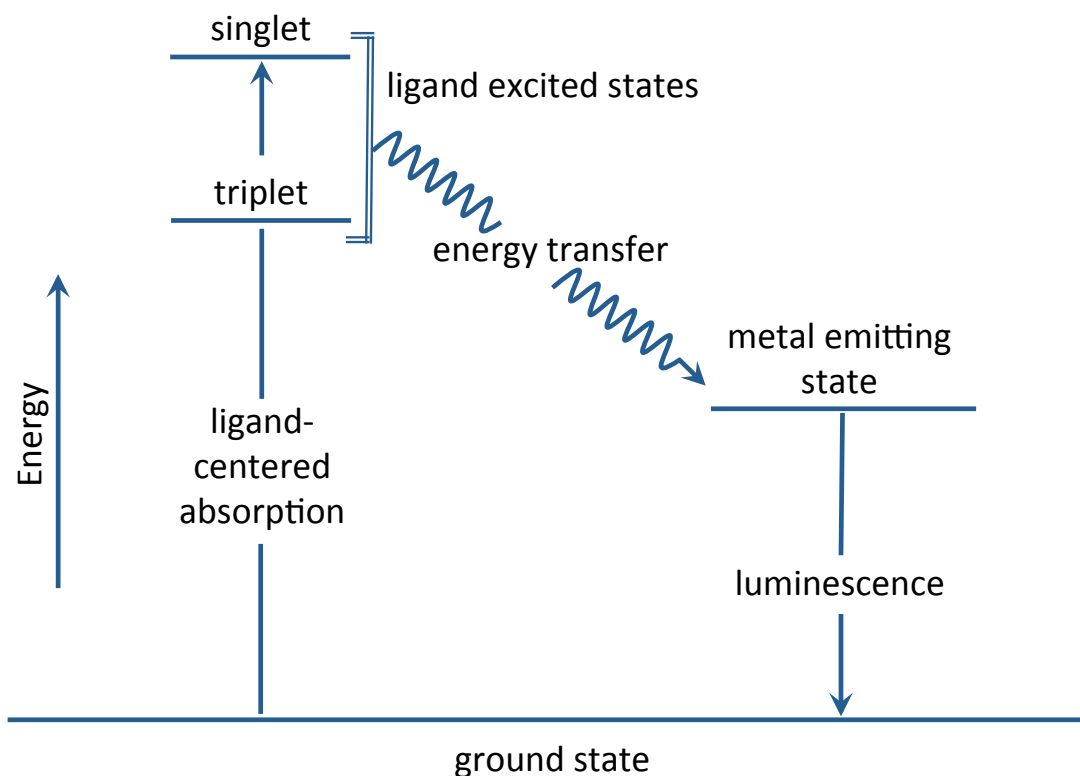
Figure 1. Schematic energy level diagram explaining the antenna effect of the ligand in Ln complexes.

One of the most popular and studied families of lanthanide complexes are β-diketonates,[12] which are rather easy to synthesize and even commercially available. Such complexes are utilized in several applications, including light-emitting devices.[12]

2.1.3. Combining Properties of Rare-Earth Emitters and Carbon Nanotubes – in a Quest for Novel Functional Hybrid Arrays

Although lanthanide diketonates have several desirable characteristics, they also exhibit some poor features, such as low thermal and photochemical stability, tendency to aggregate and undergo parasite interchromophoric interactions.[12,13] To overcome these problems and improve efficiency, various scaffolding materials have been utilized,[12-14]

including carbon nanotubes. The issue of combining carbon nanotubes with luminophores and formation of novel hybrid nanostructures was featured recently.[15] Lanthanide complexes can be attached externally to carbon nanotubes (exohedral functionalization), as it was proposed some years ago.[16] In this work, a Eu(III) complex containing aromatic ligands, tris(dibenzoylmethane) mono(1,10-phenanthroline) europium(III) (Eu(DBM)$_3$Phen), was deposited onto the walls of oxidized SWCNTs by physisorption through hydrophobic interactions (Figure 2). The resulting hybrid material possesses the features of the individual components and display the strong luminescence of europium ions. In successive studies lanthanide β-diketonates were grafted onto CNTs through layer-by-layer deposition,[17] or covalently attached with pendant alkylic chains bearing diketonate or bipyridyl termini, which coordinate lanthanide ions.[18] Kauffman et. al. reported adsorption onto the CNTs sidewalls of dendrimers which chelate lanthanide ions.[19] MWCNTs were also covered with positively charged ionic liquids and the resulting blend was further coated through electrostatic interactions with a negatively-charged europium complex.[20] Composite materials that incorporate lanthanides inside the hollow spaces of CNTs were also proposed (endohedral functionalization). Sitharaman et al. reported the growth of luminescent SWCNTs supported on a europium-based catalysts, providing *in situ* encapsulation of the rare earth ions inside the carbon nanotube.[21] A europium complex was also encapsulated inside oxidized, open tip MWCNTs yielding a luminescent host-guest assembly.[22] In this endohedral approach, the encapsulated lanthanide complex was effectively insulated from the environment by the carbonaceous walls, eliminating parasite chromophoric interactions as well as exfoliation of the complex from the hybrid material. However, the emission output is somehow weak because of the limited loading of the luminophores. Therefore, in order to make endohedral functionalized carbon nanotubes suitable for photonics or sensing, protocols for encapsulation in higher yields have to be developed.
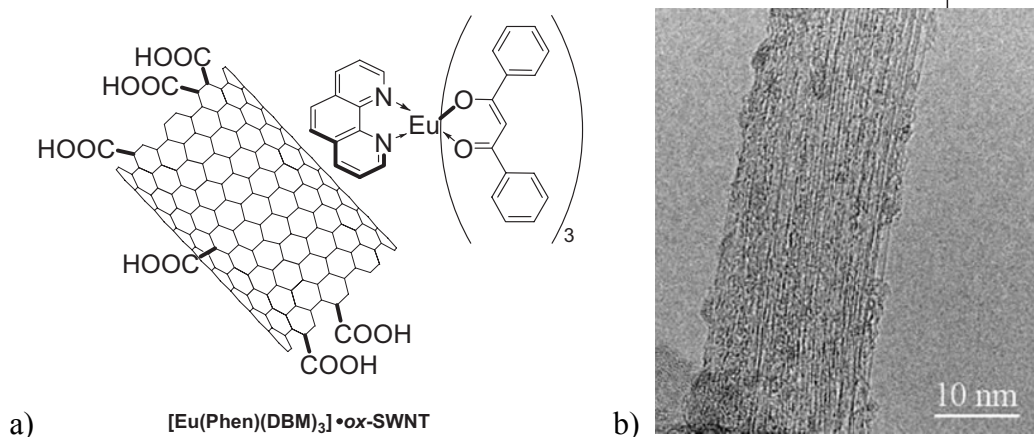
Figure 2. (a) chemical structure and (b) HR-TEM image of the hybrid [Eu(DBM)$_3$(Phen)] · ox-SWCNT complex.[15]

2.2. Synthesis and Characterization of the Hybrid Material

Exohedral decoration of CNTs still remains the most effective and promising approach to generate arrays with high chromophoric loading and advantageous luminescent properties. However, although this appears a conceptually easy procedure, there are still some issues to address, such as exfoliation of the luminophore during the processing (*i.e.* sonication or centrifugation) or lack of control on the loading of the material. Therefore, in order to prepare more robust hybrid arrays with controllable loading, we propose here a novel strategy.

The concept is to make a supramolecular nanoarchitecture composed of multiwalled carbon nanotube scaffolds covalently functionalized with positively charged dendronic branches decorated with an anionic Eu^{III} complex through ion-pairing interactions (Figs. 3 and 4). To prepare this hybrid material, as a first step, pristine MWCNTs with an external diameter of 20-30 nm were derivatized through diazotization reaction[23] using 4-[(*N*-tert-butoxycarbonyl)aminomethyl]aniline and isopentylnitrate; this formed an aryl-diazonium salt, which is able to undergo addition reaction to the carbon nanotube sidewalls.[24] Subsequently, acidic treatment (HCl/dioxane) caused cleavage of the protecting *tert*-butoxycarbonyl groups and exposed amino groups, on which the polyamidoamine (PAMAM) dendron was grown.

The growth of the PAMAM dendron is achieved by repeating cycles of a two-step reaction, each iteration resulting in a new generation of dendronic branches. The first step is a Michael addition between a methyl acrilate and free amino groups and the second is amidation of the peripheral ester units by ethylendiamine. The investigated material was equipped with a second-generation dendron, having four peripheral amino groups per grafted aryl unit. As a final step on the way to the CNT hybrid, amino groups were alkylated by addition of a glycidyl trimethylammonium salt to obtain the desired positively charged **d-MWCNTs·Cl**.

The target luminescent hybrid **d-MWCNTs·[EuL$_4$]** was prepared by dispersing in toluene **d-MWCNTs·Cl** with the excess of **[EuL]$_4$·NEt$_4$** and the ion exchange process (Figure 4). The product was subsequently purified by copious washing (in toluene and chloroform) and filtration, in order to remove the europium complex that was not attached to the carbonaceous scaffold by electrostatic interactions.
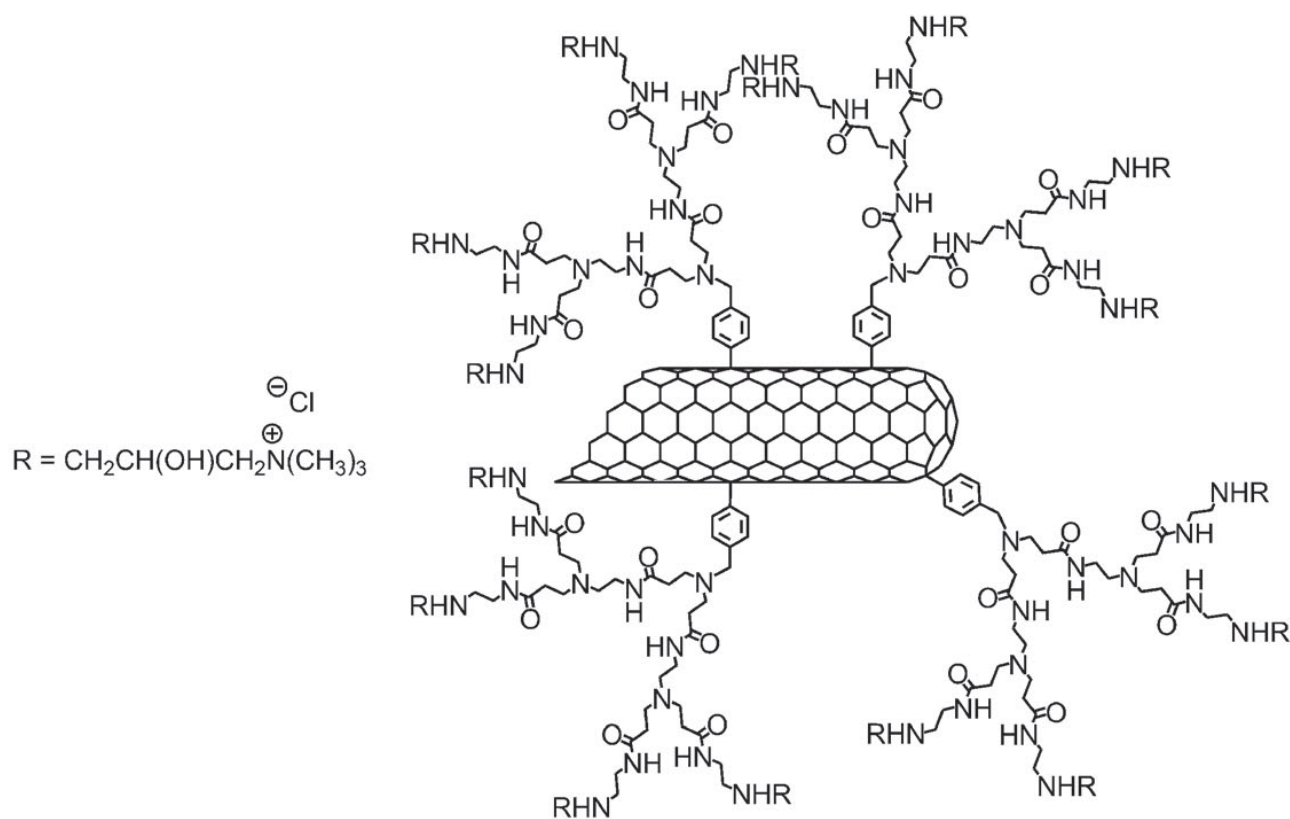
Figure 3. Structure of the carbonaceous scaffold **d-MWCNTs·Cl**, composed of MWCNTs and covalently grafted second-generation PAMAM dendrons with terminal positive charges.
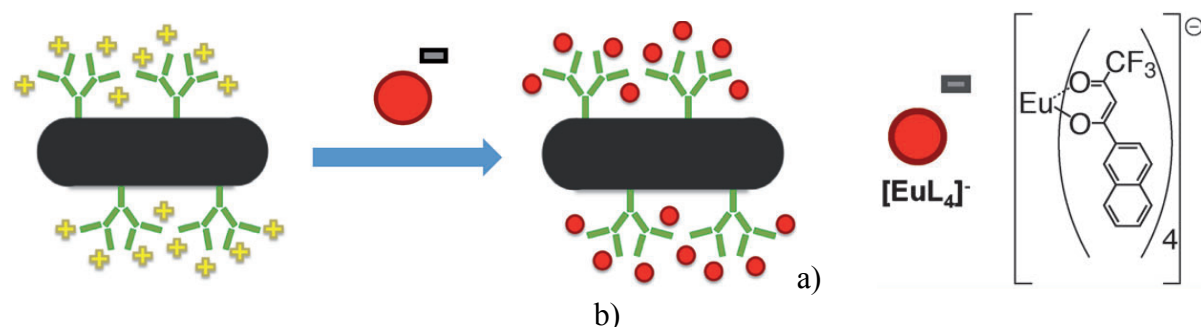
Figure 4. (a) Cartoon representation of **d-MWCNTs·Cl** and of the electrostatic coupling leading to **d-MWCNTs·[EuL₄]**; (b) the structure of the negatively charged europium complex, **[EuL]₄⁻**.

The final array **d-MWCNTs·[EuL₄]** together with the reference compounds MWCNTs, **d-MWCNTs·Cl** and **[EuL]₄·NEt₄** were then investigated by various techniques. The composition of the hybrid material was first studied by thermogravimetric analysis. Notably, in the case of **d-MWCNTs·[EuL₄]** only one pyrolysis event resulting from the presence of the grafted appendages was recorded, indicating that electrostatically functionalized dendrons behave like an individual material, with thermal stability different from its building units, **d-MWCNTs·Cl** and **[EuL]₄· NEt₄**. Moreover, very similar loadings on the carbon nanotubes were found, namely 0.07 and 0.08 mmol g^{-1} for **d-MWCNTs·Cl** and **d-MWCNTs·[EuL₄]**, indicating virtually complete anion exchange.

Elemental composition of the investigated system was determined by XPS analysis. Importantly, the results for the **d-MWCNTs·Cl** scaffold demonstrate high atomic percentage of the elements of the dendronic branches, N and Cl (4.6% and 0.7%, respectively). **d-MWCNTs·[EuL₄]** exhibits Eu and F signals corresponding, respectively, to 0.3% and 6.1%; no signal of Cl was detected confirming effective ion-exchange reaction. TEM pictures of **d-**

MWCNTs·[EuL₄] disclose the presence of the europium complex as little aggregates homogenously dispersed along the MWCNTs (Figure 5).
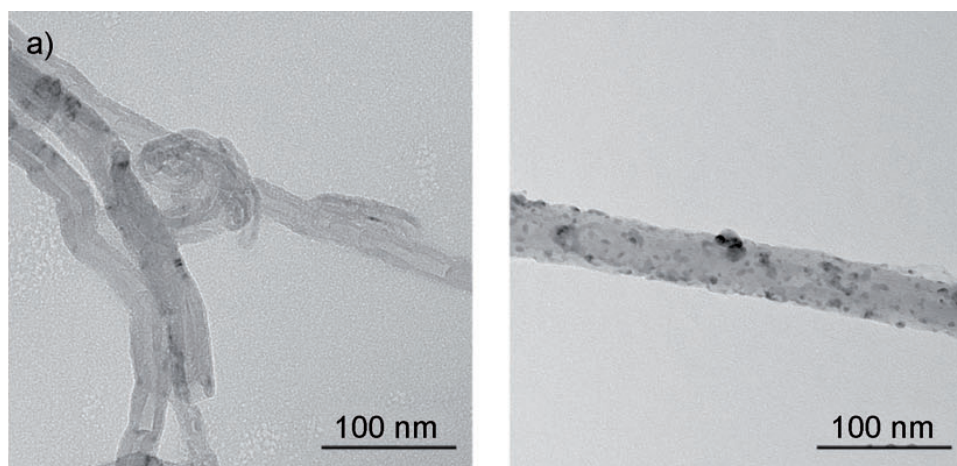
Figure 5. TEM images of (a) the carbonaceous scaffold **d-MWCNTs·Cl**, and (b) the final array **d-MWCNTs·[EuL₄]**.

The effectiveness of the ion pairing interactions in the hybrid array was evaluated by two-dimensional diffusion ordered NMR spectroscopy (DOSY NMR).[25] In a DOSY experiment, the attenuation of the NMR signal is measured during a series of pulsed-field gradient spin-echo experiments. The attenuation of the signal of a given species is an exponential function of its translational self-diffusion coefficient, D, which depends on the molecular weight and hydrodynamic properties.[26] Therefore, DOSY NMR is a sensitive tool for distinguishing if a given molecule is present in the solution as a monomer, or, for example, in a supramolecular assembly.

The D values for **[EuL₄]·NEt₄**, **d-MWCNTs·Cl** and **d-MWCNTs·[EuL₄]** were measured by ^{1}H NMR DOSY in [D₈]toluene (Figure 6). The **d-MWCNTs·Cl** scaffold and the **[EuL₄]⁻** moiety in **[EuL₄]·NEt₄** complex are characterized by very different diffusion coefficients, $0.9 \cdot 10^{-6}$ and $4.1 \cdot 10^{-6}$ cm^{2}s^{-1}. Diffusion of the scaffold slightly changed in **d-MWCNTs·[EuL₄]** ($0.7 \ 10^{-6}$ cm^{2}s^{-1}), while the **[EuL₄]⁻** moiety observed in the hybrid array

showed a dramatic decrease of the D value, dropping to $0.9 \cdot 10^{-6}$ cm^{2}s^{-1}. Moreover, only one decaying component for the **[EuL$_4$]$^-$** -centered ^{1}H NMR signal was recorded, proving efficient and strong ion-pairing interaction between the scaffold and the europium complex.

Further, from the DOSY NMR investigation, the experimental values of hydrodynamic radius of **[EuL$_4$]$^-$** was estimated to be 1.2 nm in unbounded complex and reached significantly higher value (5.8 nm) in the **d-MWCNTs·[EuL$_4$]**. The resulting values are a definitive confirmation of the ion-paired CNTs-based hybrid array.

To rule out the possibility of neutral physisorption of the europium complex onto the sidewalls of CNTs, a sample of unpurified hybrid, **U-d-MWCNTs·[EuL$_4$]**, having an excess of the complex was also studied by means of DOSY NMR. In this case, the attenuation of ^{1}H NMR signal was biexponential, which corresponds to two different D values – 1.5 (90.5%) and $5.3 \cdot 10^{-6}$ cm^{2}s^{-1} (9.5%) and prove that, contrary to the purified sample, in **U-d-MWCNTs·[EuL$_4$]** a significant amount of europium complex is not attached to the scaffold by ion-pairing interactions.
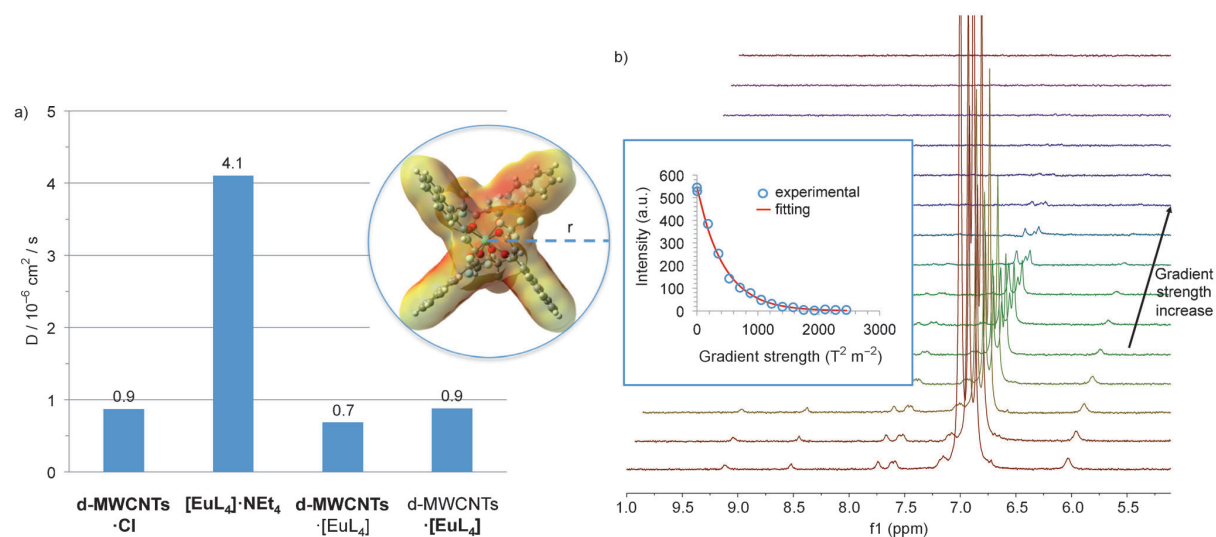
Figure 6. (a) D coefficient values for **d-MWCNTs**, **[EuL$_4$]·NEt$_4$** and **d-MWCNTs·[EuL$_4$]**; in bold, moiety for which the D value is calculated. Inset: modeled structure of **[EuL$_4$]$^-$** and representation of its hydrodynamic radius. (b) DOSY NMR spectra showing the **[EuL$_4$]$^-$** -

centered attenuating signals in **d-MWCNTs·[EuL₄]**. Inset: fitting of the experimental data to calculate *D* coefficient.

Having assessed that the Eu(III) complex is tightly bound to the carbon nanotube scaffold in MWCNTs·[EuL₄], we have investigated the photophysical properties of this hybrid material aiming in particular at testing its luminescence performance; the results are described in the following sections. Detailed procedures for the synthesis as well as characterization of the hybrid material are reported in the published manuscript.[27]

2.3. Photophysical Properties

2.3.1. Studies in the Solid State

d-MWCNTs·[EuL₄] is a novel hybrid with inherent inhomogeneous character originating from the carbon nanotube scaffold and a random disposition of the grafted dendron appendages. In order to draw reliable conclusions about the photophysical properties of our hybrid material, four samples were studied always studied in parallel, i.e. **d-MWCNTs·[EuL₄]-1**, **d-MWCNTs·[EuL₄]-2**, **d-MWCNTs·[EuL₄]-3** and **d-MWCNTs·[EuL₄]-4**. All the samples were prepared according to the same preparation and purification procedure, and prove the reproducibility of the preparative strategy. The studies on the hybrid material were made always in parallel with investigations on the reference compounds, the carbonaceous scaffold **d-MWCNTs·Cl**, and the europium complex **[EuL₄]·NEt₄** (Figure 7).
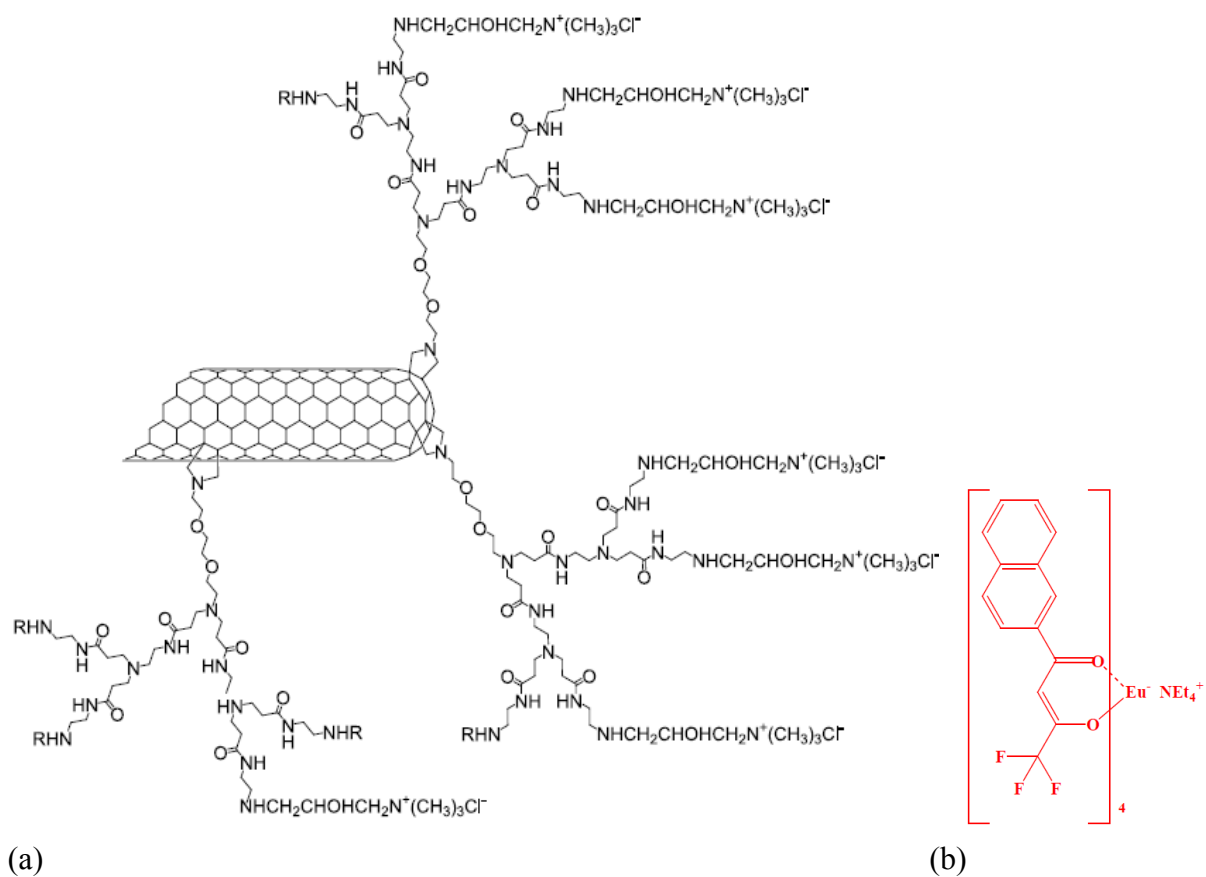
Figure 7. Chemical structure of **d-MWCNTs·Cl** scaffold (a), and **[EuL$_4$]·NEt$_4$** complex (b).

d-MWCNTs·Cl is not luminescent; its absorption profile lacks characteristic features and is dominated by the background from the light scattered by the multiwalled carbon nanotubes (Figure 8). **[EuL$_4$]·NEt$_4$** absorbs light in the UV range up to 385 nm with a maximum centered at around 330 nm. The emission profile of **[EuL$_4$]·NEt$_4$** has characteristic features of Eu(III) complexes with the most intense peak centered at 615 nm.[11,12] The lifetime is 0.29 ms and luminescence quantum yield 0.35 in the solid state (KBr).
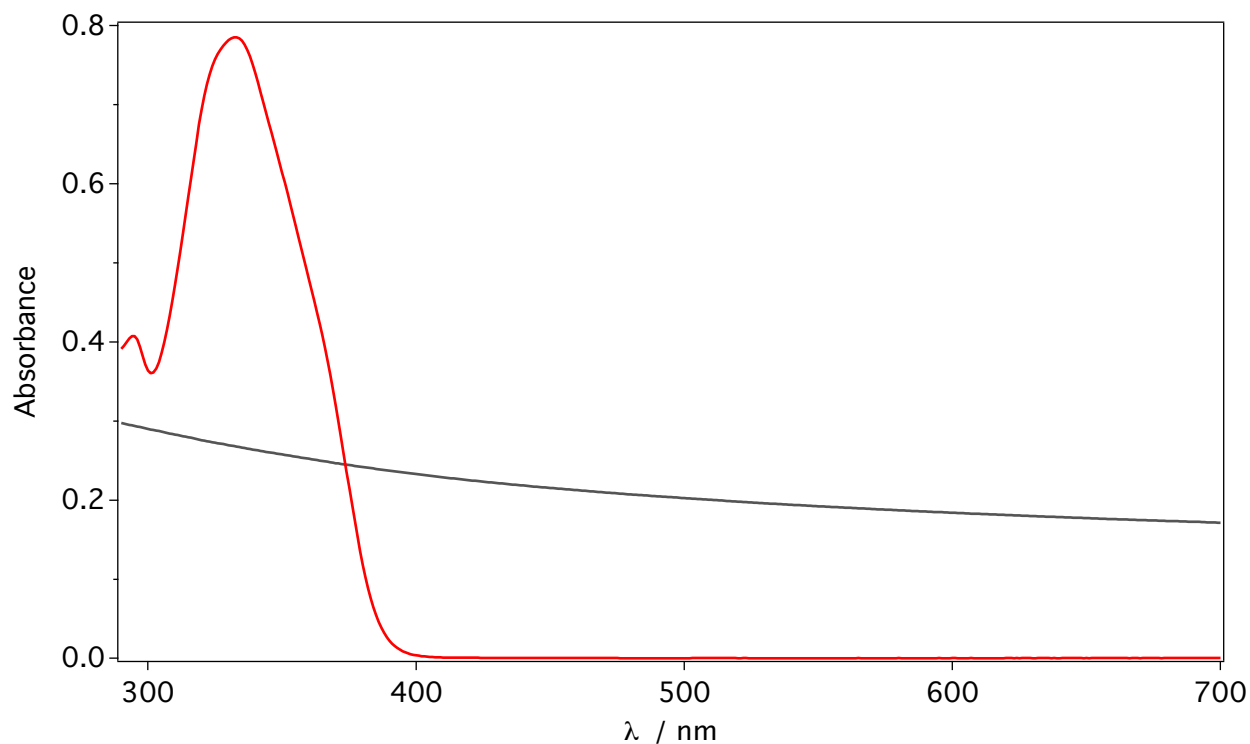
Figure 8. Absorption spectra of **d-MWCNTs·Cl** (grey) and **[EuL$_4$]·NEt$_4$** (red) in toluene.
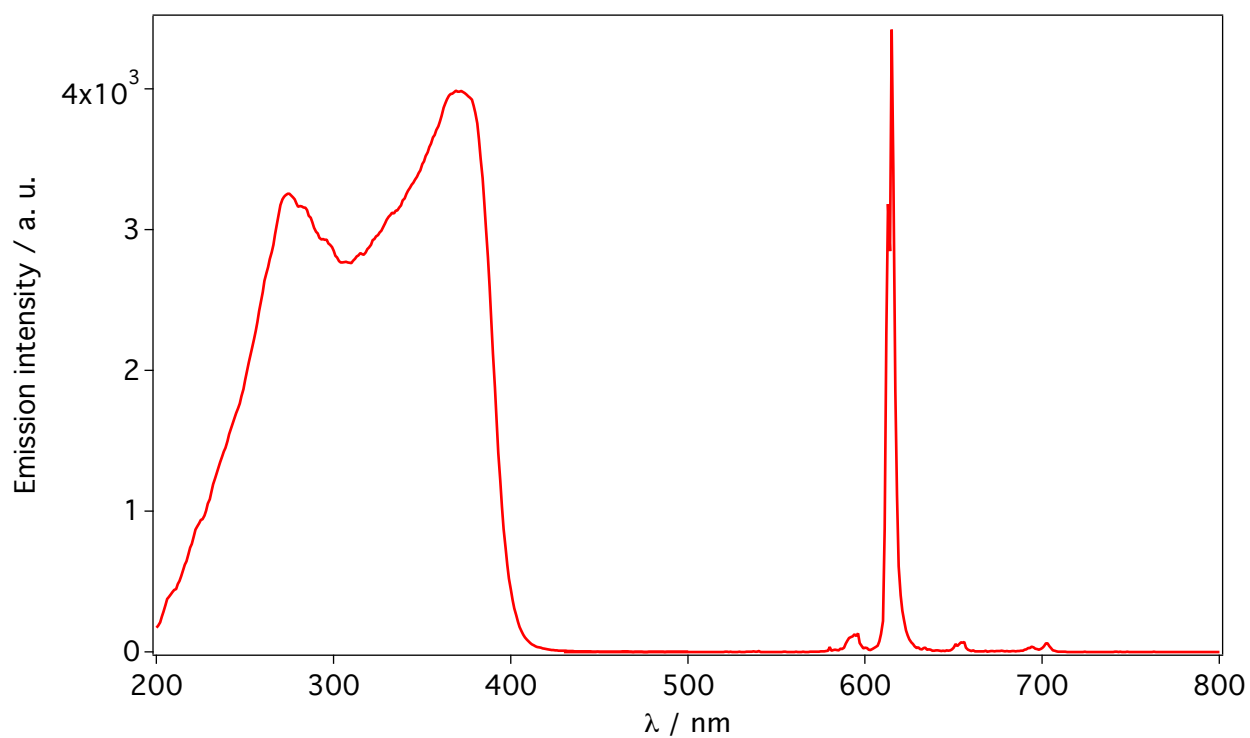
Figure 9. Excitation (left, λ_{em} = 615 nm) and emission spectra (right, λ_{exc} = 370 nm) of

[EuL$_4$]·NEt$_4$ in KBr matrix.

Investigation in KBr matrix does not require dispersion and sonication in a solvent, hence the supramolecular assembly is not disturbed. It should be taken into account that KBr is an ionic material and may undergo electrostatic interactions with our hybrid guest. However, this issue is neglected because all of the measurements were performed immediately after sample preparation.

Samples of **d-MWCNTs·[EuL₄]** in KBr were always excited where the antenna of the europium complex absorbs (i.e. 330, 350, 370 nm), maintaining identical experimental conditions throughout. The emission profile of all **d-MWCNTs·[EuL₄]** is identical at any excitation wavelengths with the most intense peak centered always at 615 nm. Importantly, emission features of the investigated hybrid are indistinguishable from **[EuL₄]·NEt₄** alone (Figure 10 and 11). The excited state lifetime in KBr matrix is 0.29 ms for **[EuL₄]·NEt₄** and for the various **d-MWCNTs·[EuL₄]** samples the following values were measured: 0.28, 0.29, 0.29 and 0.31 ms. Taking into account experimental uncertainties, these excited state lifetimes are virtually identical and suggest that neither quenching of the Eu(III) complex by the MWCNT framework through energy transfer, nor self-quenching among lanthanide complex units occur. Therefore the luminophore/substrate assembling through dendronic branches is capable of preserving the emission features of the Eu(III) units.

Notably, the excitation spectra of **d-MWCNTs·[EuL₄]** match those of the free complex (Figure 12), whereas no emission from free ligands is observed in the UV region. These findings further validate the ion exchange of the complex with the branches of the dendron.
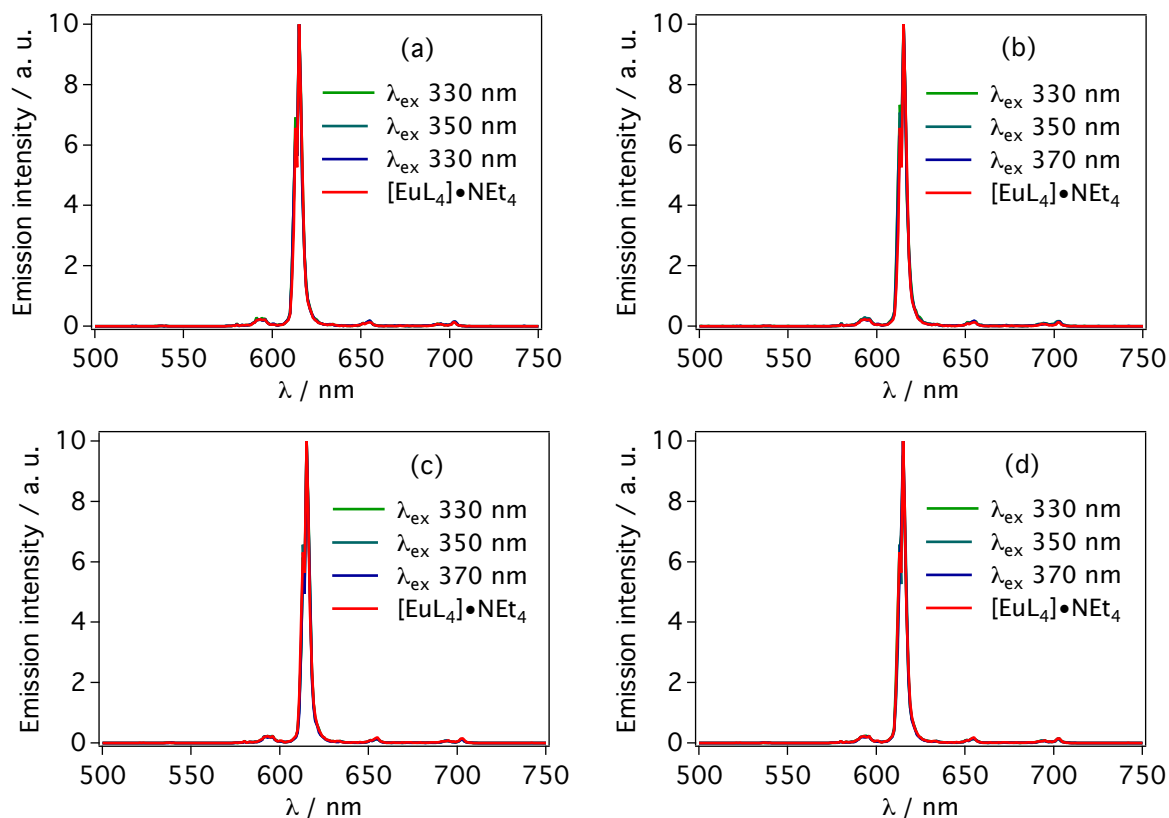
Figure 10. Normalized emission spectra of (a) **d-MWCNTs·[EuL₄]-1**; (b) **d-MWCNTs·[EuL₄]-2**; (c) **d-MWCNTs·[EuL₄]-3**; (d) **d-MWCNTs·[EuL₄]-4** in KBr matrix excited at 330 nm, 350 nm, 370 nm. Emission spectrum of **[EuL₄]·NEt₄** (red line, λ$_{exc}$ = 350) for a comparison.
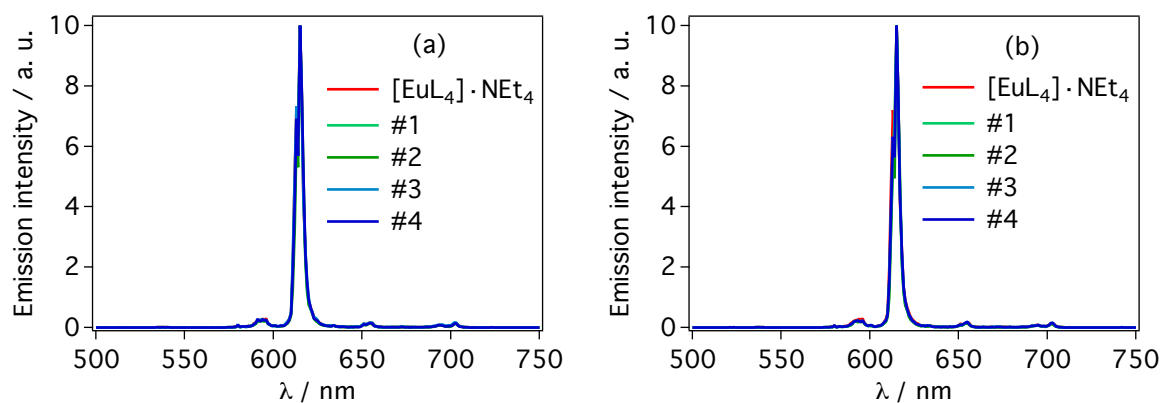
Figure 11. Normalized emission spectra of **d-MWCNTs·[EuL₄]-1**, **d-MWCNTs·[EuL₄]-2**, **d-MWCNTs·[EuL₄]-3**, **d-MWCNTs·[EuL₄]-4** and **[EuL₄]·NEt₄** in KBr matrix excited at (a) 330 nm, (b) 370 nm.
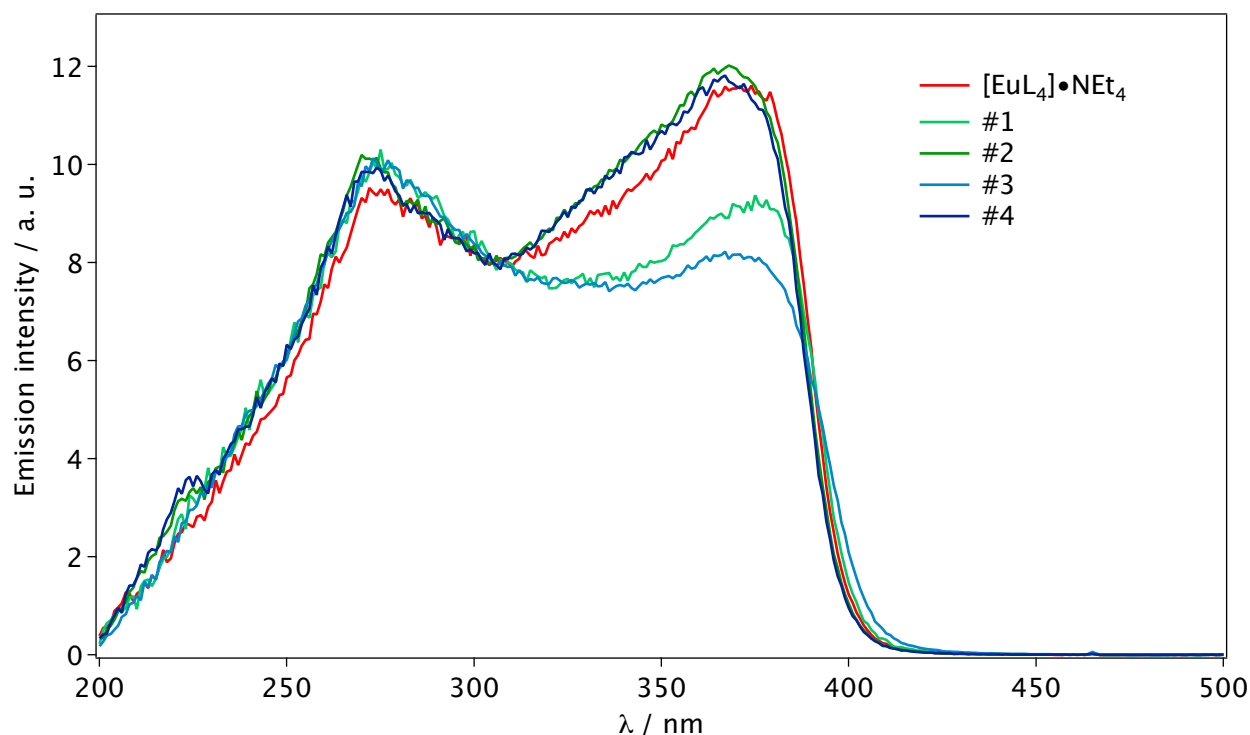
Figure 12. Excitation spectra of **d-MWCNTs·[EuL₄]-1**, **d-MWCNTs·[EuL₄]-2**, **d-MWCNTs·[EuL₄]-3**, **d-MWCNTs·[EuL₄]-4** and **[EuL₄]·NEt₄** in KBr matrix recorded at λ_{em} = 615 nm.

Solid-state luminescence quantum yields (Φ_{em}) were measured for the four **d-MWCNTs·[EuL₄]** samples by exciting at 350 nm (λ_{exc}) (Table 1). Small differences among luminescence quantum yield values can be attributed to experimental uncertainties. The values are slightly lower than that of **[EuL₄]·NEt₄** (0.35), but still in the range of experimental error.

To investigate the influence of the carbonaceous scaffold on luminescence efficiency, the solid-state luminescence quantum yield was determined using excitation wavelengths in

the 310-380 nm spectral window. In this range of λ_{exc}, the absorption spectrum of the scaffold is flat while the absorption of Eu complex crosses its maximum and minimum (Fig. 8). This experiment should answer the question if there is any light partitioning between the scaffold and the antenna of **[EuL$_4$]·NEt$_4$** complex; in case, an excitation-dependent luminescence efficiency of the complex in the hybrid should be observed. Measurements were performed for two samples and for both of them Φ_{em} values are independent of λ_{exc} indicating that the carbonaceous scaffold is not affecting the process of light absorption by the europium luminophore.

Table 1. Emission quantum yield of the hybrid array **d-MWCNTs·[EuL$_4$]-(1-4)** and reference complex **[EuL$_4$]·NEt$_4$** in KBr matrix.

	Φ_{em}
d-MWCNTs·[EuL$_4$]-1	0.27
d-MWCNTs·[EuL$_4$]-2	0.33
d-MWCNTs·[EuL$_4$]-3	0.29
d-MWCNTs·[EuL$_4$]-4	0.26
[EuL$_4$]·NEt$_4$	0.35

2.3.2. Studies in Solution

In order to (i) deeply investigate the impact of the carbonaceous scaffold on the luminescent performance of the ion-paired europium complex and (ii) confirm that the differences in luminescence quantum yield measured in the solid state are due to the experimental uncertainty and not to competitive absorption by the d-MWCNTs scaffold, photophysical studies in solution were also carried out.

The absorption of d-MWCNTs is in fact fairy negligible compared to that of the **[EuL₄]·NEt₄** solutions, as derived from absorption spectra of **d-MWCNTs·[EuL₄]** in toluene or dichloromethane (Figure 13), which are optically transparent and do not exhibit any absorption background attributable to the carbon nanomaterial.
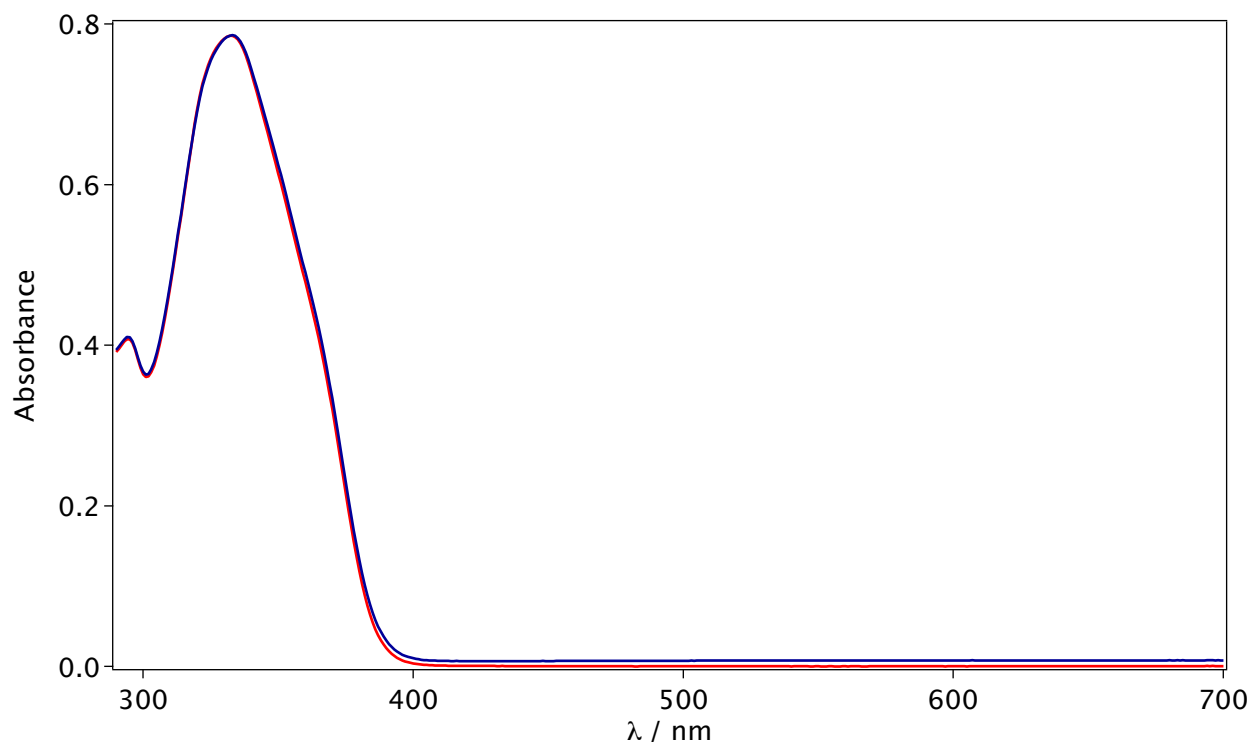
Figure 13. Absorption spectra of **d-MWCNTs·[EuL₄]** (blue) and **[EuL₄]·NEt₄** (red) in toluene.

This result can be rationalized considering that the load of **[EuL₄]⁻** ions on **d-MWCNTs⁺** is very high (see section *Synthesis and Characterization of the Investigated Material*) and the **[EuL₄]⁻**-centered maximum molar extinction coefficient (ε) is 70,000 M^{-1} cm^{-1} (330 nm). The ε value of carbon nanotubes is very difficult to determine and only recently it has been assessed in the NIR region for SWNT.[36] Therefore a direct comparison between the absorption capability of luminophores vs. substrate cannot be made. For a very rough appraisal, it can be noticed that C_{60} exhibits an ε value of 50,000 M^{-1}cm^{-1} at 330 nm

(Figure 14), namely 5.6 times lower than four units of **[EuL$_4$]$^-$** attached to a single dendronic branch.
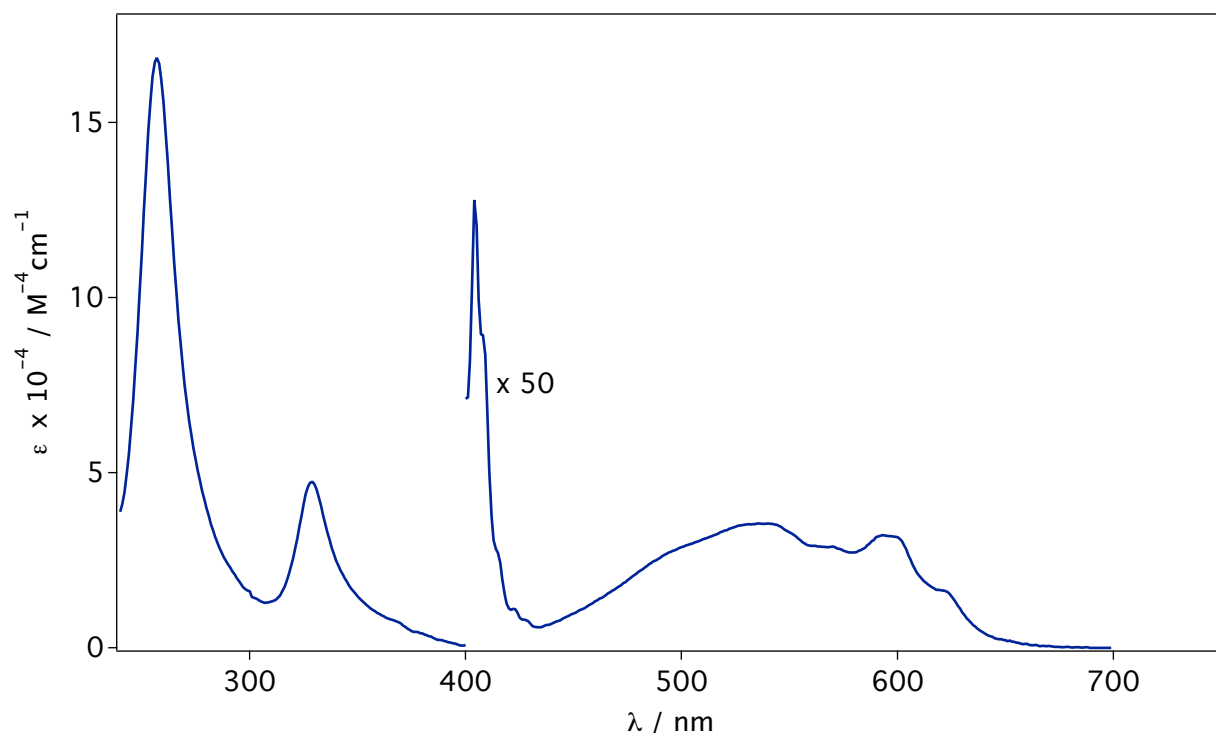
Figure 14. Extinction coefficient of C$_{60}$ in CH$_2$Cl$_2$.[28]

Further photophysical studies in solution were inspired by DOSY NMR measurements, which were performed on **d-MWCNTs·[EuL$_4$]** in methanol (MeOH) and dimethylsulfoxide (DMSO) solutions. These solvents have strong coordinating properties and cause dissociation of the β-diketonate ligand from the metal core of the europium complex, thus hampering the effective ion-pairing in the hybrid array. The results of the solvent-dependent DOSY show that, in methanol, the attenuation of the **[EuL$_4$]$^-$** signal is monoexponential with a corresponding D value of 5.8 10^{-6} cm^{2}s^{-1} indicating that the Eu(III) complex is not bound to the scaffold. In DMSO, a biexponential attenuation of the **[EuL$_4$]$^-$**-centered signal was observed, corresponding to D coefficients of 4.7 and 0.4 10^{-6} cm^{2}s^{-1},

indicating that a fraction of complex electrostatically attached to the scaffold is still present in solution (ca. 6%).

Excitation and emission spectra of **d-MWCNTs·[EuL₄]** together with **[EuL₄]·NEt₄** as a reference are presented in Figure 15. In all solvents, the photophysical features of the europium complex are not affected by the presence of the carbonaceous scaffold, be it ion-paired or not. Broadening of the signals of Eu(III) emission in MeOH and DMSO results from the instability of the complex.
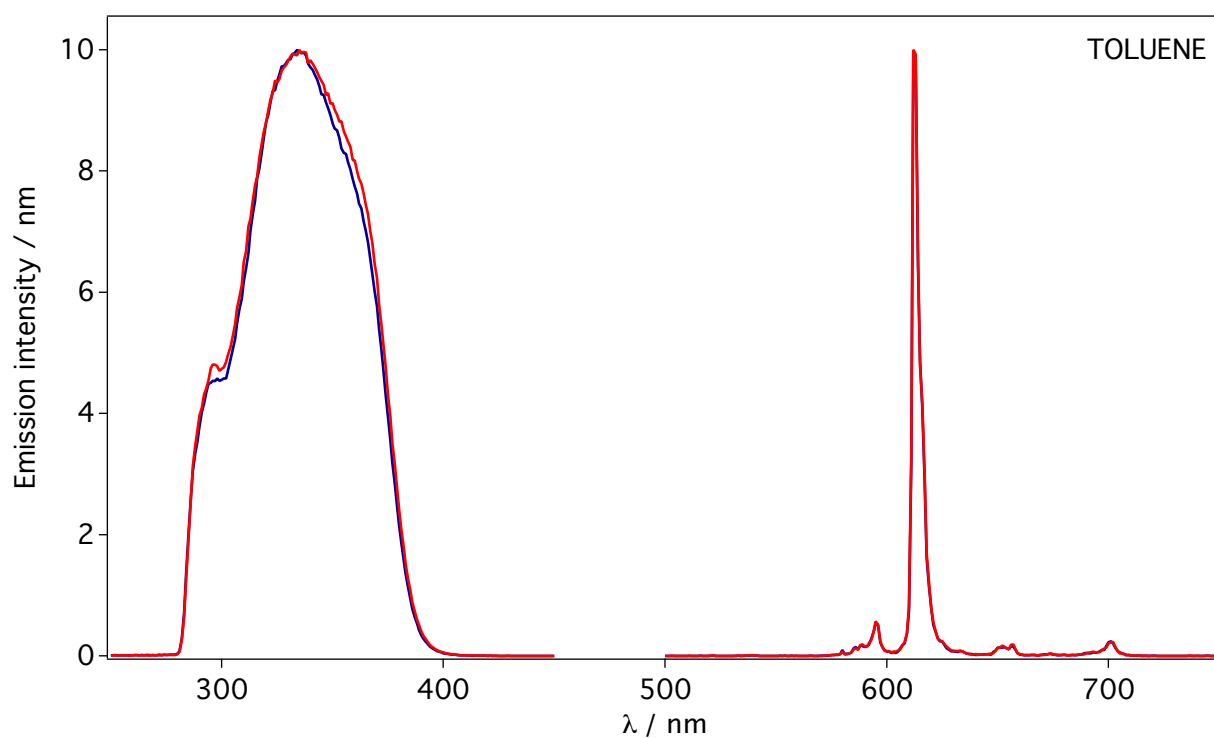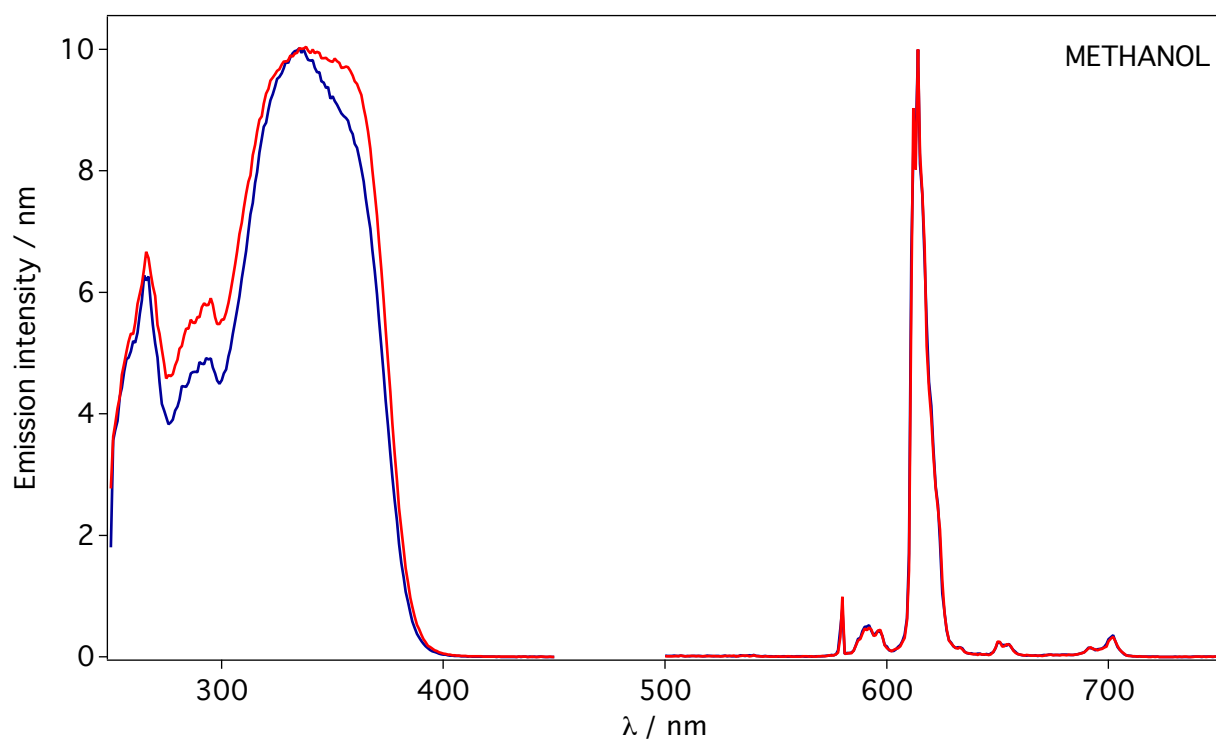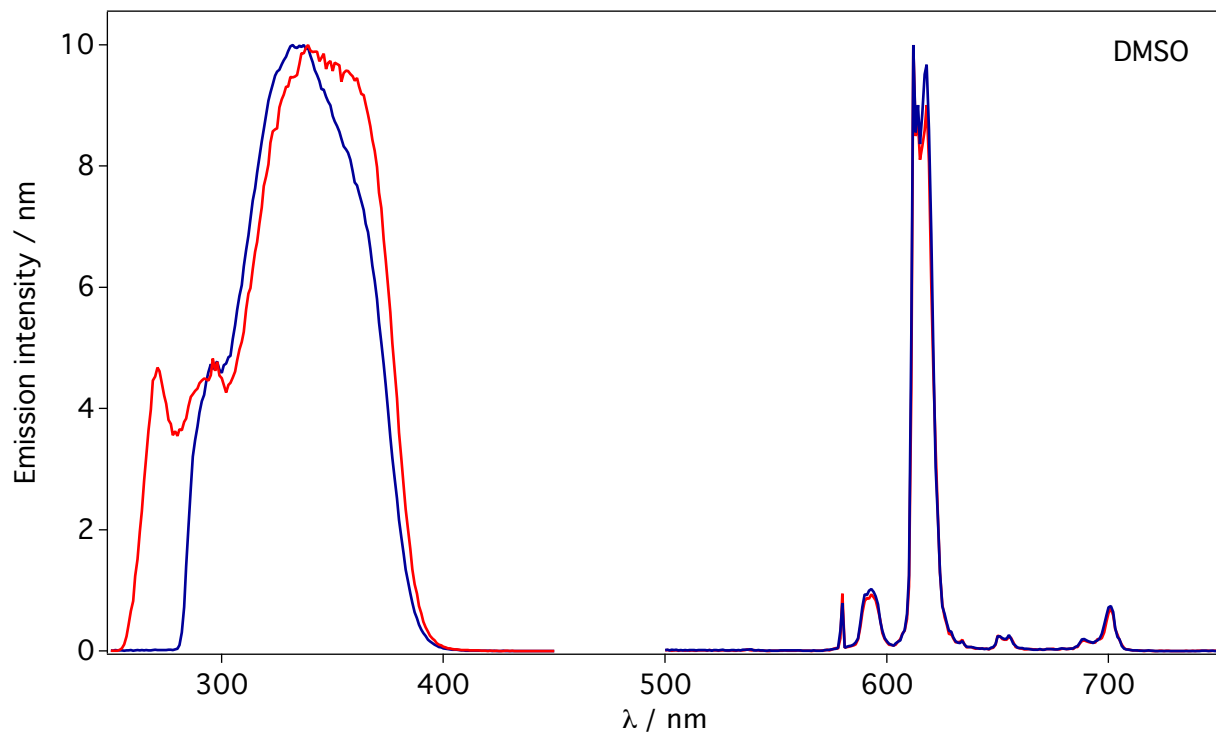
Figure 15. Excitation (λ_{em} = 615 nm) and emission (λ_{exc} = 350 nm) spectra of **d-MWCNTs·[EuL4]** (blue) and **[EuL4]·NEt4** (red) in various solvents.

The Φ_{em} and excited state lifetimes for the ionic couples **[EuL$_4$]·NEt$_4$** and **d-MWCNTs·[EuL$_4$]** are found to be identical in toluene (37% and 0.47 ms). Also in MeOH, where the detachment of the luminophores occurs, identical lifetimes were found (0.27 ms), confirming that the Eu(III)-centered luminescent properties are the same, regardless of the presence of an electrostatic interactions between the dendron-derived carbon nanotubes and the emitter.

2.4. Conclusion

We have described a novel hybrid luminescent material, **d-MWCNTs·[EuL$_4$]**, in which a multiwalled carbon nanotube scaffold is buried in a positively charged dendron ion-paired with a negatively-charged Eu(III) complex, **[EuL$_4$]$^-$**. This array was first analyzed by various techniques, including TGA, XPS and electron microscopy. The effectiveness of the ion-pairing interaction with the dendron-derived MWCNTs has been demonstrated for the first time by means of solvent-dependent DOSY NMR measurements, which have revealed different diffusion coefficients for ionic complexes **[EuL$_4$]·NEt$_4$** and **d-MWCNTs·[EuL$_4$]**.

Four samples of the material were studied in the solid state (KBr matrix) to ensure the reproducibility of the synthesis and the constant photophysical performance of this innovative hybrid. The system was further studied in solvents with different coordinating properties. The results show that the combination of MWCNT with lanthanide emitters through dendronic branches and electrostatic interactions, leads to a strongly emitting, highly soluble carbon material in which **d-MWCNTs** act as a photochemically inert scaffold exhibiting negligible UV-VIS absorption compared to the grafted luminescent dendrons and no quenching interactions. Thanks to the very high loading of the emissive species and the unchanged luminescence performances of the resulting hybrid material in the solid state, this approach

holds great promise for the preparation of substrates to be incorporated in real-life photo- and electroluminescent devices.

References

(1)   Iijima S. *Nature* **1991**, *354*, 56-58.

(2)   (a) Robertson, N.; McGowan, C. A. *Chem. Soc. Rev.* **2003**, *32*, 96-103. (b) Baughman, R. H.; Zakhidov, A. A.; de Heer, W. A. *Science* **2002**, *297*, 787-792. (c) Dresselhaus, M.; Dresselhaus, G.; Avouris, P. *Carbon Nanotubes: Synthesis, Properties and Applications*; Springer-Verlag, Berlin, 2001. (d) Ajayan, P. M.; Zhou, O. Z. *Top. Appl. Phys.* **2001**, *80*, 391-425. (e) Ajayan, P. M. *Chem. Rev.* **1999**, *99*, 1787-1799. Dai, H. *Acc. Chem. Res.* **2002**, *35*, 1035–1044.

(3)   (a) Baughman, R. H.; Zakhidov, A. A.; de Heer W. A. *Science* **2002**, *297*, 787–792. (b) Zhao, Q.; Gan, Z.; Zhuang, Q. *Electroanalysis* **2002**, *14*, 1609–1613. (c) Terrones, M. *Ann. Rev. Mater. Res*. **2003**, *33*, 419–501. (d) Popov, V. N. *Mater. Sci. Eng. R. Rep.* **2004**, *43*, 61–102. (e) Bianco, A.; Kostarelos, K.; Partidos, C. D.; Prato, M. *Chem. Commun.* **2005**, *5*, 571–577. (f) Lacerda, L.; Bianco, A.; Prato, M.; Kostarelos, K. *Adv. Drug. Deliv. Rev.* **2006**, *58*, 1460–1470.

(4)   Ebbesen, T. W.; Ajayan, P. M. *Nature* **1992**, *358*, 220-222.

(5)   Guo, T.; Nikolaev, P.; Thess, A.; Colbert, D. T.; Smalley, R. E. *Chem. Phys. Lett.* **1995**, *243*, 49-54

(6)   (a) Kitiyanan, B.; Alvarez, W. E.; Harwell, J. H.; Resasco, D. E. *chem. Phys. Lett.* **2000**, *317*, 497-503. (b) Endo, M.; Takeuchi, K.; Igarashi, S.; Kobori, K.; Shiraishi, M.; Kroto, H. W. *J. Phys. Chem. Solids* **1993**, *54*, 1841-1848.

(7)   (a) Zhao, Y.-L.; Stoddart, J. F. *Acc. Chem. Res.* **2009**, *42*, 1161–1171. (b) Kim, S. W.; Kim, T.; Kim, Y. S.; Choi, H. S.; Lim, H. J.; Yang, S. J.; Park, C. R. *Carbon* **2012**, *50*, 3–33.

(8)   Tasis, D.; Tagmatarchis, N.; Bianco, A.; Prato, M. *Chem. Rev.* **2006**, *106*, 1105–1136.

(9)   Bünzli, J.-C. G. in *Spectroscopic Properties of Rare Earths in Optical Materials*, eds. G. K. Liu and B. Jacquier, Springer Verlag, Berlin, 2005, Vol. 83. Shionoya, S.; Yen, W. M. *Phosphor Handbook*, CRC Press Inc., Boca Raton, FL, 33431, USA, **1999**. (c) Kido, J.; Okamoto, Y. *Chem. Rev.* **2002**, *102*, 2357-2368.

(10)   Yam, V. W. W.; Lo, K. K. W. *Coord. Chem. Rev.* **1999**, *184*, 157-240.

(11)   (a) Bünzli, J.-C. G.; Piguet, C. *Chem. Soc. Rev.* **2005**, *34*, 1048. (b) Leonard, J. P.; Nolan, C. B.; Stomeo, F.; Gunnlaugsson, T. *Topics in Current Chemistry*; Balzani, V.; Campagna, S., Eds. Springer Berlin Heidelberg: Berlin, Heidelberg, 2007; Vol. 281, pp. 1–43.

(12)   Binnemans, K. in *Handbook on the Physics and Chemistry of Rare Earths*; Gschneidner Jr., K. A.; Bünzli, J.-C. G.; Pecharsky, V. K., Eds. Elsevier V.B. North-Holland, Amsterdam, 2005, Vol. 35 p. 107-251

(13)   Pagnot, T.; Audebert, P.; Tribillon, G. *Chem. Phys. Lett.* **2000**, *322*, 572-578.

(14)   Binnemans, K. *Chem. Rev.* **2009**, *109*, 4283-4374. b) Bünzli, J.-C. G.; Eliseeva, S. V.; J. Rare Earths 2010, 28, 824-842.

(15)   Mohanraj, J.; Armaroli, N. *J. Phys. Chem. Lett.* **2013**, *4*, 767–778.

(16)   Accorsi, G.; Armaroli, N.; Parisini, A.; Meneghetti, M.; Marega, R.; Prato, M.; Bonifazi, D. *Adv. Funct. Mater.* **2007**, *17*, 2975–2982.

(17)   Wu, H.-X.; Cao, W.-M.; Wang, J.; Yang, H.; Yang, S.-P. *Nanotechnology* **2008**, *19*, 345701.

(18)   (a) Kong, L.; Tang, J.; Liu, J.; Wang, Y.; Wang, L.; Cong, F. *Mater. Sci. Eng. C* **2009**, *29*, 85-91. (b) Zhao, C.; Song, Y.; Qu, K.; Ren, J.; Qu, X. *Chem. Mater.* **2010**, *22*, 5718-5724; (c) Xin, X.; Pietraszkiewicz, M.; Pietraszkiewicz, O.; Chernyayeva, O.; Kalwarczyk, T.; Gorecka, E.; Pociecha, D.; Li, H.; Hołyst, R. *Carbon* **2012**, *50*, 436-443.

(19)   Kauffman, D. R.; Shade, C. M.; Uh, H.; Petoud, S.; Star, A. *Nat. Chem.* **2009**, *1*, 500-506.

(20)   Maggini, L.; Traboulsi, H.; Yoosaf, K.; Mohanraj, J.; Wouters, J.; Pietraszkiewicz, M.; Pietraszkiewicz, O.; Armaroli, N.; Bonifazi, D. *Chem. Commun.* **2011**, *47*, 1626-1628.

(21)   Sitharaman, B.; Rajamani, S.; Pramod, K. A. *Chem. Commun.* **2011**, *47*, 1607-1609.

(22)   Maggini, L.; Mohanraj, J.; Traboulsi, H.; Parisini, A.; Accorsi, G.; Armaroli, N.; Bonifazi, D. *Chem. Eur. J.* **2011**, *17*, 8533-8537.

(23)   Bahr, J. L.; Yang, J.; Kosynkin, K.; Bronikowski, C. V.; Smalley, R. E.; Tour, J. M. *J. Am. Chem. Soc.* **2001**, *123*, 6536-6542.

(24)   Quintana, M.; Prato, M. *Chem. Commun.* **2009**, 6005-6007.

(25)   Loening, N. M.; Keeler, J.; Morris, G. A. *J. Magn. Reson.* **2001**, *153*, 103-112.

(26)   (a) Morris, K. F.; Johnson Jr., C. S. *J. Am. Chem. Soc.* **1992**, *114*, 3139-3141. (b) Johnson Jr., C.

S. *Prog. Nucl. Magn. Res. Spectr.* **1999**, *34*, 203-256. (c) Nilsson, M.; Connell, M. A.; Davis, A. L.; Morris, G. A. *Anal. Chem.* **2006**, *78*, 3040-3045. (d) Gounarides, J. S.; Chen, A.; Shapiro, M. J. *J. Chromatogr. B* **1999**, *725*, 79-90.

(27)   Maggini, L.; Toma, F. M.; Feruglio, L.; Malicka, J. M.; Da Ros, T.; Armaroli, N.; Prato, M.; Bonifazi, D. *Chem. Eur. J.* **2012**, *18*, 5889–5897.

(28)   Accorsi, G.; Armaroli, N. *J. Phys. Chem. C* **2010**, *114*, 1385–1403.

Extended Gel Nanostructures of a Functional Squaraine Dye by Ultrasound Stimulation

3.1. Introduction

Since 1831 it has been known that acoustic waves have an impact on fluids. In that year Michael Faraday published "*On a peculiar class of acoustic figures*" where he described rings and symmetrical patterns on the fluid surface upon exposure to sound.[1] After this discovery, the phenomenon and its role in science was largely ignored for a whole century until Richard and Loomis investigated the role of ultrasounds, i.e. acoustic waves that have frequency higher than 20 kHz and lay beyond the human ear reception. In their pioneering work, they observed that ultrasonic energy can alter reaction rates and studied the biological effects on small animals. Nowadays, ultrasonic irradiation is applied in medicine, with echography being probably the best-known example. In materials science and pharmaceutical industry, ultrasounds are used in the preparation of micro and nanomaterials, in various processes requiring the handling of mixtures such as dispersion, homogenization or solubilization, as well as in cleaning of surfaces.[2] Ultrasounds are also able to drive chemical reactions and play a significant role in chemistry. Sonochemistry has attracted interest in sustainable processing and green chemistry since the energy of acoustic waves can serve as a convenient and environmentally friendly alternative to operating through harsh conditions or with hazardous materials.[2,3] Moreover, the application of ultrasonic waves may reduce time and energy consumption as well as improve the selectivity of a reaction.[2,3,4]

When interacting with a volume of a fluid, the energy of ultrasounds is mostly dissipated through macroscopic effects, such as heating and moving the fluid around. However, the importance of ultrasounds in materials science arises from the events that occur at the microscopic level, related to a phenomenon called cavitation.[5] When the ultrasonic wave propagates through a liquid medium, cyclic changes of pressure cause fluctuating condensation and rarefaction of the fluid. During the rarefaction of the liquid medium, molecules may be moved apart to distances at which van der Waals interactions are not able

to keep the liquid intact anymore. At this point, a small bubble with gasses can be generated or a bubble existing previously in the medium grows. The bubble swells and compresses at the rhythm of pressure changes and eventually implodes releasing high energy in a tiny area (so-called hot spot). Consequently, the temperature and pressure gradients lead to shock waves, microstreaming and turbulences. Other associated physical events that significantly affect the fate of materials are rapid local cooling rates and localized pressure increases.

The unique conditions associated with the cavitation effect are responsible for the sonochemical and sonoluminescent effects as well as other applications in materials science. However, it is rather counterintuitive that these extreme conditions generated in liquid media by ultrasounds can drive a gelator to form extended self-assembly and gel as a final material. In general, the commonly employed methods and conditions in soft matter engineering are very mild, in order to ensure the integrity of the final self-assembled material in solution. Considering the relative softness of self-assembled materials, the first report on sonication-induced gelation was rather surprising, because ultrasonic energy is expected to have a destructive impact on intramolecular interactions.[6] However, the interaction of ultrasonic waves with soft matter has been well known in medical diagnosis and transdermal drug delivery.[7] Gels, similar to water, are excellent media to transmit ultrasound energy into the target and being more viscous than water are easier to handle during the treatment. Another area of research where ultrasounds contributed to a substantial progress is the crystallization of molecules and materials.[8] Ultrasound helps the primary nucleation process by modifying the conditions for supersaturation thereby reducing the induction period between the attainment of supersaturation and the commencement of nucleation and crystallization. In addition, the excellent mixing conditions maintained by the sonication-induced shockwaves, have been shown to reduce the aggregation of crystals and allow the crystals to grow larger by controlling local nucleus population. In spite of the lessons from these totally different areas

of research, supramolecular chemist overlooked these findings until 2005 when Naota and Koori first observed sol to gel transition of organic solvents containing a dinuclear palladium complex that switches its conformation under the influence of ultrasound to generate stabilizing intermolecular π-stacking interactions (Fig. 1).[9] Since this discovery, a surge of activities in the field of sonication-induced gelation yielded a variety of organic sonogelators.[10] Naota and coworkers subsequently reported palladium-bound peptides that can cause gelation upon ultrasonic irradiation.[11] Other families of sound-triggered gelators include metal complexes,[12] peptides,[13,14] organic dyes[15] and hydrogen bonded gelators.[13-16] Dendronic L-glutamic acid derivatives were found capable of gelating a wide range of solvents, from water to toluene,[13a] while petrol can be transformed to gel by benzylammonium cinnamate salts.[17] However, organic sonogelators have been rarely exploited for the development of functional gel phase materials,[13d,14d,f] especially those composed of organic dyes.[15] For instance, Yi, Huang and co-workers have reported a family of cholesterol appended naphthalimide molecules showing gelation[15a,b] as well as morphological changes accompanied with a sol-to-gel transition[15c] under the influence of ultrasonic sound waves. Sonogelation of quinacridone derivatives functionalized with urea[15d] or cholesterol[15e,f] moieties have been demonstrated by Zhang, Wang and co-workers. Jung et al. have observed that sonication could modulate the aggregation as well as gelation properties of a porphyrin-palladium(II) complex.[15g]
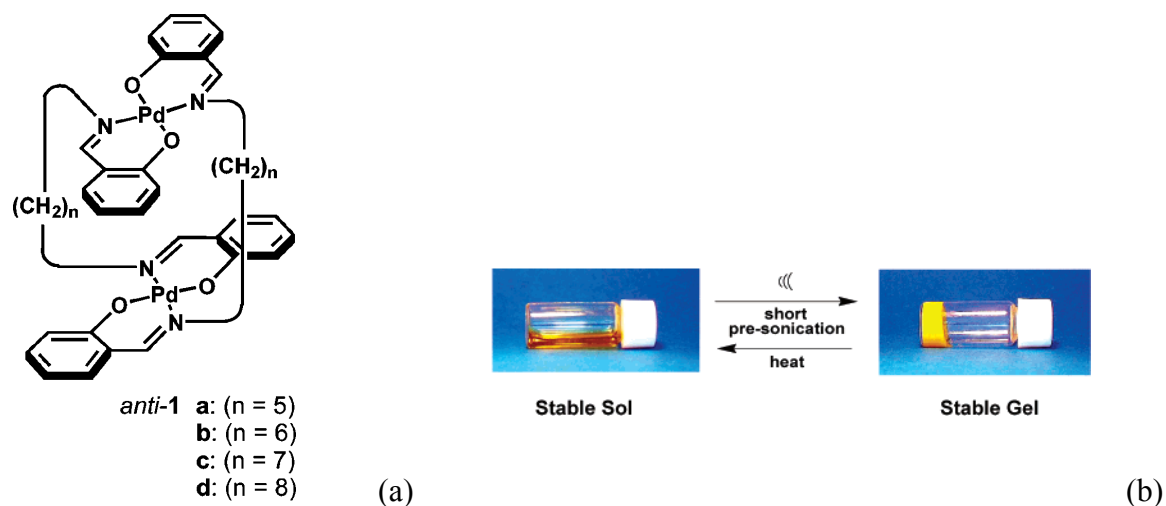
Figure 1. (a) Molecular structure of the first reported system that self-assemble upon sonication; (b) demonstration of the sol-gel transition.[9]

The occurrence of sound-induced self-assembly has a complex and not always clear explanation.[10] Undoubtedly, ultrasonic energy generates particular conditions unaffordable by other stimuli such as light or temperature. It seems that a system excited by ultrasound gains new relaxation pathways, which lead to a network of entangled self-assembled structures able to immobilize the solvent. Importantly, sound-triggered sol-to-gel transitions can be thermoreversibile. Under silent conditions, a system with a sound-triggered organogelator evolves to its lowest energy state, be it a homogenous solution or a precipitate, establishing relaxed conformations of the gelator and consequent non-covalent interactions. When ultrasounds are applied, this natural evolution of the system is biased. During exposure to ultrasonic waves, suitable conformational changes occur and the gelator is trapped in a new growing network of intermolecular interactions. This alternative establishment of non covalent interactions leading to the formation of large, often fibrillar aggregates immobilizing liquids can be observed macroscopically as a sol-gel transition of the sound-triggered organogelator.

The field of sound-triggered self-assembly is developing but is still far from applications. In soft matter sound has been applied as a stimulus somehow recently, and is not yet widely explored as sound-induced crystallization. Time has come to understand, describe, apply, and take full advantage of the potential of ultrasound-triggered self-assembly.

Squaraines are an interesting class of polymethine-type dyes with resonance-stabilized zwitterionic structure. The unique combination of photostability and optical properties that span from the visible to the near-infrared region make squaraine dyes attractive for various applications in the areas of biology, chemistry, and material science.[18] Aggregation properties of squaraines have been extensively studied in mixed solvents, organized media and in the presence of metal ions.[18b-e] However, there are only very few reports on the formation of extended supramolecular nanostructures of functional squaraine derivatives.[19] The first example has come from the research group of Whitten, which reported the self-assembly of a cholesterol tethered squaraine derivative, forming gel fiber networks incorporating organic solvents.[19a] Ajayaghosh and coworkers reported a cation stirred expression of supramolecular chirality and morphological transition from spheres to helices of a chiral tripodal squaraine dye.[19c,d] In another study, it was demonstrated that metal complexation promoted one-dimensional nanostructure formation of a tailor made squaraine dye, yielding an enhancement of molar absorptivity due to the quantum confinement effect.[19e] Evaporation induced self-assembly of a simple squaraine dye into micrometer long aligned nanowires has been reported by Zhang, Lee and co-workers.[19f] Very recently, Mayerhöffer and Würthner have elucidated the thermodynamic and mechanistic aspects of a hydrogen-bonded assembly of a squaraine dye that forms extended fiber-like aggregates.[19h]

Construction of self-assembled structures of squaraine dyes continues to be challenging and has become important in the context of their renowned interest in light energy harvesting.[20] Herein we report the self-assembling properties of the squaraine derivative **GA-**

SQ, which forms extended nanostructures and gels upon application of ultrasound. With the help of spectroscopic and microscopic techniques, we demonstrate a nucleation and growth mechanism for the observed self-assembly, an aspect rarely studied in the area of sonication induced gelation.[15b,16f] Furthermore, the addition of a minuscule amount of single wall carbon nanotubes (SWCNTs) as nanoscale substrate has been found to considerably influence the morphological properties of sonogels of **GA-SQ** by promoting a heterogeneous nucleation process.

3.2. Synthesis and Characterization of the Squaraine Gelator GA-SQ

Compounds **1**, **2** and **4** were prepared as per reported procedures.[21] The preparation of compound **1** was achieved by first reacting methyl 3,4,5-trihydroxybenzoate with 1-bromododecane in the presence of K_2CO_3.[21a] The ester group of this compound was then hydrolyzed using KOH in ethanol to yield the corresponding carboxylic acid derivative.[21a] The compound thus obtained was converted to the aminoethylbenzamide derivative **1** by reacting with excess ethylenediamine in the presence of benzotriazol-1-yloxytris(dimethylamino)phosphonium hexafluorophosphate (BOP), an amide coupling reagent (Scheme 1).[21b] Alkylation of *N*-methylaniline with ethyl 4-bromobutyrate in the presence of NaOAc and I_2, followed by hydrolysis using 5% KOH, afforded *N*-methyl-*N*-(carboxypropyl)aniline **2**.[21c,d] 3-(4-(*N*,*N*-dibutylamino)phenyl)-4-hydroxy-cyclobut-3-ene-1,2-dione **4** was prepared by reacting squaryl chloride[21e] with *N*,*N*-dibutyl aniline.[21f]

The amide bond formation between aminoethylbenzamide derivative **1** and *N*-methyl-*N*-(carboxypropyl)aniline **2** using BOP reagent in the presence of triethylamine gave **3** in 87% yield (Scheme 1). Reaction of **3** with the semisquaraine derivative **4** in a 1:1 stoichiometry, under reflux conditions in 2-propanol using tributyl orthoformate as the catalyst, resulted in the formation of the squaraine gelator **GA-SQ** (Scheme 1). The crude product first isolated by

filtration was further purified by column chromatography on neutral alumina and provided the pure product as a greenish blue solid in 37% yield.
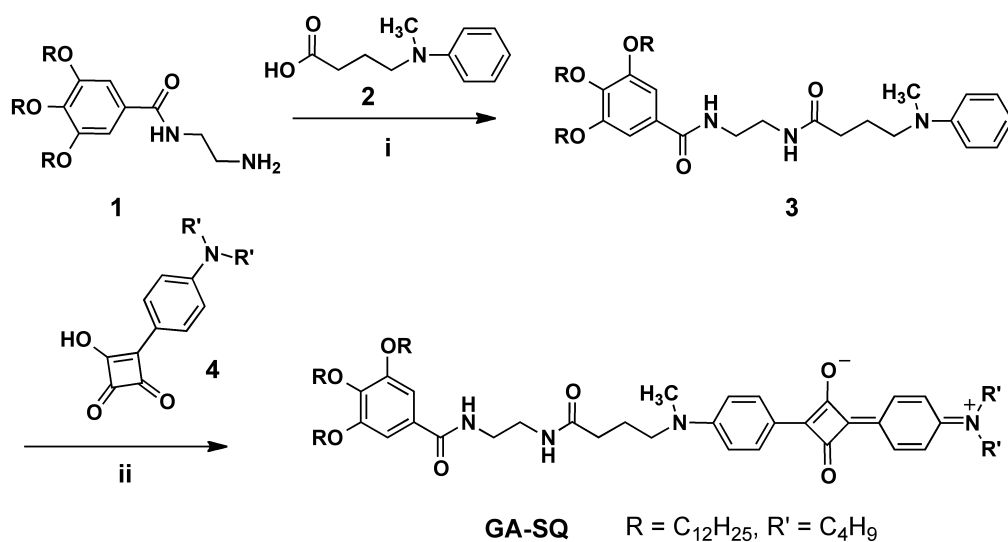
Scheme 1. Synthesis of **GA-SQ** gelator.[a]

[a] Reagents and conditions: (i) BOP reagent, triethylamine, dry CH_2Cl_2, r.t., 3 h, 80%; (ii) dry 2-propanol, tributyl orthoformate, 90 °C, 20 h, 37%.

The FT-IR spectrum of **GA-SQ** in $CDCl_3$ showed an intense band at 1589 cm^{-1} characteristic of pseudoaromatic squarate moiety (Figure 2).[21f] The amide carbonyl group of **GA-SQ** clearly discerned as a sharp band at 1660 cm^{-1} (Figure 2). In the ^1H NMR spectrum of **GA-SQ** in $CDCl_3$ (Figure 3), a singlet at δ 3.04 ppm corresponds to the resonance of –NCH_3 protons. The signal at δ 3.41–3.48 ppm is ascribed to the methylene protons of –CH_2NCH_3 and –CH_2NCH_2–, the resonance of which overlaps to appear as a multiplet. The signals at δ 6.7, 8.29 and 8.33 ppm are assigned to the protons of the diphenyl squaraine unit. The peak at δ 7.02 ppm is attributed to the aromatic protons of the alkoxy substituted gallic acid moiety. ^{13}C NMR (Figure 4) and gradient heteronuclear single quantum correlation (gHSQC) (Figure 5) spectra in $CDCl_3$ are in agreement with the structure of **GA-SQ**. The MALDI-TOF mass spectrum exhibits the 1175.27 $[M]^+$ ion peak along with 1197.92 [M + Na]$^+$ and 1214.37 [M + K]$^+$ peaks (Figure 6).
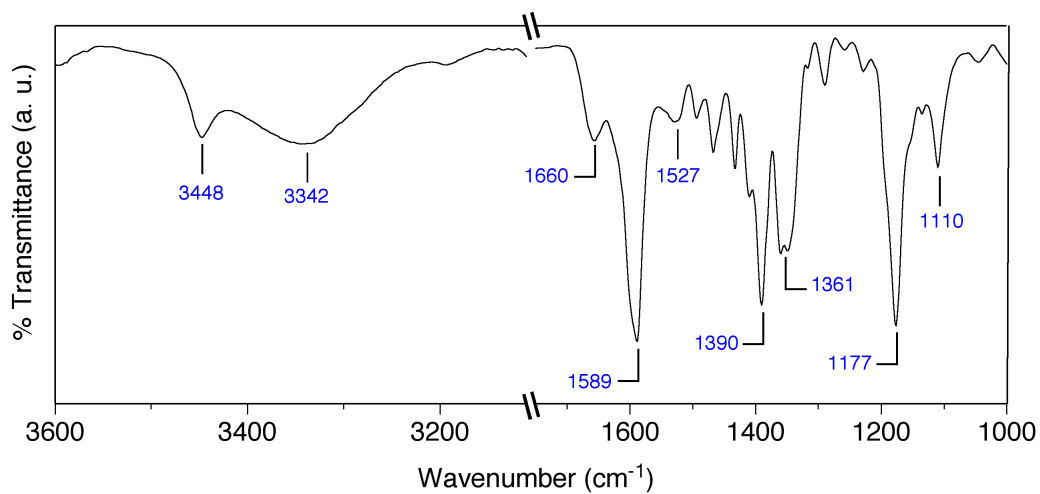
Figure 2. FT-IR spectrum of **GA-SQ** in CDCl$_3$ (4 mM).
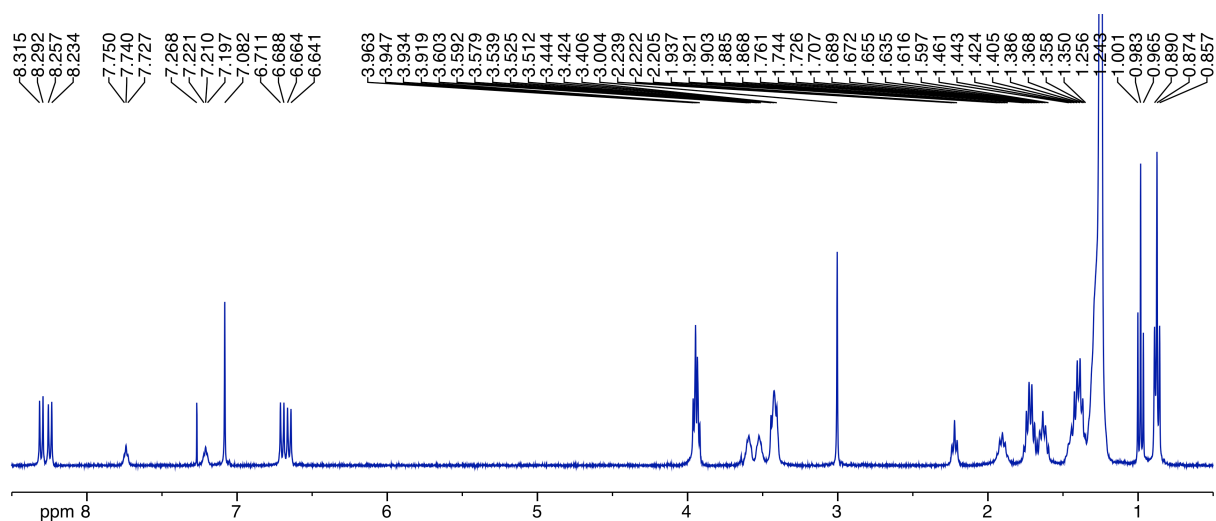
Figure 3. ^{1}H NMR (400 MHz, 298 K) spectrum of **GA-SQ** in CDCl$_3$.
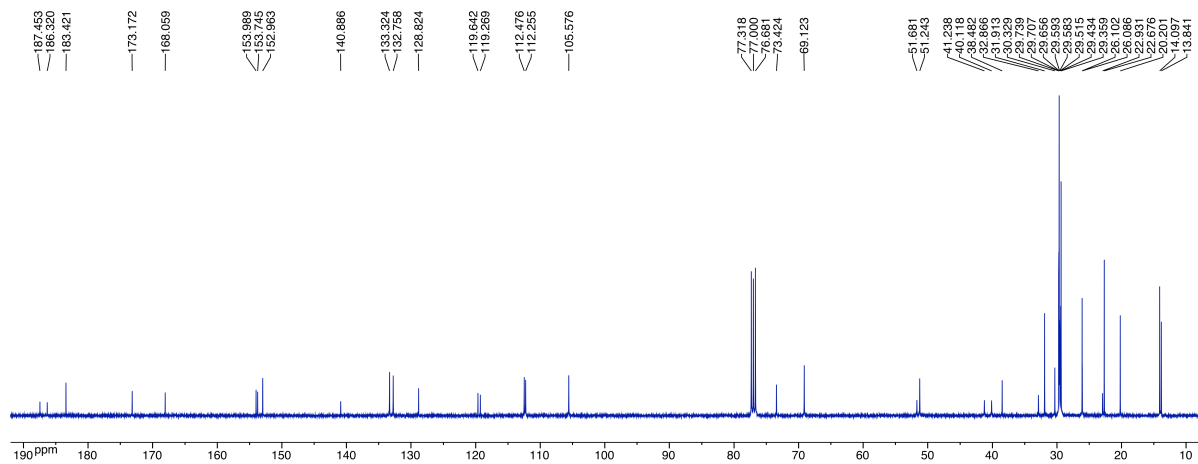
Figure 4. ^{13}C NMR (100 MHz, 298 K) spectrum of **GA-SQ** in CDCl$_3$
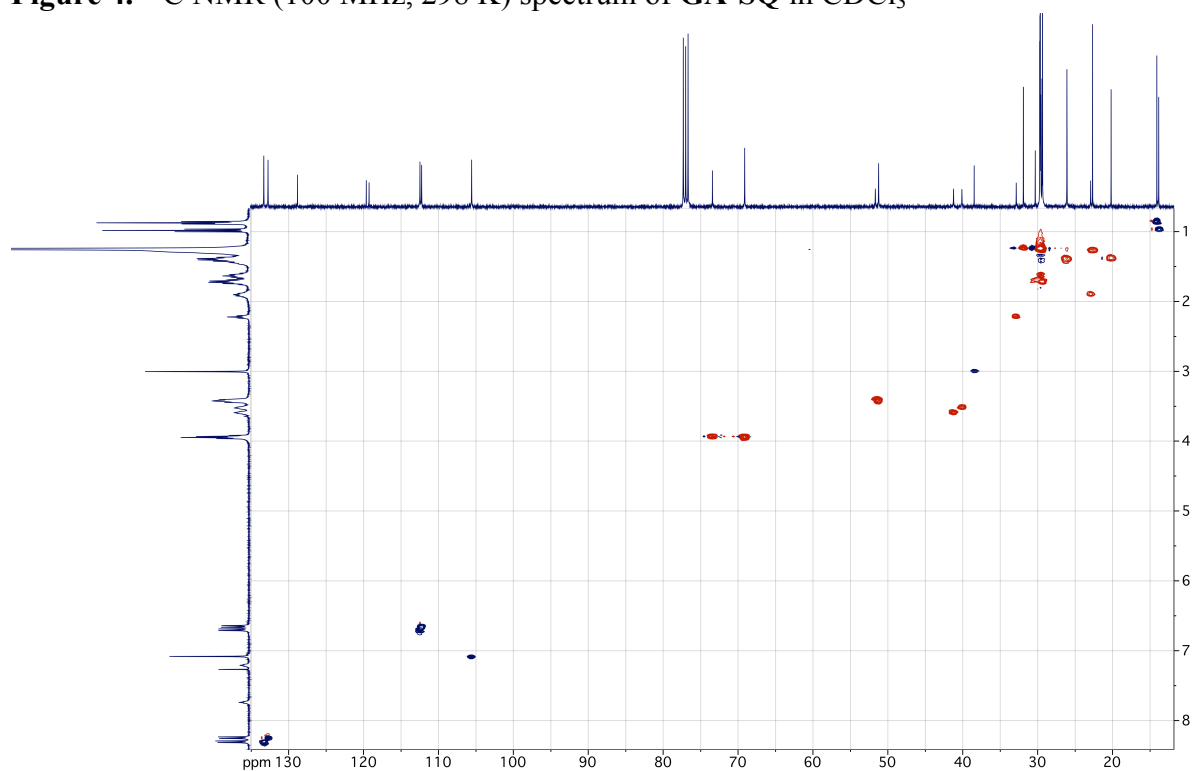
Figure 5. ^{1}H, ^{13}C–gHSQC spectrum (298 K) of **GA-SQ** in CDCl$_3$.
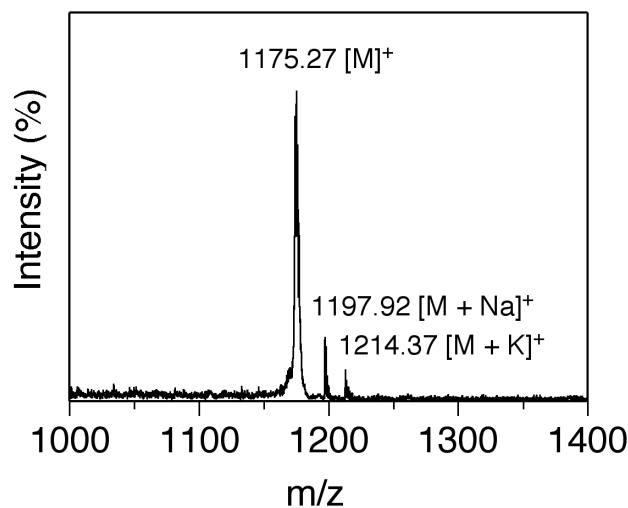
Figure 6. MALDI-TOF spectrum of **GA-SQ** (matrix: α-cyano-4-hydroxycinnamic acid).

The absorption and emission spectra of **GA-SQ** in chloroform display a single band with the λ_{max} at 635 and 650 nm respectively with a relatively small Stokes shift $\Delta\nu_{st} = 412$ cm^{-1} (Figure 7). These optical features are very similar to the standard squaraine dyes derived from the reaction of squaric acid with N,N-dialkyl anilines.[21f]
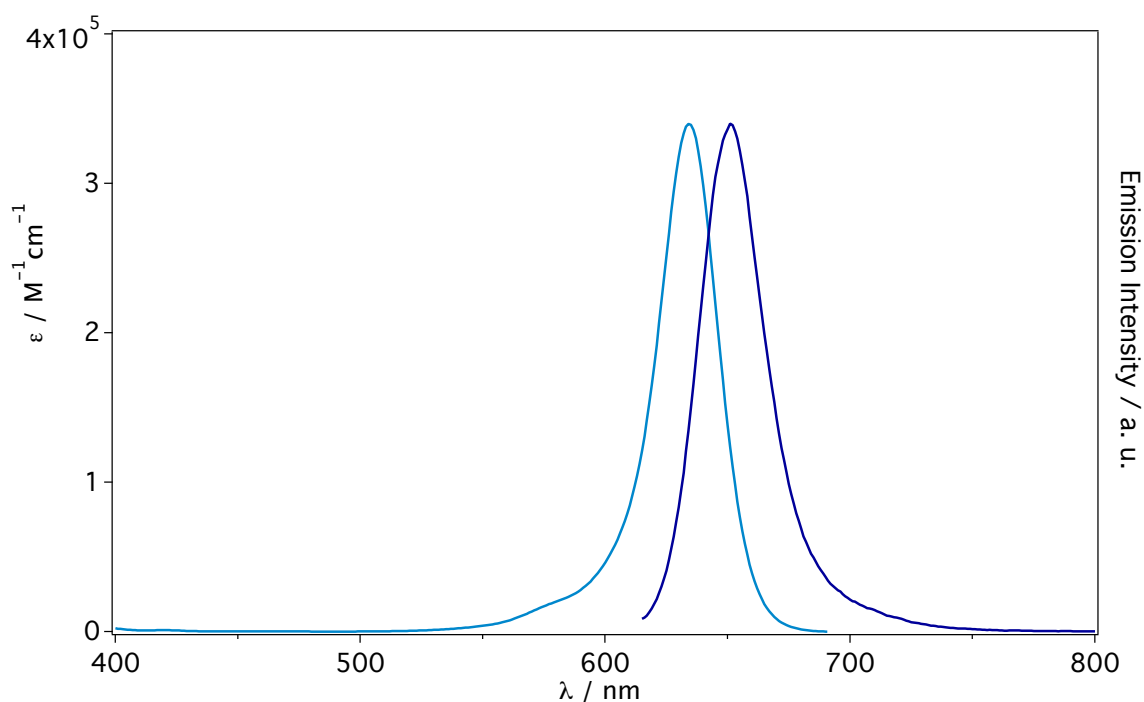
Figure 7. Absorption and emission spectra of **GA-SQ** in CHCl$_3$ (c = 0.02 mM, l = 1 cm, λ_{exc} = 600 nm).

3.2. Studies on the Self-Assembly of the Squaraine Organogelator

Gel formation is normally obtained by heating a required amount of gelator in a suitable solvent and subsequent cooling of the resultant homogenous solution either to room temperature or below.[22] The driving force for the formation of gel nanostructures is considered to be a supersaturation mediated nucleation and growth.[22b] The gelator **GA-SQ**,[22] owing to the presence of hydrophobic dodecyl chains, zwitterionic squaraine dye moiety, and amide functional groups exhibits multifaceted solubility character. In relatively polar solvents like $CHCl_3$, CH_2Cl_2 and THF **GA-SQ** is easily soluble and therefore, unsuitable for gelation studies. In aliphatic and aromatic solvents it is either insoluble or become soluble by heating at high temperature, but precipitates quickly on cooling. Interestingly, in protic polar solvents such as aliphatic alcohols, **GA-SQ** becomes soluble at high temperatures, while upon cooling exhibits two types of behavior. When a solution of **GA-SQ** in *n*-butanol is heated to 70 °C and then let spontaneously cool down to room temperature, no apparent changes were observed. However, on rapid cooling to 0 °C by inserting the sample in an ice bath, **GA-SQ** forms aggregates and the process is accompanied by a color change of the solution from cyan to dark violet (Figure 8 inset). In order to visualize the morphology of these aggregates we carried out detailed electron microscopic studies. The aggregates of **GA-SQ** were cast on freshly cleaved mica and carbon coated copper grid, air-dried and imaged by scanning electron microscopy (SEM) and transmission electron microscopy (TEM), respectively. SEM images show the formation of nanorings and ill-defined fibrous structures (Figure 8a). TEM analysis confirms that the aggregates entail nanorings surrounded by networks of short fibers that are a few micrometers in length (Figure 8b).
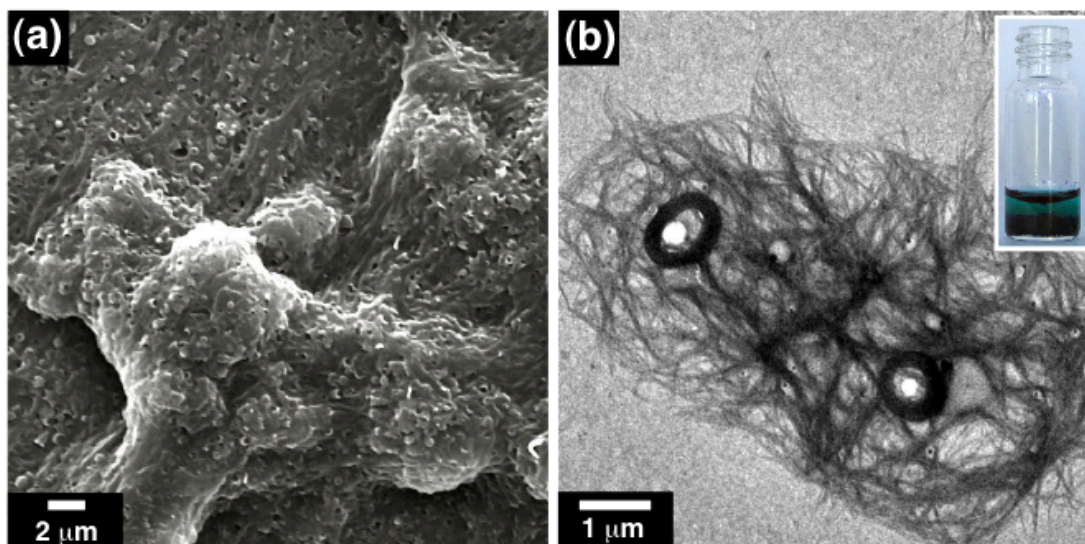
Figure 8. (a) SEM and (b) TEM images of **GA-SQ** self-assembled aggregates obtained by rapid cooling of a hot *n*-butanol solution (4 mM) to 0 °C. The inset shows the photograph of the corresponding self-assembled precipitates formed in *n*-butanol.

Even though the aggregates of **GA-SQ** failed to entrap solvent molecules and did not lead to gelation, the presence of polymorphic nanostructures was quite encouraging. These polymorphic nanostructures are most likely originated from two kinds of nuclei formed during the primary crystallization process. Previous studies have demonstrated that regulating the formation of nuclei, its distribution and growth at the early stages of the self-assembling process would modify the kinetic pathways of supramolecular gel formation and consequent macroscopic properties.[22b] In this regard, application of ultrasound has gained a lot of attention. Ultrasound is known to stimulate the primary nucleation process at a lower supersaturation level, which otherwise would not occur with other methods.[8,10] Sonication also helps to break the seeds and disperse it uniformly in solution. In addition, the cavitation and streaming effect of the ultrasound waves ensure the bulk-phase mass transfer of solute to the surface of growing crystal, thereby promoting the secondary nucleation process. Based on this knowledge, we speculated that the application of ultrasound to a solution of **GA-SQ**

might enhance the formation and growth of nuclei responsible for the formation of nanorings and fibers, by altering the condition for supersaturation. If the secondary nucleation process in the edges or sides of the developing nanostructure would create permanent junction zones, an interconnected network structure capable of trapping solvent molecules by capillary force and van der Waals interactions might eventually arise.

To examine this possibility, detailed studies on the aggregation and gelation were carried out. Homogeneous solutions of various concentrations of **GA-SQ** in *n*-butanol were prepared at 70 °C and then subjected to ultrasonication for 2 minutes (0.23 W/cm^2, 37 kHz) in a bath maintained at room temperature. As a control experiment, another batch of the same solutions was cooled to room temperature without applying sonication. In the lower concentration region (0.01 - 0.5 mM), the solutions cooled to room temperature in the presence and absence of sonication show no difference (Figure 9). Interestingly, at a higher concentration range (1 to 4 mM) the sonication treatment gradually changed the color of the solutions from cyan to dark violet, whereas concentrated solutions cooled in the absence of sonication do not show any color variation (Figure 9). This finding underpins the key role of sonication, likely related to the modified conditions of supersaturation that promote the aggregation of molecules. Though at a concentration of 1 mM some aggregate formation is observed, the solution turned into a semi gel at a slightly higher concentration of 2 mM (Figure 9). A more stable gel is obtained at a concentration 4 mM, which prevented the flow of solvent upon tilting the sample vial sidewise or upside down (Figure 9). Sonication induced gelation is also observed in other aliphatic alcoholic solvents such as ethanol and *n*-propanol with a slightly higher critical gelator concentration of 4.5 and 4.25 mM respectively.
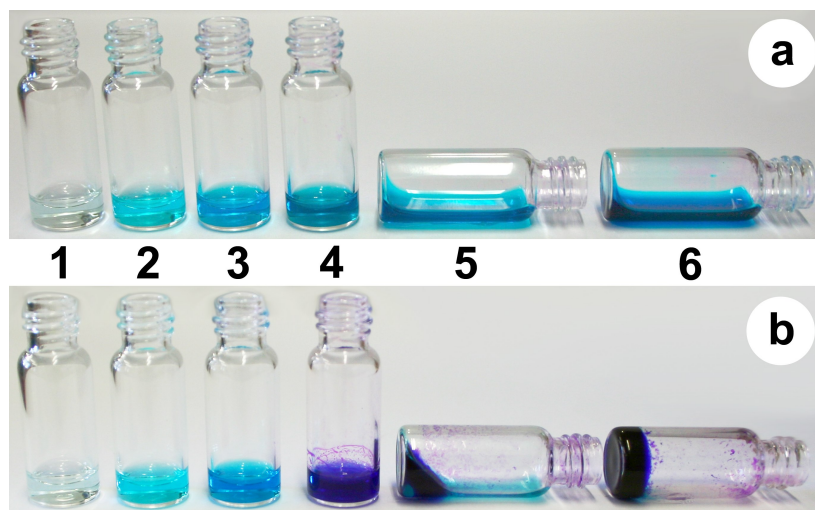
Figure 9. Photographs of the **GA-SQ** solutions in *n*-butanol cooled to room temperature (a) in absence and (b) presence of ultrasonic irradiation. Numbers correspond to the following concentration: 1 = 0.01 mM, 2 = 0.1 mM, 3 = 0.5 mM, 4 = 1 mM, 5 = 2 mM and 6 = 4 mM.

Insight on aggregation and gelation process can be obtained from the characteristic absorption properties of the squaraine moiety that changes upon aggregation.[19,20] However, the high extinction coefficient of squaraines ($\sim 10^5$ M^{-1} cm^{-1}) together with the high concentrations used for these studies (mM) make it challenging to apply this technique. To circumvent these difficulties and enable a reasonable analysis, we used a special type of demountable flow cuvette with adjustable path length (Figure 10).
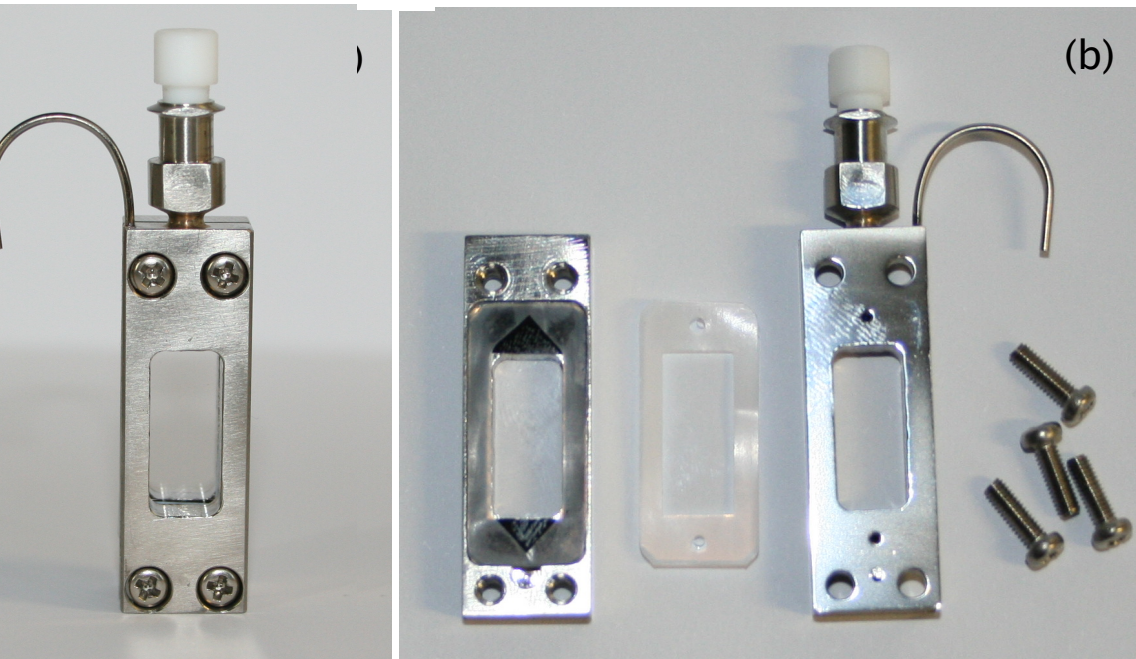
Figure 10. Photograph of the flow cuvette used for the absorption studies of **GA-SQ** samples with high concentration; (a) assembled; (b) deassembled.

UV-Vis absorption spectra of the investigated samples are presented in Figure 11 and Figure 12. In the case of samples not exposed to sonication, the absorption spectra show a sharp band with λ_{max} at 640 nm, characteristic of the monomeric squaraine dye; its intensity changes proportionally to the concentration (Figure 11), as visible by the naked-eye observation (Figure 9a). In the case of sonicated samples, solutions in the range 0.01-0.5 mM do not undergo aggregation (Figure 9b), which is confirmed by absorption spectroscopy (Figure 12a). However, for concentrations 1-4 mM, where aggregation/gelation was observed (Figure 9b), absorption spectra reveal the presence of a new blue-shifted broad band with λ_{max} at 540 nm and a tail in the region between 675 and 800 nm, along with a reduced absorption of the monomeric squaraine at 640 nm. As the concentration increases, the band corresponding to the monomeric squaraine decreases in intensity with a concomitant increase in the absorption band at shorter wavelength with a tail in the lower energy region (Figure

12b). The observed broad spectrum suggests strong association of squaraine units in the aggregates of **GA-SQ** in a *H*-type fashion. The absorption features of self-assembled **GA-SQ** closely matches the spectral features of extended *H*-aggregates of squaraine amphiphiles and gelators.[20a,25]
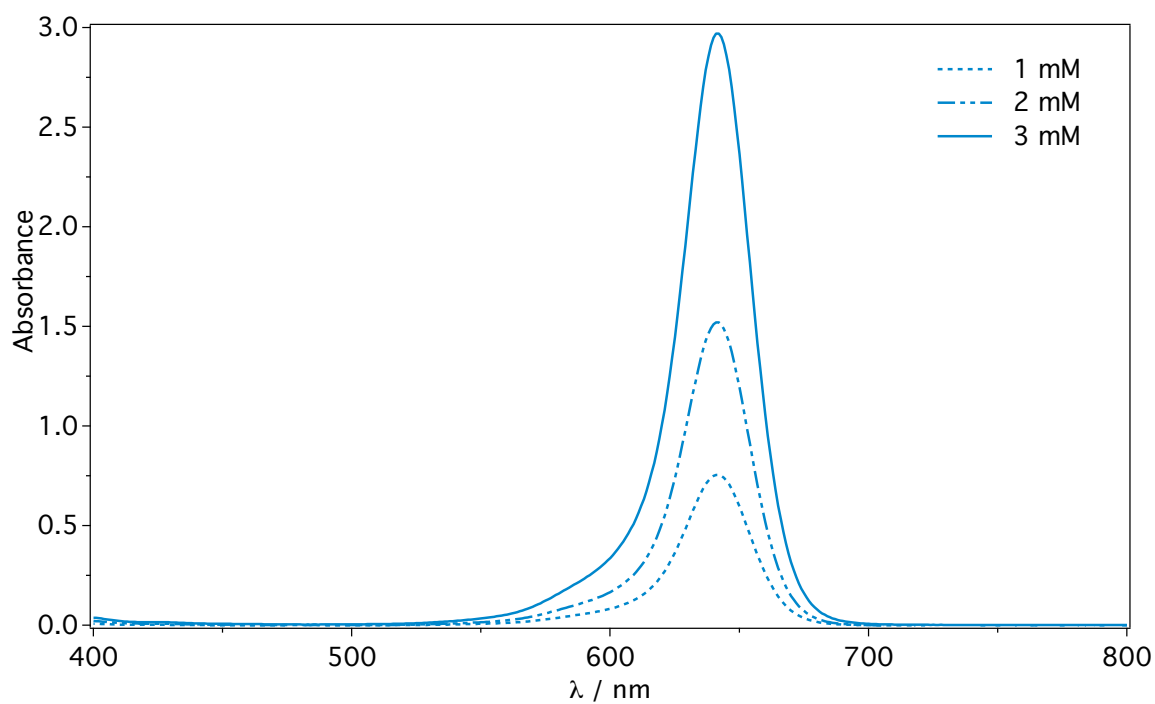
Figure 11. Absorption spectra of **GA-SQ** solutions in *n*-butanol were prepared by heating at 70 ºC and subsequent cooling to room temperature.
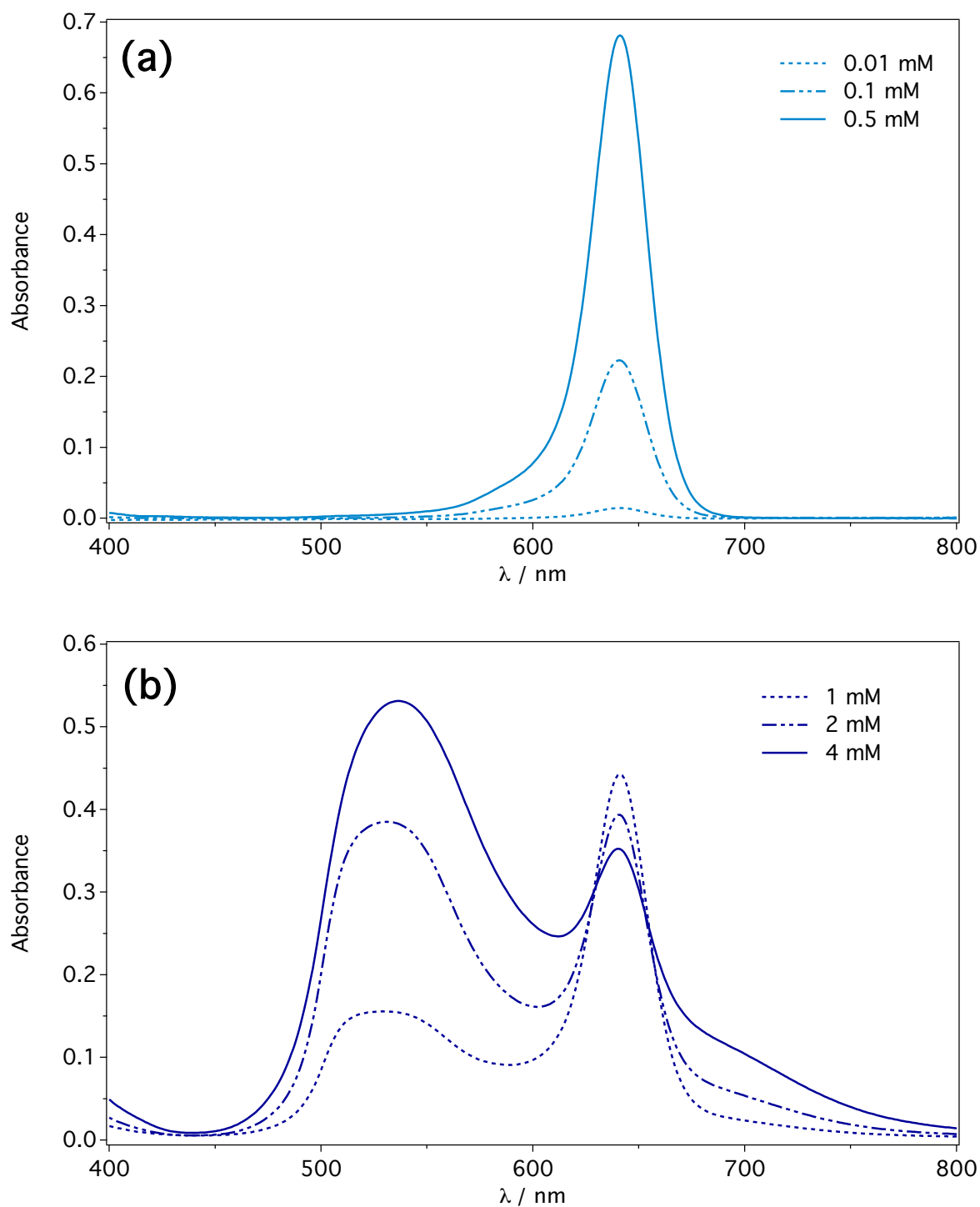
Figure 12. Absorption spectra of **GA-SQ** solutions after sonication (a) lower and (b) higher concentration region (path length, $l = 0.05$ mm).

In light of the above results, it is important to gain insight into the morphology of the self-assembled **GA-SQ** obtained upon sonication. To this end, extensive microscopy studies

were performed on *n*-butanol gel cast on suitable substrates. SEM studies of a gel (4 mM) cast on freshly cleaved mica surface reveal the formation of entangled fibrous networks characteristic of self-assembled gels (Figure 13a). The width of the fibers varies from 50 to 400 nm and the length is extended to several micrometers. TEM analysis of a diluted gel (2 mM) cast on carbon coated copper grid confirms these dimensional values (Figure 13b). The width and length of the thinnest fiber that can be distinguished is approximately 30 nm and few micrometers. The branching of fibers and the tangling of thin fibers to thicker fibrous structures can be also visualized from the TEM micrograph. The atomic force microscopy (AFM) studies on a dilute *n*-butanol gel (2 mM) cast on a freshly cleaved mica surface are also in agreement with the fiber-like morphology of the gel assembly, as observed with SEM and TEM.
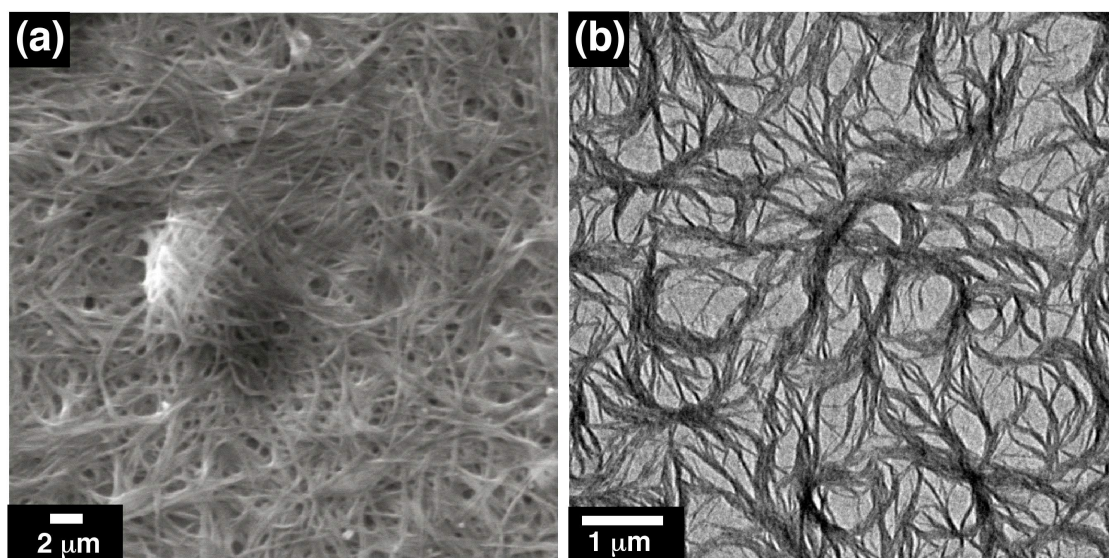
Figure 13. (a) SEM and (b) TEM images of sonication induced self-assembly of **GA-SQ** in *n*-butanol. The concentration used for SEM and TEM studies are 4 and 2 mM respectively.

The above results prompted us to attempt a rationalization of the noncovalent interactions responsible for the self-assembly of **GA-SQ**. It is well known that hydrogen

bonding and van der Waals interactions play a crucial role in the self-assembly of molecules leading to gelation of solvents[22,25] and the best technique to probe this is FT-IR spectroscopy. A secondary amide group is characterized by three distinct infrared absorptions corresponding to symmetric N-H stretch (amide A band), C=O stretch (amide I band) and a combination of the N-H deformation and of the C-N stretch (amide II band).[26] These IR absorptions show change in energy (frequency) when involved in hydrogen-bonding.[26] The IR spectrum of **GA-SQ** in CDCl$_3$ (4 mM, Figure 14a) displays two bands at 3448 and 3342 cm^{-1} that can be assigned as amide A bands. The aliphatic and aromatic amide carbonyl (amide I) appears as a single band at 1660 cm^{-1} and the amide II band at 1527 cm^{-1}. By contrast, the IR spectrum of **GA-SQ** in the xerogel state exhibits a completely different behavior (Figure 14b). Thus, the amide A bands appear at 3301 and 3265 cm^{-1}, with a shift of 147 and 77 cm^{-1} respectively. The amide I band split up as two bands displayed at 1650 and 1620 cm^{-1}, while the amide II shifts to 1539 cm^{-1}. The significant shifts of amide A and I bands to the lower frequency, and the amide II band to the higher frequency region are clear indication of strong hydrogen bonding in the gel state.[26]
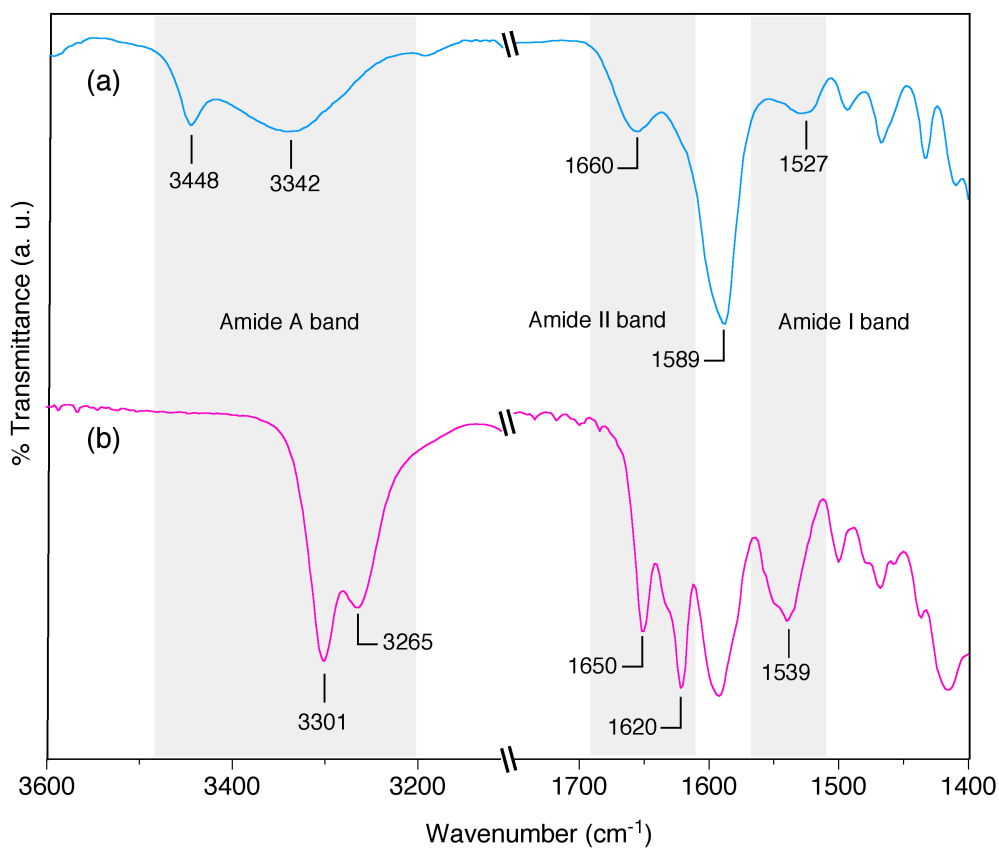
Figure 14. FT-IR spectra of **GA-SQ** (a) in CDCl$_3$ (4 mM) (b) xerogel film of *n*-butanol sonogel (4 mM).

Another clear change is the shift of symmetric and asymmetric CH$_2$ vibrations of **GA-SQ** in gel state to 2849 and 2918 cm^{-1} in comparison to those in CDCl$_3$, where they are observed at 2856 and 2928 cm^{-1} respectively (Figure 15). This observation implies that the alkyl chains of **GA-SQ** in the gel state are in all *trans* configuration and interdigitated.[28] Similar observations were made in the case of **GA-SQ** self-assembled precipitates formed by rapid cooling to 0 °C (Figure 16).
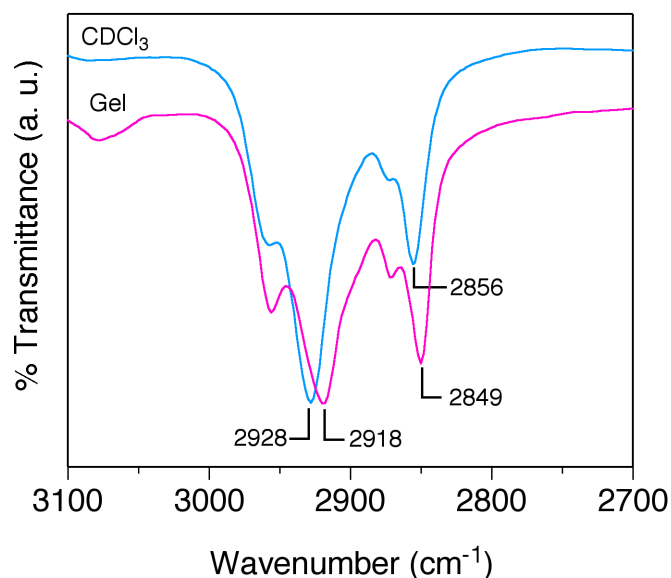
Figure 15. The FT-IR spectra of **GA-SQ** in CDCl₃ (4 mM) and xerogel film of n-butanol sonogel (4 mM) showing the asymmetric and symmetric methylene stretching.
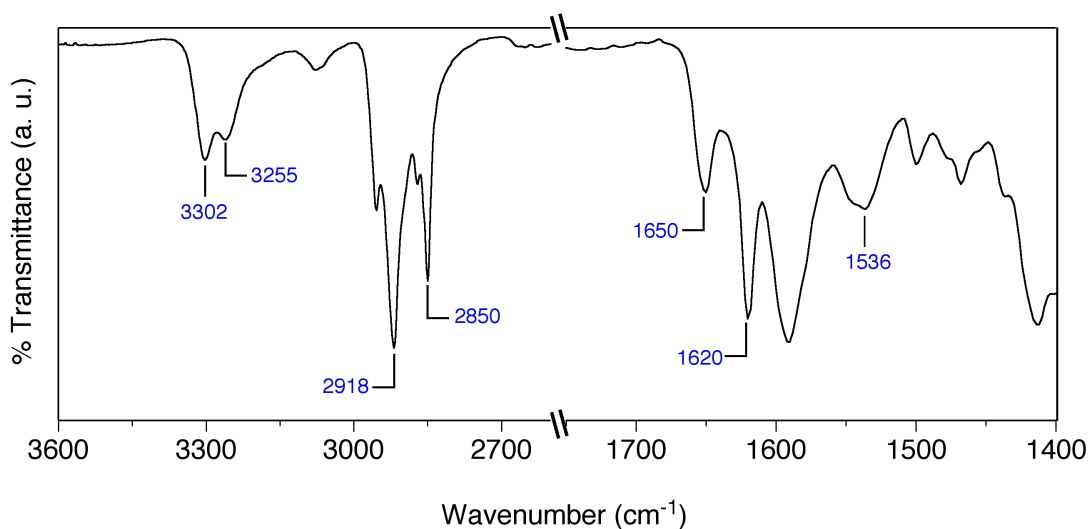
Figure 16. FT-IR spectra of **GA-SQ** self-assembled aggregates precipitated on rapid cooling of a hot n-butanol solution (4 mM) to 0 ℃.

To investigate the involvement of the squaraine moiety in the observed aggregation properties of **GA-SQ**, temperature dependent electronic absorption studies were performed, using the 2 mM *n*-butanol solution of **GA-SQ** that responds to sonication (Figure 17). As the temperature is increased from 20 to 56 ℃, the broad absorption in the wavelength region from

470 to 570 nm and the tail band observed between 675-800 nm exhibit a decrease in intensity with a concomitant increase in the absorption at 640 nm. These transitions are accompanied two isosbestic points at 575 and 675 nm. The absorption spectra at higher temperatures are found to be similar to those in CHCl$_3$, where **GA-SQ** mainly exists as a monomeric species. The absorption blue shift of the broad band with respect to the monomer suggests that the squaraine units are involved in *H*-type aggregation.[19c-e,h,24b] On the other hand, the presence of the red-shifted tail extended to the near IR region suggests the contribution of intermolecular charge transfer interaction in the aggregate formation.[24a] The formation of *H*-type aggregates is further confirmed by variable temperature emission studies (Figure 18). At low temperatures, the fluorescence of **GA-SQ** self-assembly is found to be completely quenched, which is a characteristic feature of *H*-type aggregation.[19c-e,h] The emission band is restored at higher temperatures due to conversion of self-assembled **GA-SQ** into monomeric species.
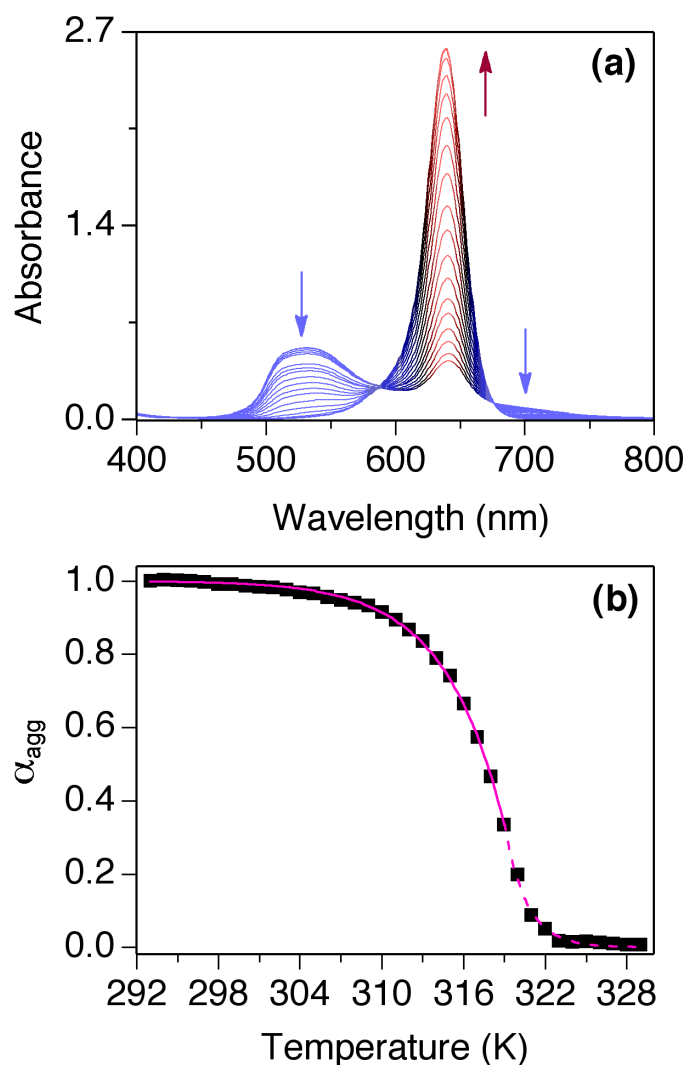
Figure 17. (a) Temperature dependent absorption spectra of **GA-SQ** *n*-butanol gel (2 mM) prepared by sonication (path length, $l = 0.05$ mm). Arrows indicates relative changes in absorption with increase in temperature from 20 to 56 °C. (b) The plot of fraction of aggregates (α_{agg}) versus temperature fitted within elongation (solid line) and nucleation (dashed line) regimes.

The melting curve obtained from the temperature dependent absorption studies is shown in Figure 17b. In order to demonstrate the involvement of nucleation and growth process in the observed self-assembly of **GA-SQ**, we have attempted to analyze the curve on the basis of the model proposed by van der Schoot, Schenning and Meijer.[19h,28] According to

this model, the fraction of aggregated molecules (α_{agg}) in the elongation and nucleation

regime can be defined by the following equations (1) and (2) respectively.

$$\alpha_{agg} = \alpha_{SAT} \left(1 - \exp\left[\frac{-h_e}{RT_e^2} (T - T_e) \right] \right) \qquad (1)$$

$$\alpha_{agg} = K_a^{1/3} \exp\left[(2/3\, K_a^{-1/3} - 1) \frac{h_e}{RT_e^2} (T - T_e) \right] \qquad (2)$$

The melting curve can be fitted with such elongation and nucleation functions. In the

elongation regime the fit provides the molecular enthalpy released due to noncovalent

interactions, h_e (−194 kJ/mol) and elongation temperature T_e (320.5 K). The other parameters

are the universal gas constant (R), absolute temperature (T) and α_{SAT}, a parameter necessary

to equate $\alpha_{agg}/\alpha_{SAT}$ to unity. Fit of the nucleation regime gave the equilibrium constant K_a

(5.3 x 10^{-3}) for the activation step at T_e. The satisfactory fit of the melting curve suggests the

cooperative assembly of molecules in the nucleation and elongation process.[19h,23e,28]

To look closely into the packing of the molecules in the self-assembled structures of

GA-SQ that are formed under different conditions, we have performed X-ray diffraction

(XRD) studies. Figure 18a shows the XRD pattern of the **GA-SQ** xerogel film, which exhibits

several well-resolved peaks characteristics of long range crystalline ordering of the molecules.

These peaks can be grouped and indexed in two different sets based on the ratio of the *d*

values. The first group shows reflections with *d* spacing of 4.17 (*100*), 2.08 (*200*), 1.39 (*300*),

1.04 (*400*), 0.69 (*600*), 0.59 (*700*) nm. This implies that, in the gel state, molecules maintain a

lamellar structure (Figure 18a inset) with the interlayer distance corresponding to 4.17

nm.[27b,29] A second group of peaks with *d* values of 1.74 (*010*), 0.86 (*020*), 0.43 (*040*), 0.29

(*060*) and 0.22 (*080*) nm indicate lateral packing of the molecules in the lamellar arrangement.

The intense and broad reflection at 2θ 20.6° (*040*) is found to consist of two shoulder peaks

with *d* spacing of 0.41 and 0.39 nm and can be ascribed to stacking of aromatic units assisted

by secondary amide hydrogen bonding[31] and crystalline packing of interdigitated alkyl chains respectively.[27a,29d] Next, we have investigated the XRD of **GA-SQ** self-assembled precipitates formed by heating and rapid cooling to 0 ºC. The diffractions peaks obtained from a thin film of precipitates are found to be less sharp in comparison to that of xerogel film (Figure 18b). Other noticeable differences are the absence of reflections corresponding to (*100*) and (*010*) planes and the presence of a diffuse halo due to the disordered packing of alkyl chains.[30c] The result of XRD studies suggest a less ordered lamellar arrangement of molecules in the polymorphic nanostructures observed for self-assembled precipitates in comparison to the sonication induced gel where only one kind of nanostructure formation is observed.
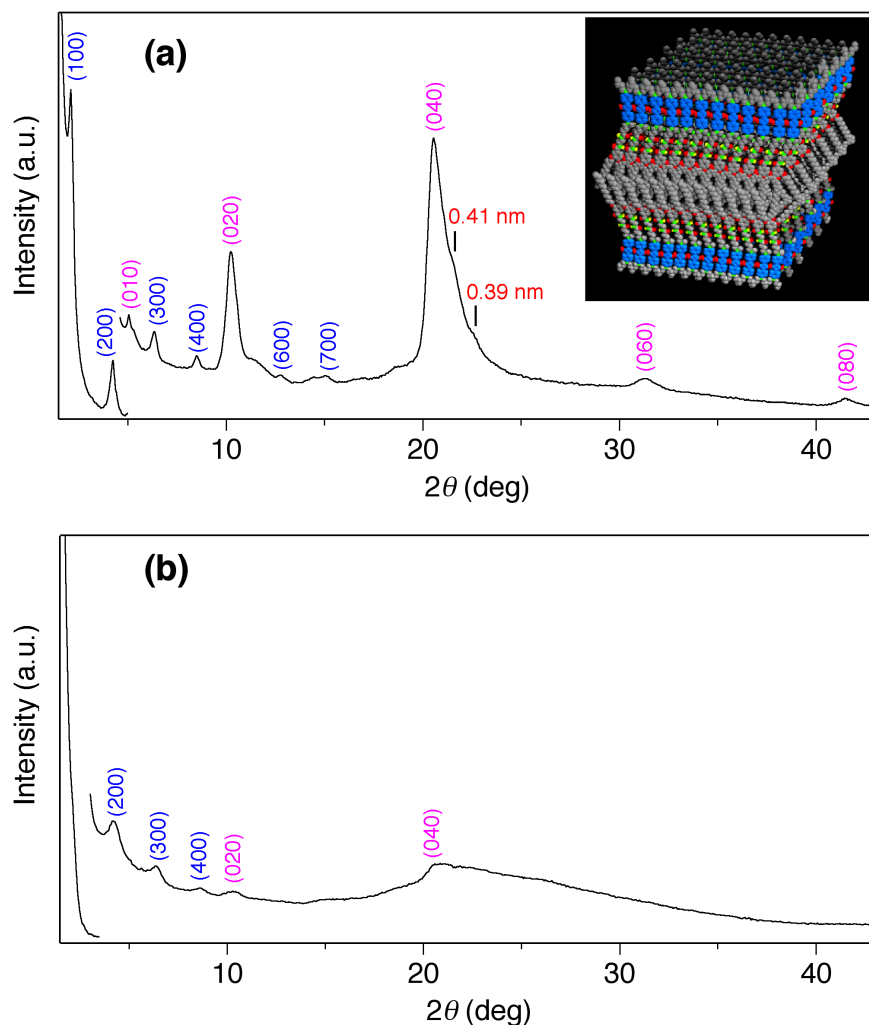
Figure 18. XRD patterns of **GA-SQ** (a) xerogel film of *n*-butanol gel (4 mM) prepared by sonication and (b) film of self-assembled aggregates obtained by rapid cooling of a hot *n*-butanol solution (4 mM) to 0 ºC. Inset shows schematic of possible lamellar packing diagram of **GA-SQ**.

3.4. Effect of Single Walled Carbon Nanotubes as a Nanoscale Substrate in the Sonication-Induced Self-Assembly of the Squaraine Organogelator

In principle, homogenous nucleation from the interior of a solution is difficult to occur.[22b] Generally, all nucleation events are heterogeneous in nature and always involve some kinds of substrates. Heterogeneous nucleation effectively decreases the energy barrier

for nucleation.[22b] For example, in the case of crystallization of molecules, seeding of crystal enhances the crystallization process. Similarly, in the case of polymers[31] and proteins,[32] the presence of substrates such as CNTs induce the crystallization process. CNTs are good choice as a nanoscale substrate also in supramolecular self-assembly, because of their propensity to facilitate the epitaxial growth of interacting molecules.[33] Furthermore, the involvement of CNTs in the nucleation and growth process of a supramolecular soft material can give rise to interesting properties. With this objective, we decided to study the influence of SWCNTs on the sonication induced self-assembling behavior of **GA-SQ**.

A very small amount of SWCNTs (~0.1 mg / 0.5 ml) was added to solutions of **GA-SQ** with concentration ranges from 0.01 to 4 mM. These samples were first heated at 70 ºC and then subjected to sonication for 5 min. Control experiments were also performed by sonicating another batch of the solutions prepared without adding SWCNTs. After sonication, the 0.01 mM solution of **GA-SQ** with SWCNTs showed no color change, likewise the control sample. When the concentration of **GA-SQ** was raised to 0.1 mM, the solution with SWCNTs changed its color indicating an aggregation process; at a concentration of 0.5 mM the formation of dark violet aggregates was observed (Figure 19a). On the contrary, sonication was not found to affect the **GA-SQ** solution in the reference samples without SWCNTs (Figure 19b). This observation indicates that the synergic effect of sonication and SWCNTs accelerates the aggregate formation of **GA-SQ** even at low concentrations. This underpins SWCNTs mediated heterogeneous nucleation and growth of **GA-SQ**.[31,32,34] Interestingly, after sonication of 1 and 2 mM solutions with SWCNTs, formation of semigel and stable gel were observed respectively (Figure 19a). In the absence of SWCNTs (see above) the semigel and gel of **GA-SQ** were observed for 2 and 4 mM respectively (Figure 9b). This means that the critical gelation concentration is reduced upon addition of a miniscule amount of SWCNTs. Further evidence to the role of ultrasonic waves in the SWCNTs mediated heterogeneous

nucleation of **GA-SQ** solutions is obtained from a control experiment in which the same solutions were heated to 70 ºC and left cooled spontaneously till room temperature. Without application of ultrasound, none of them were able to undergo aggregation (Figure 20).
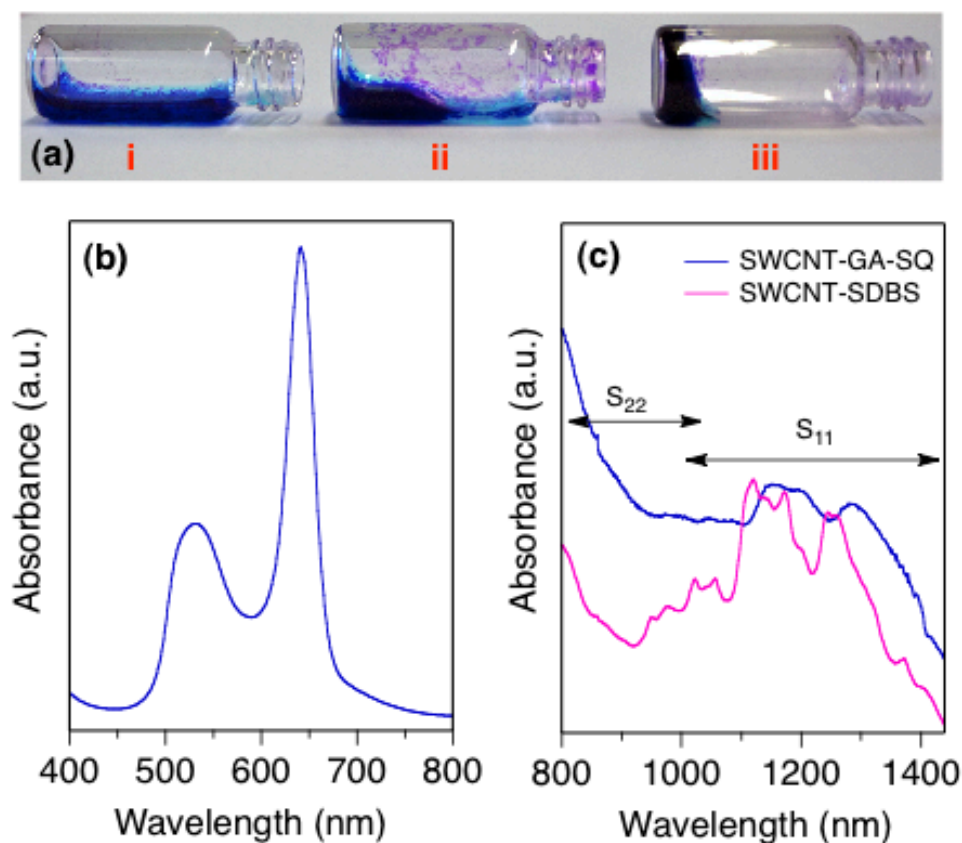
Figure 19. (a) Photograph showing the changes of **GA-SQ** *n*-butanol solutions containing 0.1 mg of SWCNTs after ultrasound irradiation for 5 min. Numbers correspond to the following concentration: i = 0.5, ii = 1 and iii = 2 mM. (b) Absorption spectrum of sonication induced aggregates of **GA-SQ** formed in the presence of 0.1 mg of SWCNTs (*n*-butanol, c = 0.5 mM, path length, l = 0.5 mm). (c) The absorption spectra of the same sample in the range 800-1400 nm showing van Hove singularities of SWCNTs. For a reference the absorption spectrum of SWCNTs dispersed in SDBS is also shown.
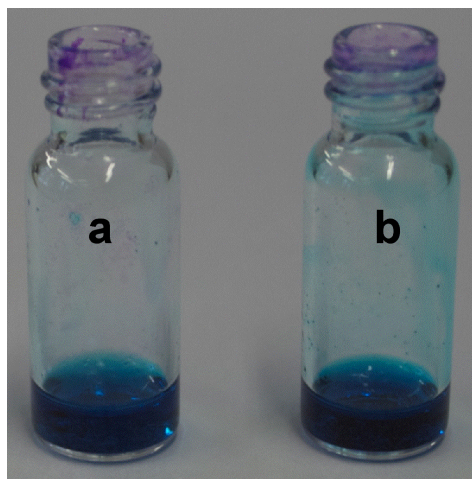
Figure 20. Photograph showing the changes of **GA-SQ** n-butanol solutions a) = 2 mM b) 4 mM containing 0.1 mg of SWCNTs after heating and cooling to room temperature (25 ºC).

The presence and involvement of SWCNTs in the observed self-assembly of **GA-SQ** can be easily probed by optical spectroscopy, through inspection of the peculiar absorption features of SWCNTs. Thus, the absorption spectrum of an aggregated solution of **GA-SQ** (0.5 mM), prepared by adding SWCNTs followed by heating and sonication, was recorded. The absorption spectrum shows the formation of the band corresponding to aggregated species of **GA-SQ** (λ_{max} = 540 nm, Figure 19b). In addition, the spectrum clearly exhibits well-defined absorption bands in the near IR region indicating van Hove singularities of dispersed SWCNTs (Figure 19c).[34,35] The absorptions corresponding to the electronic transitions of semiconducting nanotubes are observed between 750 and 900 nm (S_{22}) and 1000-1500 nm (S_{11}). The absorption features of metallic nanotubes are overlapped with the strong absorption of squaraines in the 400-700 nm region. The spectrum of SWCNTs dispersed in **GA-SQ** aggregates is then compared with that of SWCNTs dispersed in solution of sodium dodecylbenzenesulfonate (SDBS) in D_2O (Figure 19c). Even though the effect of solvent cannot be completely ruled out, a clear red shift and broadening of the first order semiconducting electronic transition S_{11} (1000-1500 nm) in the **GA-SQ** aggregates is

observable, most likely due to electronic interactions of the aromatic units of **GA-SQ** with SWCNTs.[36,37] Further evidence for the interaction between **GA-SQ** and SWCNTs is obtained from FT-IR studies. The aromatic C-H bending mode of **GA-SQ** observed between 700-900 cm^{-1} decreases its intensity in the presence of SWCNTs, indicating the strong interaction of aromatic moieties of **GA-SQ** with SWCNTs (Figure 21).[38]
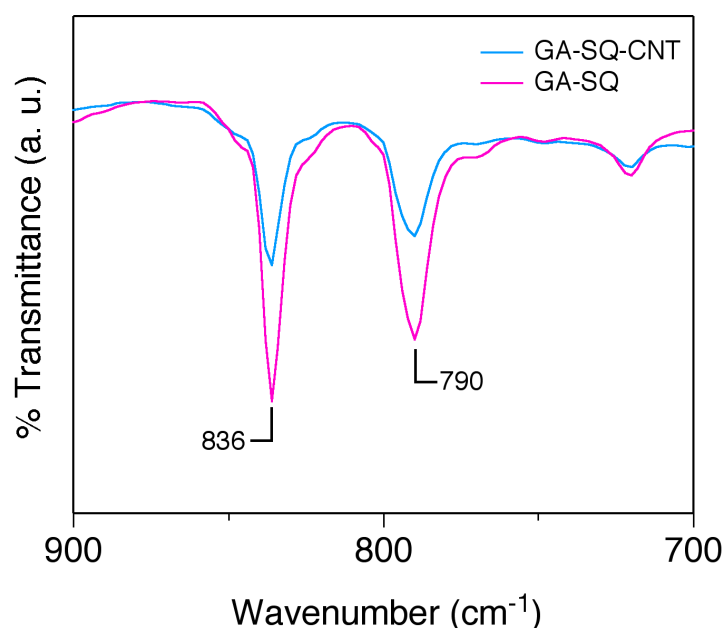
Figure 21. The FT-IR spectra of **GA-SQ** (2 mM) and SWCNTs doped **GA-SQ** (2 mM) xerogel films showing the aromatic C-H bending.

After having observed the impact of SWCNTs on the aggregation and optical properties of the **GA-SQ** self-assembly, we investigated their effect on the nanoscale morphology. SEM and TEM studies of **GA-SQ** gel (2 mM) showed the presence of micrometer long supramolecular nanotapes along with very few toroidal structures (Figure 22a and 22b). Merging of individual nanotapes results in bundles whose width varies from 30 to 300 nm. It should be noted that in the absence of SWCNTs, **GA-SQ** gel showed a rather different fiber-like morphology (Figure 13). The substantial difference in morphology

observed in the presence of very small amounts of SWCNTs indicates their influence in the self-assembling process of the squaraine molecule. The TEM studies of **GA-SQ** aggregates at lower concentration (0.5 mM) gave insight into this aspect. TEM micrograph of the sample clearly showed the formation of toroids as well as bundles of tapes (Figure 22c and 22d). In some cases these toroidal assemblies are found to open up as part of the tapes and their bundles.
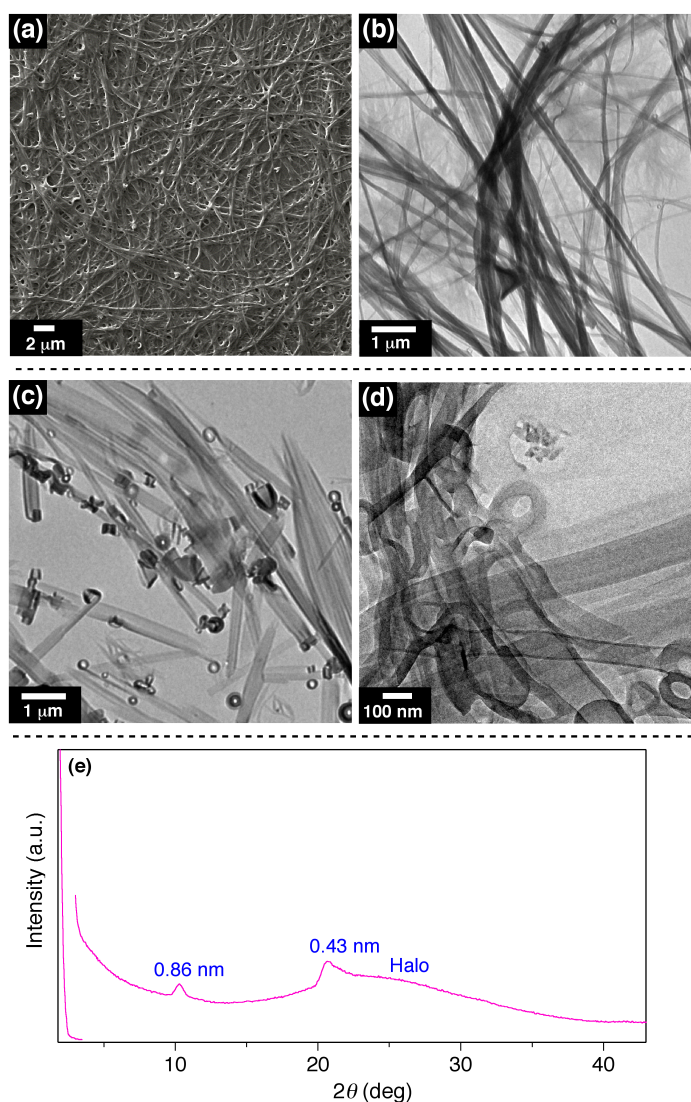
Figure 22. Effect of SWCNTs on the morphology of **GA-SQ** assembly. (a) SEM and (b) TEM images of **GA-SQ** gel (2 mM). (c) and (d) TEM images of **GA-SQ** aggregate (0. 5

mM). (e) XRD patterns of the xerogel film. The samples were prepared by adding a miniscule amount of SWCNTs to a hot solution of **GA-SQ** in *n*-butanol followed by sonication.

The observed difference in morphology is further confirmed by XRD studies. In contrast to the XRD profile of sonication-induced gel (Figure 18a), the gel formed in the presence of SWCNTs showed a XRD profile consisting of only few peaks (Figure 8e). It displayed two diffraction peaks at 2θ 20.68 and 10.28 with d spacing of 0.43 and 0.86 nm respectively. The peak at 2θ 20.68 is found to be broad and a contain a small shoulder peak presumably due to the presence of reflection corresponding to stacking of aromatic units assisted by hydrogen bonding.[30] The presence of a diffuse halo in the wide-angle region indicates alkyl chains are packed in a disordered manner.[30c]

3.5. Conclusion

We have shown that a suitably designed squaraine dye equipped with dodecyloxy galloyl diamide unit (**GA-SQ**), undergoes ultrasound triggered self-assembly and gelation, a hitherto unknown property for this class of molecules. The application of ultrasound is found to modify the conditions for the supersaturation mediated nucleation and growth of **GA-SQ** self-assembly, which is apparent from the reluctance of the squaraine derivative to undergo aggregation by heating and slow cooling without sonication. On the other hand, self-assembly induced by just heating and rapid cooling to 0 ºC results in the formation of precipitates consisting of polymorphic nanostructures. Extended morphological analysis reveals that sonication prompts the formation of only one kind of nuclei leading to extended crystalline fibrous structures. Interestingly, the sonication of **GA-SQ** solutions containing a minuscule amount of SWCNTs promotes self-assembling in a lower concentration regime, where mere sonication has no effect. The presence of the nanoscale substrate yields a nanotape-like morphology, which highlights the importance of nucleation events in shaping the final self-

assembled material.[38] For the sonication induced gelation of **GA-SQ,** nucleation and growth is mainly determined by the crystalline packing of hydrophobic alkyl chains and hydrogen bonding, which promote the π-π stacking of the aromatic units. While, in the presence of SWCNTs, the adsorption of molecules on the heterogeneous surface, leads to a nucleation process assisted by π-stacking and hydrogen bonding. In this scenario, the establishment of a crystalline arrangement of the hydrophobic alkyl chains is more unlikely.

The strategy presented in this study paves the way to the rational preparation of nanostructured composites made of technologically relevant components such as functional dyes (squaraines) and carbon allotropes (fullerenes, CNTs and graphene), with cheap and facile methods. The application of these intimately mixed composites as active materials in organic electronic devices for light-energy conversion and related application is a subject worth of investigation.

References

(1)   Faraday, M. *Philos. Trans. R. Soc. London*, **1831**, *121*, 299-340.

(2)   (a) Suslick, K. S.; Price, G. J. *Annua. Rev. Mater. Sci.*, **1999**, *29*, 295. (b) Gedanken, A.; Tang, X; Wang, Y.; Perkas, N.; Koltypin, Y.; Landau, M. V.; Vradman, L.; Herskowitz, M. *Chem. Eur. J.* **2001**, *7*, 4546-4552 (c) Suh, W. H.; Jang, A. R.; Suh, Y.-H.; Suslick, K. S. *Adv. Mat.* **2006**, *18*, 1832-1837.

(3)   Crum, L. A., Mason, T. J.; Reisse, J.; Suslick, K. S. *Sonochemstry and Sonoluminescence*, Kluwer, Dordrecht, **1999**, vol. 524.

(4)   (a) Suslick, K. S. *Science*, **1990**, *247*, 1439-1445. (b) Gedanken, A. *Chem. Eur. J.* **2008**, *14*, 3840-3853.

(5)   (a) Suslick, K. S.; Flannigan, D. J. *Annu. Rev. Phys. Chem.* **2008**, *56*, 659-683. (b) Skrabalak, S. E. *Phys. Chem. Chem. Phys.* **2009**, *11*, 4930-4942.

(6)   Paulusse, J. M. J.; van Beek, D. J. M.; Sijbesma, R. P. *J. Am. Chem. Soc.* **2007**, *129*, 2392–2397.

(7)   (a) Watson, T. *Ultrasonics* **2008**, *48*, 321–329. (b) Prausnitz, M. R.; Langer, R. *Nat. Biotechnol.* **2008**, *26*, 1261–1268.

(8)   (a) Thompson, L. H.; Doraiswamy, L. K. *Chem. Eng. Sci.* **2000**, *55*, 3085–3090. (b) Ruecroft, G.; Hipkiss, D.; Ly, T.; Maxted, N.; Cains, P. W. *Org. Process Res. Dev.* **2005**, *9*, 923–932. (c) Luque de Castro, M. D.; Priego-Capote, F. *Ultrason. Sonochem.* **2007**, *14*, 717–724.

(9)   Richards, W. T.; Loomis, A. L. *J. Am. Chem. Soc.* **1927**, *49*, 3086–3100.

(10)   (a) Paulusse, J. M. J.; Sijbesma, R. P. *Angew. Chem., Int. Ed.* **2006**, *45*, 2334–2337. (b) Bardelang, D. *Soft Matter* **2009**, *5*, 1969–1971. (c) Cravotto, G.; Cintas, P. *Chem. Soc. Rev.* **2009**, *38*, 2684–2697.

(11)   Isozaki, K.; Takaya, H.; Naota, T. *Angew. Chem., Int. Ed.* **2007**, *46*, 2855–2857.

(12)   (a) Weng, W.; Beck, J. B.; Jamieson, A. M.; Rowan, S. J. *J. Am. Chem. Soc.* **2006**, *128*, 11663–11672. (b) Zhang, S.; Yang, S.; Lan, J.; Tang, Y.; Xue, Y.; You, J. *J. Am. Chem. Soc.* **2009**, *131*, 1689–1691. (c) He, Y.; Bian, Z.; Kang, C.; Jin, R.; Gao, L. *New J. Chem.* **2009**, *33*, 2073–2080. (d) Sambri, L.; Cucinotta, F.; De Paoli, G.; Stagni, S.; De Cola, L. *New J. Chem.* **2010**, *34*, 2093–2096. (e) Kotal, A.; Paira, T. K.; Banerjee, S.; Mandal, T. K. *Langmuir* **2010**, *26*, 6576–6582. (f) Komiya, N.; Muraoka, T.; Iida, M.; Miyanaga, M.; Takahashi, K.; Naota, T. *J. Am. Chem. Soc.* **2011**, *133*, 16054–16061.

(13)   (a) Li, Y.; Wang, T.; Liu, M. *Tetrahedron* **2007**, *63*, 7468–7473. (b) Wang, X.; Kluge, J. A.; Leisk, G. G.; Kaplan, D. L. *Biomaterials* **2008**, *29*, 1054–1064. (c) Bardelang, D.; Camerel, F.; Margeson, J. C.; Leek, D. M.; Schmutz, M.; Zaman, M. B.; Yu, K.; Soldatov, D. V.; Ziessel, R.; Ratcliffe, C. I.; Ripmeester, J. A. *J. Am. Chem. Soc.* **2008**, *130*, 3313–3315. (d) Bardelang, D.; Zaman, M. B.; Moudrakovski, I. L.; Pawsey, S.; Margeson, J. C.; Wang, D.; Wu, X.; Ripmeester, J. A.; Ratcliffe, C. I.; Yu, K. *Adv. Mater.* **2008**, *20*, 4517–4520. (e) Wang, Y.; Zhan, C.; Fu, H.; Li, X.; Sheng, X.; Zhao, Y.; Xiao, D.; Ma, Y.; Ma, J. S.; Yao, J. *Langmuir* **2008**, *24*, 7635–7638.

(14)   (a) Xie, Z.; Zhang, A.; Ye, L.; Feng, Z.-g. *Soft Matter* **2009**, *5*, 1474–1482. (b) Ke, D.; Zhan, C.; Li, A. D. Q.; Yao, J. *Angew. Chem., Int. Ed.* **2011**, *50*, 3715–3719. (c) Maity, S.; Kumar, P.; Haldar, D. *Soft Matter* **2011**, *7*, 5239–5245. (d) Maity, S.; Sarkar, S.; Jana, P.; Maity, S. K.; Bera, S.; Mahalingam, V.; Haldar, D. *Soft Matter* **2012**, *8*, 3960–3966. (e) Maity, I.; Rasale, D. B.; Das, A. K. *Soft Matter* **2012**, *8*, 5301–5308. (i) Afrasiabi, R.; Kraatz, H.-B. *Chem. –Eur. J.* **2013**, *19*, 1769–1777.

(15)   (a) Wu, J.; Yi, T.; Shu, T.; Yu, M.; Zhou, Z.; Xu, M.; Zhou, Y.; Zhang, H.; Han, J.; Li, F.; Huang, C. *Angew. Chem., Int. Ed.* **2008**, *47*, 1063–1067. (b) Wu, J.; Yi, T.; Xia, Q.; Zou, Y.; Liu, F.; Dong, J.; Shu, T.; Li, F.; Huang, C. *Chem. –Eur. J.* **2009**, *15*, 6234–6243. (c) Yu, X.; Liu, Q.; Wu, J.; Zhang, M.; Cao, X.; Zhang, S.; Wang, Q.; Chen, L.;

Yi, T. *Chem. –Eur. J.* **2010**, *16*, 9099–9106. (d) Dou, C.; Wang, C.; Zhang, H.; Gao, H.; Wang, Y. *Chem. –Eur. J.* **2010**, *16*, 10744–10751. (e) Dou, C.; Li, D.; Gao, H.; Wang, C.; Zhang, H.; Wang, Y. *Langmuir* **2010**, *26*, 2113–2118. (f) Dou, C.; Li, D.; Zhang, H.; Gao, H.; Zhang, J.; Wang, Y. *Sci. China Chem.* **2011**, *54*, 641–650. (g) Cho, Y.; Lee, J. H.; Jaworski, J.; Park, S.; Lee, S. S.; Jung, J. H. *New J. Chem.* **2012**, *36*, 32–35. (h) Liu, Z.-X.; Feng, Y.; Yan, Z.-C.; He, Y.-M.; Liu, C.-Y.; Fan, Q.-H. *Chem. Mater.* **2012**, *24*, 3751–3757.

(16)   (a) Wang, C.; Zhang, D.; Zhu, D. *J. Am. Chem. Soc.* **2005**, *127*, 16372–16373. (b) Anderson, K. M.; Day, G. M.; Paterson, M. J.; Byrne, P.; Clarke, N.; Steed, J. W. *Angew. Chem., Int. Ed.* **2008**, *47*, 1058–1062. (c) Cao, Y.; Tang, L. M.; Wang, Y. J.; Zhang, B. Y.; Jia, L. K. *Chem. Lett.* **2008**, *37*, 554–555. (d) Yamanaka, M.; Fujii, H. *J. Org. Chem.* **2009**, *74*, 5390–5394. (e) You, Y.-Z.; Yan, J.-J.; Yu, Z.-Q.; Cui, M.-M.; Hong, C.-Y.; Qu, B.-J. *J. Mater. Chem.* **2009**, *19*, 7656–7660. (f) Wang, R.-Y.; Liu, X.-Y.; Li, J.-L. *Cryst. Growth Des.* **2009**, *9*, 3286–3291. (g) Deng, C.; Fang, R.; Guan, Y.; Jiang, J.; Lin, C.; Wang, L. *Chem. Commun.* **2012**, *48*, 7973–7975.

(17)   Trivedi, D. R.; Dastidar, P. *Chem. Mat.* **2006**, *63*, 1470-1478.

(18)   (a) Law, K.-Y. *Chem. Rev.* **1993**, *93*, 449–486. (b) Ajayaghosh, A. *Acc. Chem. Res.* **2005**, *38*, 449–459. (c) Sreejith, S.; Carol, P.; Chithra, P.; Ajayaghosh, A. *J. Mater. Chem.* **2008**, *18*, 264–274. (d) Yagi, S.; Nakazumi, H. *Top. Heterocycl. Chem.* **2008**, *14*, 133–181. (e) McEwen, J. J.; Wallace, K. J. *Chem. Commun.* **2009**, 6339–6351. (f) Gassensmith, J. J.; Baumes, J. M.; Smith, B. D. *Chem. Commun.* **2009**, 6329–6338. (g) Beverina, L.; Salice, P. *Eur. J. Org. Chem.* **2010**, 1207–1225. (h) Avirah, R. R.; Jayaram, D. T.; Adarsh, N.; Ramaiah, D. *Org. Biomol. Chem.* **2012**, *10*, 911–920.

(19)   (a) Geiger, C.; Stanescu, M.; Chen, L.; Whitten, D. G. *Langmuir* **1999**, *15*, 2241–2245. (b) Jyothish, K.; Hariharan, M.; Ramaiah, D. *Chem. –Eur. J.* **2007**, *13*, 5944–5951. (c)

Ajayaghosh, A.; Chithra, P.; Varghese, R. *Angew. Chem., Int. Ed.* **2007**, *46*, 230–233. (d) Chithra, P.; Varghese, R.; Divya, K. P.; Ajayaghosh, A. *Chem. –Asian J.* **2008**, *3*, 1365–1373. (e) Ajayaghosh, A.; Chithra, P.; Varghese, R.; Divya, K. P. *Chem. Commun.* **2008**, 969–971. (f) Zhang, C.; Zhang, X.; Zhang, X.; Fan, X.; Jie, J.; Chang, J. C.; Lee, C.-S.; Zhang, W.; Lee, S.-T. *Adv. Mater.* **2008**, *20*, 1716–1720. (g) Wu, J.; Yi, T.; Zou, Y.; Xia, Q.; Shu, T.; Liu, F.; Yang, Y.; Li, F.; Chen, Z.; Zhou, Z.; Huang, C. *J. Mater. Chem.* **2009**, *19*, 3971–3978. (h) Mayerhöffer, U.; Würthner, F. *Chem. Sci.* **2012**, *3*, 1215–1220. (i) Ohsedo, Y.; Miyamoto, M.; Oono, M.; Shikii, K.; Tanaka, A. *RSC Adv.* **2013**, *3*, 3844–3847.

(20) (a) Silvestri, F.; Irwin, M. D.; Beverina, L.; Facchetti, A.; Pagani, G. A.; Marks, T. J. *J. Am. Chem. Soc.* **2008**, *130*, 17640–17641. (b) Wang, S.; Hall, L.; Diev, V. V.; Haiges, R.; Wei, G.; Xiao, X.; Djurovich, P. I.; Forrest, S. R.; Thompson, M. E. *Chem. Mater.* **2011**, *23*, 4789–4798. (c) Chen, G.; Sasabe, H.; Wang, Z.; Wang, X.-F.; Hong, Z.; Yang, Y.; Kido, J. *Adv. Mater.* **2012**, *24*, 2768–2773. (d) Deing, K. C.; Mayerhöffer, U.; Würthner, F.; Meerholz, K. *Phys. Chem. Chem. Phys.* **2012**, *14*, 8328–8334.

(21) (a) Ghosh, S.; Li, X.-Q.; Stepanenko, V.; Würthner, F. *Chem. –Eur. J.* **2008**, *14*, 11343–11357. (b) Dawn, A.; Fujita, N.; Haraguchi, S.; Sada, K.; Shinkai, S. *Chem. Commun.* **2009**, 2100–2102. (c) Chen, H.; Herkstroeter, W. G.; Perlstein, J.; Law, K.-Y.; Whitten, D. G. *J. Phys. Chem.* **1994**, *98*, 5138–5146. (d) Stanescu, M.; Samha, H.; Perlstein, J.; Whitten, D. G. *Langmuir* **2000**, *16*, 275–281. (e) De Selms, R. C.; Fox, C. J.; Riordan, R. C. *Tetrahedron Lett.* **1970**, *11*, 781–782. (f) Keil, D.; Hartmann, H. *Dyes Pigm.* **2001**, *49*, 161–179.

(22) Terech, P.; Weiss, R. G. *Chem. Rev.* **1997**, *97*, 3133–3160. (b) Li, J.-L.; Liu, X.-Y. *Adv. Funct. Mater.* **2010**, *20*, 3196–3216.

(23)   Trialkoxy galloyl amide unit is an efficient self-assembly inducing segment, see: (a) Kitahara, T.; Shirakawa, M.; Kawano, S.-i.; Beginn, U.; Fujita, N.; Shinkai, S. *J. Am. Chem. Soc.* **2005**, *127*, 14980–14981. (b) Li, Y.; Wong, K. M.-C.; Tam, A. Y.-Y.; Wu, L.; Yam, V. W.-W. *Chem. –Eur. J.* **2010**, *16*, 8690–8698. (c) Das, A.; Ghosh, S. *Chem. Commun.* **2011**, *47*, 8922–8924. (d) Stone, D. A.; Tayi, A. S.; Goldberger, J. E.; Palmer, L. C.; Stupp, S. I. *Chem. Commun.* **2011**, *47*, 5702–5704. (e) Aparicio, F.; García, F.; Sanchez, L. *Chem. –Eur. J.* **2013**, *19*, 3239–3248.

(24)   (a) Law, K.-Y. *J. Phys. Chem.* **1988**, *92*, 4226–4231. (b) Liang, K.; Law, K.-Y.; Whitten, D. G. *J. Phys. Chem.* **1994**, *98*, 13379–13384. (c) Chen, H.; Farahat, M. S.; Law, K.-Y.; Whitten, D. G. *J. Am. Chem. Soc.* **1996**, *118*, 2584–2594.

(25)   (a) Fages, F.; Vögtle, F.; Žinić, M. *Top. Curr. Chem.* **2005**, *256*, 77–131. (b) Ajayaghosh, A.; George, S. J.; Schenning, A. P. H. J. *Top. Curr. Chem.* **2005**, *258*, 83–118. (c) Yagai, S. *J. Photochem. Photobiol., C* **2006**, *7*, 164–182. (d) González-Rodríguez, D.; Schenning, A. P. H. J. *Chem. Mater.* **2011**, *23*, 310–325.

(26)   (a) Skrovanek, D. J.; Howe, S. E.; Painter, P. C.; Coleman, M. M. *Macromolecules* **1985**, *18*, 1676–1683. (b) Herrebout, W.; Clou, K.; Desseyn, H. O.; Blaton, N. *Spectrochim. Acta, Part A* **2003**, *59*, 47–59. (c) Jahnke, E.; Weiss, J.; Neuhaus, S.; Hoheisel, T. N.; Frauenrath, H. *Chem. –Eur. J.* **2009**, *15*, 388–404.

(27)   (a) Kameta, N.; Masuda, M.; Minamikawa, H.; Shimizu, T. *Langmuir* **2007**, *23*, 4634−4641. (b) Nakanishi, T.; Michinobu, T.; Yoshida, K.; Shirahata, N.; Ariga, K.; Möhwald, H.; Kurth, D. G. *Adv. Mater.* **2008**, *20*, 443−446. (c) Jin, W.; Yamamoto, Y.; Fukushima, T.; Ishii, N.; Kim, J.; Kato, K.; Takata, M.; Aida, T. *J. Am. Chem. Soc.* **2008**, *130*, 9434–9440.

(28)   (a) Jonkheijm, P.; van der Schoot, P.; Schenning, A. P. H. J.; Meijer, E. W. *Science* **2006**, *313*, 80–83. (b) Smulders, M. M. J.; Schenning, A. P. H. J.; Meijer, E. W. *J. Am. Chem. Soc.* **2008**, *130*, 606–611.

(29)   (a) Estroff, L. A.; Leiserowitz, L.; Addadi, L.; Weiner, S.; Hamilton, A. D. *Adv. Mater.* **2003**, *15*, 38–42. (b) Ryu, J.-H.; Lee, E.; Lim, Y.-b.; Lee, M. *J. Am. Chem. Soc.* **2007**, *129*, 4808–4814. (c) Yagai, S.; Kinoshita, T.; Higashi, M.; Kishikawa, K.; Nakanishi, T.; Karatsu, T.; Kitamura, A. *J. Am. Chem. Soc.* **2007**, *129*, 13277–13287. (d) Cao, H.; Yuan, Q.; Zhu, X.; Zhao, Y.-P.; Liu, M. *Langmuir* **2012**, *28*, 15410–15417.

(30)   (a) Lewis, F. D.; Yang, J.-S.; Stern, C. L. *J. Am. Chem. Soc.* **1996**, *118*, 2772–2773. (b) Abbel, R.; van der Weegen, R.; Pisula, W.; Surin, M.; Leclère, P.; Lazzaroni, R.; Meijer, E. W.; Schenning, A. P. H. J. *Chem. –Eur. J.* **2009**, *15*, 9737–9746. (c) Diring, S.; Camerel, F.; Donnio, B.; Dintzer, T.; Toffanin, S.; Capelli, R.; Muccini, M.; Ziessel, R. *J. Am. Chem. Soc.* **2009**, *131*, 18177–18185.

(31)   Li, L.; Li, B.; Hood, M. A.; Li, C. Y. *Polymer* **2009**, *50*, 953–965.

(32)   (a) Linse, S.; Cabaleiro-Lago, C.; Xue, W.-F.; Lynch, I.; Lindman, S.; Thulin, E.; Radford, S. E.; Dawson, K. A. *Proc. Nat. Acad. Sci. U. S. A.* **2007**, *104*, 8691–8696. (b) Thauvin, C.; Rickling, S.; Schultz, P.; Célia, H.; Meunier, S.; Mioskowski, C. *Nat. Nanotech.* **2008**, *3*, 743–748. (c) Asanithi, P.; Saridakis, E.; Govada, L.; Jurewicz, I.; Brunner, E. W.; Ponnusamy, R.; Cleaver, J. A. S.; Dalton, A. B.; Chayen, N. E.; Sear, R. P. *ACS Appl. Mater. Interfaces* **2009**, *1*, 1203–1210.

(33)   (a) Srinivasan, S.; Ajayaghosh, A. Interaction of Carbon Nanotubes and Small Molecules. In *Supramolecular Soft Matter: Applications in Materials and Organic Electronics*; Nakanishi, T., Ed.; Wiley & Sons: Hoboken, New Jersey, 2011; Chapter 19, pp 381-406. (b) Fukushima, T.; Aida, T. *Chem. –Eur. J.* **2007**, *13*, 5048–5058.

(34)   (a) Srinivasan, S.; Babu, S. S.; Praveen, V. K.; Ajayaghosh, A. *Angew. Chem., Int. Ed.* **2008**, *47*, 5746–5749. (b) Tan, Z.; Ohara, S.; Naito, M.; Abe, H. *Adv. Mater.* **2011**, *23*, 4053–4057. (c) Samanta, S. K.; Subrahmanyam, K. S.; Bhattacharya, S.; Rao, C. N. R. *Chem. –Eur. J.* **2012**, *18*, 2890–2901.

(35)   (a) Backes, C.; Schmidt, C. D.; Hauke, F.; Böttcher, C.; Hirsch, A. *J. Am. Chem. Soc.* **2009**, *131*, 2172–2184. (b) Backes, C.; Mundloch, U.; Ebel, A.; Hauke, F.; Hirsch, A. *Chem. –Eur. J.* **2010**, *16*, 3314–3317. (c) Sprafke, J. K.; Stranks, S. D.; Warner, J. H.; Nicholas, R. J.; Anderson, H. L. *Angew. Chem., Int. Ed.* **2011**, *50*, 2313–2316. (d) Romero-Nieto, C.; García, R.; Herranz, M. Á.; Ehli, C.; Ruppert, M.; Hirsch, A.; Guldi, D. M.; Martín, N. *J. Am. Chem. Soc.* **2012**, *134*, 9183–9192.

(36)   (a) Yanagi, K.; Iakoubovskii, K.; Matsui, H.; Matsuzaki, H.; Okamoto, H.; Miyata, Y.; Maniwa, Y.; Kazaoui, S.; Minami, N.; Kataura, H. *J. Am. Chem. Soc.* **2007**, *129*, 4992–4997. (b) Tsuchikawa, R.; Ahn, H.-Y.; Yao, S.; Belfield, K. D.; Ishigami, M. *J. Phys.: Condens. Matter* **2011**, *23*, 202204. (c) Xu, Y.; Malkovskiy, A.; Pang, Y. *Chem. Commun.* **2011**, *47*, 6662–6664.

(37)   (a) Zhang, J.; Lee, J. K.; Wu, Y.; Murray, R. W. *Nano Lett.* **2003**, *3*, 403–407. (b) Srinivasan, S.; Praveen, V. K.; Philip, R.; Ajayaghosh, A. *Angew. Chem., Int. Ed.* **2008**, *47*, 5750–5754.

(38)   (a) van der Laan, S.; Feringa, B. L.; Kellogg, R. M.; van Esch, J. *Langmuir* **2002**, *18*, 7136–7140. (b) Babu, S. S.; Möhwald, H.; Nakanishi, T. *Chem. Soc. Rev.* **2010**, *39*, 4021–4035. (c) Tevis, I. D.; Palmer, L. C.; Herman, D. J.; Murray, I. P.; Stone, D. A.; Stupp, S. I. *J. Am. Chem. Soc.* **2011**, *133*, 16486–16494. (d) Gopal, A.; Varghese, R.; Ajayaghosh, A. *Chem. –Asian J.* **2012**, *7*, 2061–2067.

Chapter 4

Experimental Section

4.1. Photophysical Studies

The photophysical studies were carried out in solvents of spectrofluorimetric grade without further purification. Absorption spectra were recorded with a Perkin–Elmer Lambda 950 UV/vis/NIR spectrophotometer in Hellma quartz cells ($l = 1$ cm). Absorption studies of the gelation/aggregation processes in n-butanol were carried out in a demountable flow cuvette with an option to vary path lengths using spacers of different thickness (FLAB-50-UV-01, GL Sciences, Japan). Molar absorption values (ε) were calculated by applying the Lambert–Beer law to the absorbance spectra ($A_{max} < 0.7$) of the compounds. The temperature of the samples was varied with HAAKE F3-C digital heated/refrigerated water bath (HAak Mess-Technick Gmbh u. Co., Germany), which can be manually connected to cuvette holder and, externally controlled.

Steady-state photoluminescence spectra were recorded in the right angle mode with an Edinburgh FLS920 spectrometer (continuous 450 W Xe lamp), equipped with a Peltier-cooled Hamamatsu R928 photomultiplier tube (185–850 nm) or a Hamamatsu R5509-72 supercooled photomultiplier tube (193 K, 800–1700 nm range). Emission quantum yields were determined according to the approach described by Demas and Crosby,[1] using quinine sulfate ($\Phi_{em} = 0.546$ in air-equilibrated acid water solution, 1 M H_2SO_4) and [Ru(bpy)$_3$Cl$_2$] ($\Phi_{em} = 0.028$ in air-equilibrated water solution)[2] as standards. Capillary tubes immersed in liquid nitrogen in a coldfinger quartz Dewar were used for measurements of solvent frozen glasses at 77 K. Temperature dependent photoluminescence was recorded on SPEX-Flourolog F112X spectrofluorimeter using front face geometry. Steady-state photoluminescence in the solid state was recorded using KBr discs in the right angle mode with an Edinburgh FLS920 spectrometer. Luminescence quantum yield, Φ_{em}, have been calculated by corrected emission spectra obtained from an apparatus consisting of a barium sulfate coated integrating sphere, Edinburgh FLS920 spectrometer, continuous 450 W Xe lamp as light source and a R928

photomultiplayer tube as signal detector, following the procedure described by De Mello et al.[3]

Fluorescence lifetimes were measured with (i) an IBH 5000F time-correlated single-photon counting device, by using pulsed NanoLED excitation source; analysis of the luminescence decay profiles against time was accomplished with the Decay Analysis Software DAS6 provided by the manufacturer; (ii) a Perkin-Elmer LS-50B spectrofluorimeter equipped with a pulsed Xe lamp and in gated detection mode; the phosphorescence decay analysis was performed with the PHOSDecay software provided by the manufacturer.

4.2. Electrochemistry

Electrochemical experiments have been performed at room temperature, after argon purging, with an AMEL 5000 electrochemical system in dichloromethane (DCM, Carlo Erba RPE, distilled over phosphoric anhydride and stored under argon pressure) and $0.1 \ mol \cdot L^{-1}$ tetrabuthylammonium perchlorate (TBAP, Fluka, crystallized from methanol and vacuum dried). Cyclic voltammetries have been performed in a home made three-compartment cell with Pt disc electrode (diameter 1 mm), Pt wire counter electrode and aqueous KCl Satured Calomel Electrode (SCE) whose potential is -0.47 V vs. ferrocene/ferricinium (Fc/Fc$^+$).[4]

4.3. Gelation Studies and Sample Preparation for IR and XRD Analysis

A weighed amount of the **GA-SQ** in an appropriate solvent (0.5 mL) was placed in a sealed glass vial (1 cm diameter) and dissolved by heating at 70 ºC. The solution was then subjected to sonication ($0.23 \ W/cm^2$, 37 kHz, bath temperature 25 ºC, Elmasonic S10H,) for 2 minutes. The sonication-induced gelation was considered successful if no sample flow was observed upon tilting the sample vial upside down. To study the effect of carbon nanotubes,

SWCNTs were purchased from Unidym Inc (purified HiPco-SWCNTs, batch number: P2150) and used as received. A miniscule amount of SWCNTs (~0.1 mg/0.5 ml) was added quickly to a solution of **GA-SQ** in *n*-butanol prepared by heating at 70 ºC and the mixture was subjected to sonication for 5 min.

References

(1)   Crosby, G. A.; Demas, J. N. *J. Phys. Chem.* **1971**, *75*, 991.

(2)   Meech, S. R.; Phillips, D. *J. Photochem*. **1983**, *23*, 193.

(3)   de Mello, J. C.; Wittmann, H. F.; Friend, R. H. *Adv. Mater.* **1997**, *9*, 230-232.

(4)   Gratzner, J.; Kuta, J. *Pure Appl. Chem.* **1984**, *56*, 461-466.

List of Publications

Joanna M. Malicka, Anjamkudy Sandeep, Filippo Monti, Elisa Bandini, Massimo Gazzano, Choorikkat Ranjith, Vakayil K. Praveen, Ayyappanpillai Ajayaghosh and Nicola Armaroli *"Extended Gel Nanostructures of a Functional Squaraine Dye by Ultrasound Stimulation"*, *submitted*

Laura Maggini, Tomas Marangoni, Benoit Georges, **Joanna M. Malicka**, K. Yoosaf, Andrea Minoia, Roberto Lazzaroni, Nicola Armaroli, and Davide Bonifazi. "Azobenzene-based supramolecular polymers for processing MWCNTs*" Nanoscale* **2013**, *5*, 634–645.

Laura Maggini, Francesca M. Toma, Luigi Feruglio, **Joanna M. Malicka**, Tatiana Da Ros, Nicola Armaroli, Maurizio Prato, and Davide Bonifazi "Luminescent Blooming of Dendronic Carbon Nanotubes through Ion-Pairing Interactions with an Eu[III] Complex" *Chem. Eur. J.* 2012, *18*, 5889-5897.

Julien Iehl, Michel Holler, Jean-François Nierengarten, K. Yoosaf, **Joanna M. Malicka**, Nicola Armaroli, and Béatrice Delavaux-Nicot "Photo-induced Energy Transfer in a Th-Symmetrical Hexakis-adduct of C 60Substituted with π-Conjugated Oligomers" *Aust. J. Chem.* 2011, *64*, 153-159.

Selected Presentations

J. M. Malicka "*Photophysical Studies of Systems Synthesized within FINELUMEN network*" Finelumen International Conference 19-20 Settembre 2012, Philips High-Tech Campus, Eindhoven, the Netherlands; Poster Presentation.

J. M. Malicka, A. Kremer, A. Zanelli, D. Bonifazi, N. Armaroli "*Photophysical and Electrochemical Properties of a Novel Antenna-Fullerene-Donor Architecture for Light Energy Conversion*" IUPAC Symposium on Photochemistry 15-20 Luglio 2012, Coimbra, Portugal; Poster Persentation – **Award for the Best Poster Presentation.**

J. M. Malicka, L. Maggini, F. M. Toma, L. Feruglio, T. Da Ros, N. Armaroli, M. Prato, D. Bonifazi "Luminescent Blooming of Dendronic Carbon Nanotubes through Ion-Pairing Interactions with an Eu[III] Complex" Electronic Processes in Organic Materials – Exploring the Fundamentals of Organic Electronics; Gordon Research Conference 3-8 Giugno 2012, Lucca, Italy; Poster Presentation.